FINAL TECHNICAL REPORT

GROUND MOTION SITE EFFECTS IN THE WABASH VALLEY REGION FROM THE 18 JUNE 2002 DARMSTADT EARTHQUAKE

Award Number: 04HQGR0095

Principal Investigator: Edward W. Woolery

University of Kentucky
Department of Earth and Environmental Sciences
101 Slone Research Building
Lexington, KY 40506-0053
Phone: 859.257.3016
Fax: 859.257.1147
Email: woolery@uky.edu
http://www.uky.edu/AS/Geology/

Program Element: CU/I

Key Words: Engineering Seismology, Strong ground motion, Amplification

The views and conclusions contained in this document are those of the authors and should not be interpreted as necessarily representing the official policies, either expressed or implied, of the U.S. Government.

Award Number: 04HQGR0095

GROUND MOTION SITE EFFECTS IN THE WABASH VALLEY REGION FROM THE 18 JUNE 2002 DARMSTADT EARTHQUAKE

Edward W. Woolery, *Dept. of Earth and Environmental Sciences, University of Kentucky, 101 Slone Bldg., Lexington, Ky. 40506-0053, Tel: 859.257.3016, Fax: 859.257.1147, Email: woolery@uky.edu*,

ABSTRACT

The M4.6 southwestern Indiana (Darmstadt) earthquake of 18 June 2002 triggered 46 blast monitors in Indiana, Illinois, and Kentucky. The ground motions recorded by the blast monitors were between 6 and 9 times greater than the predictive relationships suggested. Consequently, the study objective was to understand the role of the site effect in this disparity. Integrated dynamic site investigations at the blast monitor locations, equivalent-linear site response, and empirical relationships were used to assess the role of the site effects associated with the Darmstadt earthquake ground motions. The observed free-field particle velocity records, peak accelerations and 5 percent damped PSA's for the earthquake, generally exceeded ground motions predicted for the top of the bedrock by factors of two or more, even after soil amplifications were taken into consideration.

The ambient noise and S-wave horizontal-to-vertical spectral ratio methods, as well as the V_{30} classification method, were also used estimate site effects for ground motions of >2 Hz at the blast monitors. The goal was to determine if any of the methods were robust enough to use as a general reconnaissance tool for estimating site effects in the area. The results indicated the horizontal-to-vertical ratio of the ambient noise method is too inconsistent to use as site-specific seismic hazard tool. The horizontal-to-vertical ratio of the S-wave method for estimating site effects maybe useful if there are a significant number of events recorded at a site to derive a statistical average; however, based on the results of this single event, its usefulness as a site-specific seismic hazard tool is suspect. The data also indicated that there is significant scatter in the V_{30} site classification scheme; therefore it too is unreliable for use as a site-specific seismic hazard tool.

NONTECHNICAL SUMMARY

The M4.6 southwestern Indiana (Darmstadt) earthquake of 18 June 2002 triggered 46 blast monitors in Indiana, Illinois, and Kentucky. The resulting free-field records have provided a unique opportunity to assess the role of seismic hazard amplification and the methods for measuring them in this area of the central United States. This study found that the disparity between the observed and expected ground motions is not entirely due to the amplification effects of the soil overburden. In addition, the results showed that the less rigorous methods for measuring ground-motion site effects performed poorly in this area.

INTRODUCTION

The 18 June 2002 M4.6 (4.9 $m_{b,Lg}$) Darmstadt earthquake was located at coordinates 37.966°N/87.775° in southwestern Indiana. The epicenter is near the center of the southern Illinois, southwestern Indiana, and western Kentucky coalfields, where numerous blast monitors are permanently installed. The earthquake triggered 46 blast monitors in the area, and two blast monitors at limestone quarries in Indiana and Kentucky (Fig. 1). The ground motions recorded by the blast monitors were between 6 and 9 times greater than the predictive relationships suggested (Fig. 2) (e.g., Atkinson and Boore, 1995). Consequently, the study objective was to understand the role of the site effect in this disparity. The blast-monitor recordings were used to constrain the site effects in the June 18, 2002 ground motions. Specifically, the earthquake ground-motion parameters observed from the blast-monitor data were compared to the ground-motion parameters predicted from linear-equivalent earthquake site response models, NEHRP provisions for seismic hazard amplification, and horizontal-to-vertical spectral ratios (HVSR) of ambient noise and earthquake S-waves.

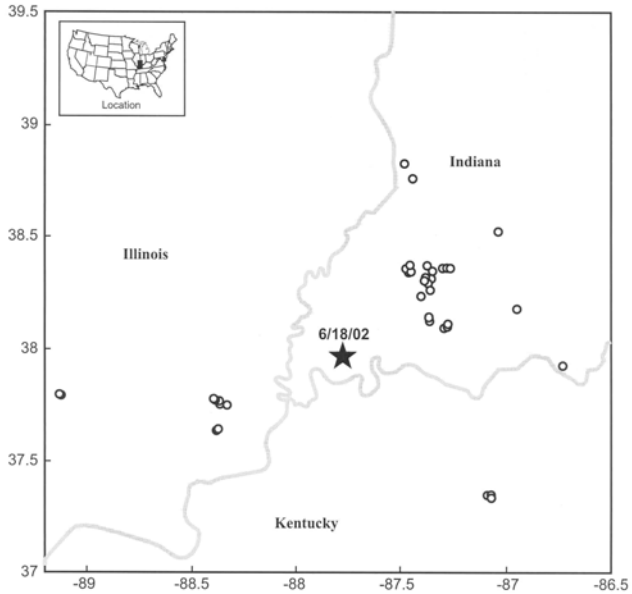

Figure 1. The locations of blast monitors (open circles) are shown relative to the earthquake epicenter (solid star) (from Street et al., 2005).

The epicenter of the June 18, 2002, earthquake is also located in the Nuttli and Herrmann (1978) defined Wabash Valley seismic zone, and the Wheeler and Cramer (2002) defined

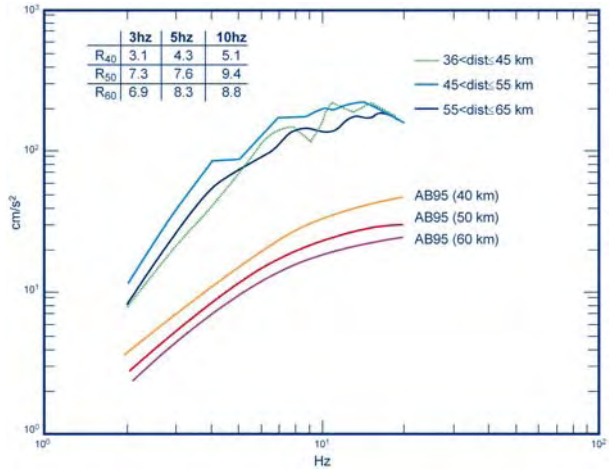

Figure 2. The observed ground motions were between 6 and 9 times greater than predictive relationships suggest (e.g., Atkinson and Boore, 1995).

Tristate Seismicity source zone (Fig. 3). Since 1820, 17 moderately damaging (i.e., Modified Mercalli VI-VII) earthquakes have occurred in the area of the seismic zones, and paleoseismological geotechnical evidence suggests that the area within the seismic zones has been shaken by at least four large (M6.0±0.5 to M7.5±0.5) late Pleistocene to middle Holocene earthquakes (Obermeier *et al*., 1991, 1992; Munson *et al*., 1992, 1997; Pond and Martin, 1997) (Fig. 3). Consequently, a moderate earthquake, such as the event on June 18, 2002, is not unexpected in the area.

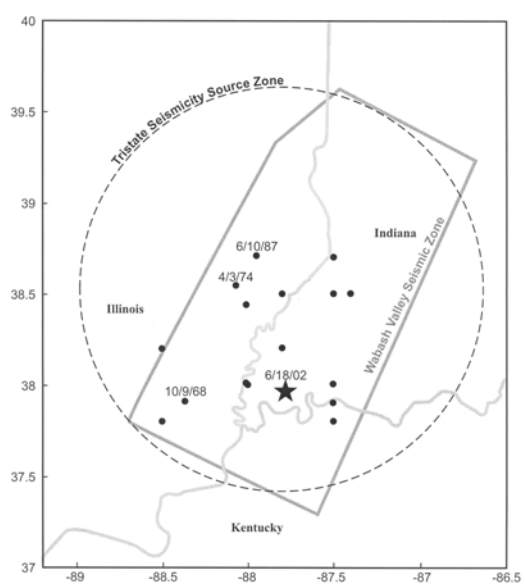

Figure 3. The location of the June 18, 2002, earthquake (filled star) is given relative to other MM VI or greater earthquakes in southwestern Indiana and southeastern Illinois, as well as the boundaries of the Wabash Valley seismic zone (solid lines), and the Tristate Seismicity source zone (dashed line) (from Street et al., 2005).

Site-response amplification can have a profound effect on the ground motions at a location, and is a major issue in general seismic hazard assessments. In order to assess the site effect, most estimation methods require an understanding of the dynamic site properties. These previously unknown properties at the blast monitor locations were defined using shear-wave (SH) refraction and reflection techniques. Previous published (Zhang *et al*., 1993) and unpublished *SH*-wave investigations, as well as available drill hole logs, suggested the soil overburden in the region varied between 2 and 4 m in depth along ridgelines and hill tops, to nearly 30 m in the valleys. The soils are generally characterized as loess, lacustrine, and alluvial deposits that primarily consist of silts and clays with relatively lesser amounts of sand. The bedrock in the area is a Pennsylvanian cyclic-sequenced shale, sandstone, and siltstone with minor coal and limestone units. All units vary in thickness and continuity. Consequently, bedrock and associated S-wave velocity is not uniform across the area. This variability in the bedrock type and thickness also likely contributes to the site effects in some areas.

BLAST-MONITOR RECORDINGS

Modern blast monitors are high-resolution, digital particle velocity recorders with capabilities very similar to those of modern strong-motion instruments used in engineering seismology. Record lengths from the blast monitors in this study vary from 5 to 15 s, with 71 percent of the records ranging from 6 to 9 s in length. Included in the recording time is a 1 s pre-event memory, and at the end of each record is a calibration pulse for each component of the seismometer (Fig 4.). Time on the blast monitors is checked periodically, but is not maintained rigorously enough for phase studies. The response of the blast monitors in this study is flat to velocity over a frequency range of 3 to 100 Hz, and down 10 to 15% at 2 Hz.

The three-component geophones for the blast monitors are free-field installations. A typical installation consisted of placing the geophone 20- to 35-cm below ground surface (soil), and backfilling and compacting with soil. The horizontal axes of the geophones were generally oriented so that the radial component was directed toward the general area of blasting that was to be monitored.

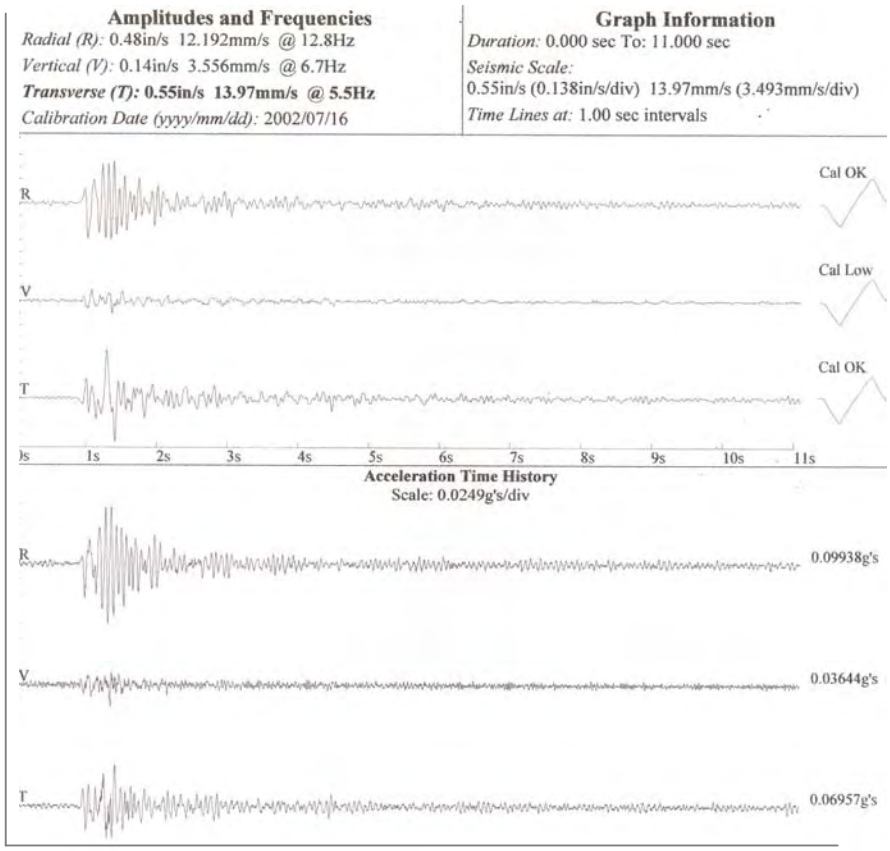

Figure 4. An example of a recorded velocity and derived acceleration time history from Site 20.

Like strong-motion recorders, blast monitors record the vertical and two horizontal components. The peak particle velocity and associated frequency of the ground motion for each component is imprinted on the record by the recorder, along with a time scale. The time scale is relative to the startup time of the recorder. With the exception of eight records, *P*-wave arrivals at the blast monitors were too small to trigger the instruments; instead, they were triggered by the *S*- or *Lg*-wave arrivals. The acceleration record was derived from the velocity record using the manufacturer's software package, Seismograph Data Analysis 2000, Version 6.0 (White Industrial Seismology, Inc., of Joplin, Mo.).

Table 1 is a list of the blast-monitor locations shown in Figure 1. Included in the table are the epicentral distances of the blast monitors to the earthquake, and the peak horizontal and vertical velocities, peak horizontal accelerations, and 5 percent damped peak spectral velocities. Also listed in the table are the frequencies with which the various ground-motion parameters are associated. An asterisk indicates sites at which the blast monitors recorded

TABLE 1

Blast monitor locations and observed peak ground-motion parameters.

Site No.	Lat/Long (°N/°W)	Dist. (km)	PPV (H) cm/s	PPV (H) Hz	PPV (V) cm/s	PPV (V) Hz	PGA cm/s^2	PGA Hz	PPSA SA	PPSA Hz
Illinois										
1*	37.746/88.337	55	1.067	7.5	0.210	9.8	51.9	9	6.06	8
			0.889	8.0			42.2	10		
2	37.750/88.361	56	1.194	8.1	0.102	12.8	81.2	7	7.34	8
			0.991	7.3			61.7	7		
3*	37.756/88.368	57	0.470	7.7	0.267	7.1	35.7	9	1.98	8
			0.419	6.4			22.7	12		
4*	37.756/88.369	57	0.521	8.2	0.279	4.8	32.5	4	1.72	8
			0.508	6.7			29.2	11		
5*	37.757/88.374	57	0.622	6.4	0.178	4.9	51.9	6	2.40	6
			0.495	6.9			48.7	9		
6*	37.758/88.375	57	0.514	9.1	0.159	6.2	27.6	6	2.25	8
			0.438	8.0			27.6	7		
7*	37.759/88.377	57	0.572	7.7	0.178	5.8	32.4	7	3.05	8
			0.508	7.1			22.6	7		
8	37.639/88.373	63	0.305	8.8	0.076	8.8	29.2	9	1.19	10
			0.241	11.1			19.5	14		
9	37.636/88.374	64	0.546	6.4	0.076	11.1	32.4	7	0.90	11
			0.292	8.0			19.5	11		
10	37.789/89.124	119	0.152	4.8	0.050	7.7	-	-	-	-
			0.127	5.2						
11	37.792/89.129	120	0.166	4.5	0.064	7.7	-	-	-	-
			0.140	5.5						
Indiana										
12	38.128/87.359	40	0.724	7.7	0.178	3.7	42.2	14	2.59	7
			0.699	4.6			39.0	14		
13	38.121/87.358	40	0.711	8.6	0.152	9.6	-	-	-	-
			0.457	11.9						
14	38.227/87.391	44	2.159	8.5	0.508	11.9	116.8	16	7.49	11
			2.057	8.5			104.1	12		
15	38.225/87.393	44	1.676	5.0	0.355	6.2	77.9	13	4.07	6
			1.270	6.4			64.9	11		
16	38.089/87.285	45	0.527	5.4	0.184	6.5	26.0	12	1.10	13
			0.324	4.7			24.3	14		
17	38.104/87.274	46	0.432	6.2	0.152	6.7	29.2	11	1.36	11
			0.419	7.5			26.0	15		
18*	38.101/87.274	46	0.434	12.8	0.146	6.9	27.6	12	1.39	15
			0.254	11.6			17.9	19		
19	38.092/87.275	46	0.508	5.5	0.127	4.3	25.9	13	1.55	7
			0.330	5.3			19.5	9		
20	38.253/87.350	49	1.397	5.5	0.356	6.7	97.4	12	6.62	12
			1.219	12.8			68.2	11		
21	38.365/87.365	50	2.438	7.8	0.356	7.2	129.8	13	10.81	7
			2.387	7.1			103.9	9		
22	38.337/87.454	50	0.356	4.6	0.127	5.8	-	-	-	-
			0.305	4.3						
23	38.295/87.377	50	1.753	7.7	0.483	8.8	77.9	9	5.04	7
			1.448	4.9			51.9	8		
24*	38.296/87.377	50	1.549	5.1	0.381	5.4	110.3	12	6.42	10
			1.321	8.8			84.4	12		
25	38.285/87.364	50	1.626	7.7	0.508	6.4	77.8	12	4.57	7
			1.245	8.3			77.8	9		
26	38.337/87.446	50	5.690	3.4	1.524	4.5	155.8	6	21.75	3
			2.083	4.2			129.9	13		

27	38.353/87.465	51	3.048	4.3	0.787	4.4	142.8	11	10.15	3
			2.718	3.4			116.9	12		
28	38.303/87.376	51	2.032	6.9	0.559	7.7	84.4	9	4.56	9
			1.778	8.0			77.9	13		
29	38.363/87.449	52	2.997	4.4	0.406	13.1	129.8	4	11.79	4
			2.032	4.0			103.9	15		
30	38.306/87.349	53	1.168	6.1	0.279	8.2	65.0	10	3.01	7
			0.737	7.5			51.9	11		
31	38.339/87.341	56	2.642	3.3	0.902	6.5	58.4	5	8.44	4
			1.372	5.4			45.5	10		
32	38.354/87.293	60	1.448	4.6	0.457	7.6	51.9	9	5.66	5
			1.016	4.4			51.8	9		
33	38.352/87.283	60	1.524	7.6	0.305	10.0	103.9	13	4.48	13
			1.118	8.5			-	-		
34	38.352/87.278	61	1.753	5.6	0.432	8.8	121.7	10	4.82	8
			1.575	8.5			84.4	18		
35	38.354/87.279	61	1.981	6.9	0.660	13.4	120.1	15	5.20	13
			1.829	9.4			100.6	13		
36	38.354/87.276	61	1.346	8.6	0.356	10.0	90.9	13	3.70	13
			1.143	7.4			64.9	11		
37	38.168/86.946	76	0.178	11.3	0.076	30.1	-	-	-	-
			0.178	14.6						
38	37.925/86.724	92	0.178	6.7	0.076	7.5	9.7	11	0.50	4
			0.171	3.5			8.1	11		
39	38.756/87.434	92	0.229	4.4	0.063	7.4	-	-	-	-
			0.179	4.7						
40	38.804/87.491	139	0.292	3.1	0.064	3.5	-	-	-	-
			0.241	3.6						
41	38.805/87.474	139	0.178	6.7	0.051	11.9	-	-	-	-
			0.127	6.4						
42	38.605/87.009	152	0.279	2.6	0.051	4.1	13.0	10	0.74	6
			0.191	9.4			9.7	3		
Kentucky										
43	37.339/87.086	92	0.229	4.4	0.064	4.3	6.5	9	0.57	5
			0.191	4.1			6.5	8		
44	37.335/87.075	93	0.140	2.6	0.051	5.1	-	-	-	-
			0.076	4.5						
45	37.335/87.073	95	0.127	3.0	0.051	5.6	-	-	-	-
			0.114	2.4						
46	38.032/85.664	184	0.051	3.7	0.038	5.1	-	-	-	-
			0.444	6.9						

Ground-motion parameters acquired from blast monitors triggered by the June 18, 2002, southwestern Indiana earthquake. Horizontal and vertical peak particle velocities (PPV), peak horizontal accelerations (PGA), and 5 percent damped pseudo-accelerations (PPSA). An asterisk indicates sites where blast monitors were triggered by the *P*-wave, whereas the other monitors were triggered by the *Sg*/*Lg*-wave arrival.

both the *P*- and *S*/*Lg*-waves. If a blast monitor was triggered more than once, there is a 50 ms calibration signal superimposed on the subsequent recordings. Three blast monitors in southern Indiana were triggered by a *P*-wave arrival, and were in the process of being retriggered at the time of the *S/Lg*-wave arrival. Data from these blast monitors were not included in the study. Peak ground accelerations were not included for some of the more distant blast monitors because the amplitudes of the traces were less than about three times the amplitude of the background noise at the site.

Eight blast monitors were triggered by the *P*-wave arrival. Figure 5 shows the *P*-wave record for site 6. The arrow in Figure 5 indicates the P_D-wave. The amplitudes of the P_D-wave at sites 4 through 7 were the maximum velocities recorded on the vertical component at those sites.

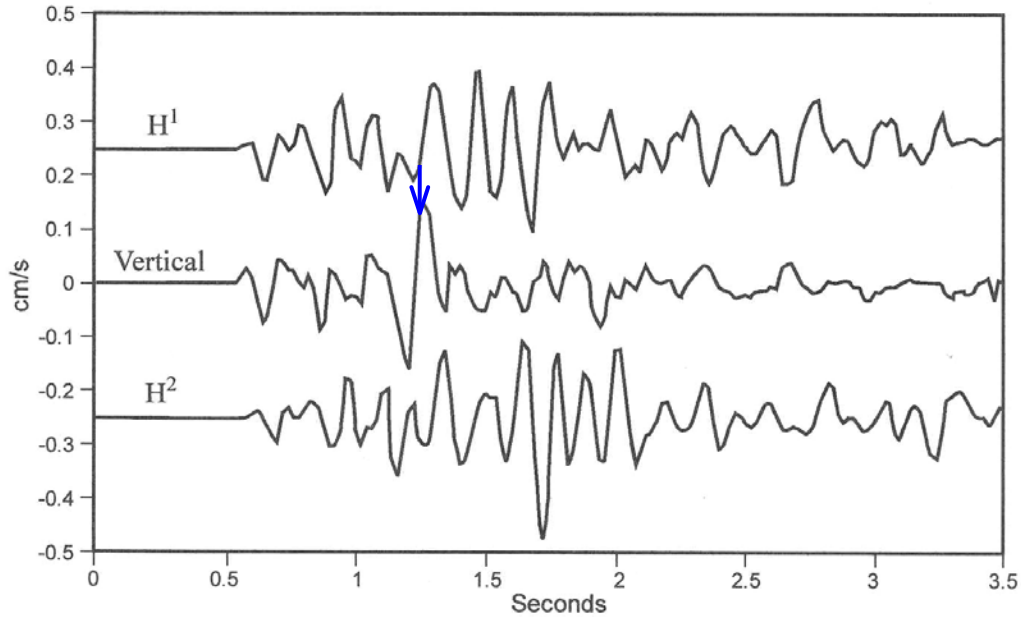

Figure 5. Typical blast-monitor record for *P*-wave traces at sites where the instrument was triggered by the *P*-wave arrival. The record is from site 6. The blue arrow above the vertical trace indicates the P_D phase arrival.

SITE CONDITIONS

Shear-wave velocity models for each site were derived from SH-wave refraction and reflection data collected using an inline spread of forty-eight 30-Hz horizontal geophones spaced at 2 m intervals and a 48-channel engineering seismograph. The energy source consisted of a section of steel H-pile that was struck horizontally by a 5.4-kg sledgehammer in a direction perpendicular to the geophone spread. The surveys were reversed (to correct for non-horizontal horizons) with five redundancy/reciprocity at various locations in each line. The seismic signal was enhanced by applying 15 horizontal impacts of the 5.4-kg hammer to the H-pile section that had a hold-down weight of ~75 kg. To ensure the accurate identification of SH-mode events, impacts were recorded on each side of the energy source. By striking each side of the source and reversing the acquisition polarity of the engineering seismograph, inadvertent P- and SV-mode energy will stack in a destructive manner, while SH-mode will stack constructively. The data were

collected at a sampling interval of either 0.25 or 0.5 ms, and processed on a PC using a commercial software package. Processing the seismic data typically consisted of applying a bandpass filter and automatic gain control (AGC). F-K filters were used with a few records to remove offline noise (e.g. irrigation pumps, farm machinery, etc.). The interpreted S-wave velocity model for each site is given in **Appendix A**.

SITE RESPONSE METHODOLOGIES

Linear-Equivalent Site Response Analysis

The site response analyses used an equivalent-linear code, EERA (Equivalent-linear Earthquake site Response Analysis) (Bardet et al., 2000). EERA is a recent exploitation of the traditional equivalent-linear SHAKE program (Schnabel et al., 1972; and Idriss and Sun, 1991). SHAKE computes one-dimensional soil responses for a system of homogeneous, visco-elastic layers of infinite horizontal extent that are subjected to vertically traveling shear waves. The program uses a continuous solution to the wave equation adapted for use with transient motions through the Fast Fourier Transform (FFT) algorithm. Non-linearity of the shear modulus and damping are approximated by the use of equivalent linear soil properties and numerically obtaining values compatible with the effective strains in each layer. SHAKE computes the response in a horizontally layered soil-rock system subjected to transient and vertical traveling shear waves. SHAKE assumes that the cyclic soil behavior can be replicated using an equivalent linear model, which has been extensively described in the geotechnical earthquake engineering literature (e.g., Idriss and Seed, 1968; Seed and Idriss, 1970; and Kramer, 1996). EERA was developed in FORTRAN 90 utilizing the basic SHAKE concepts. EERA's SHAKE implementation utilizes the dynamic array dimensioning and matrix operations in FORTRAN 90 and integrates input/output with Microsoft Excel.

The updated algorithms, like the original, assume simplified geometry and cyclic behavior of the materials. The basic assumptions made in the analyses follow [Yule and Wahl, 1996]:

1. The soil horizons are horizontal and extend infinitely.
2. The ground surface is horizontal.

3. Each soil unit can be completely defined by the shear modulus, damping function, layer thickness, and unit weight. Values are frequency independent.
4. The non-linear cyclic behavior is adequately characterized by the linear visco-elastic (Voigt) constitutive model and implemented with the equivalent linear method.
5. The incident earthquake motions are spatially uniform, horizontally polarized (SH) shear waves that are propagated vertically through the soil column.

The EERA program calculates the time histories of accelerations, velocities, displacements, stress, and strain and amplification ratio, Fourier, and response spectra as a result of an induced rock motion. Required input parameters to the algorithm include:

1. *Specification of normalized shear modulus and damping ratio*: Three relationships for shear modulus and damping were available in the program; one each for rock, sand, and cohesive soils.
2. *Acceleration time History*. The ground motions were derived by stochastic simulation and input to EERA as a rock outcrop motion. These acceleration time histories for the top of rock motions are discussed below.
3. *Soil Data*.
    a. Number of soil layers
    b. Soil type
    c. Layer thickness
    d. Shear wave velocity
    e. Shear modulus
    f. Critical damping ratio (initial estimate)
    g. Unit weight

<u>Stochastic Time Histories</u>

The stochastic simulation model proposed by Boore [1983], and recommended by Reiter [1990], was used for deriving the recommended time-histories for the Wabash Valley Region. From the mathematical representation of O'Connor and Ellingwood [1992], the spectral density of strong motions derived from the Boore model, $S_a(\omega)$, is described by the equation:

$$S_a(\omega) = CM_0 S(\omega, \omega_c) P(\omega, \omega_m)(1/R) e^{-\omega R / 2Q\beta}$$

where, C = a constant related to the source parameters, $S(\omega, \omega_c)$ = spectral density of the energy released at the source, M_o = seismic moment (dyne-cm), $P(\omega, \omega_m)$ = high-cut filter with a cutoff of ω_m, R = epicentral distance, Q = specific quality factor (which is inversely related to attenuation), β = shear-wave velocity (km/s), ω = circular frequency, ω_c = corner frequency exhibited by the spectral density of the shear waves, and ω_m = maximum circular frequency. The constant C is related to the source parameters by the equation:

$$C = (RP\ FS\ RF)/(4\pi\omega\rho^3)$$

where, RP = radiation pattern, FS = amplification due to the free-surface boundary condition, RF = reduction factor to account for the partitioning of the seismic energy into horizontal components, and ρ = density (kg/m^3).

The source parameter's seismic moment, M_o, and spectral corner frequency, $f_c = \omega_c/2\pi$, are related by the equation:

$$f_c=4.9x10^6\beta(\Delta\sigma/M_o)^{1/3}$$

where, f_c is in Hertz, $\Delta\sigma$ = stress drop in bars, and M_o is in dyne-cm [Brune 1970, 1971]. Seismic moment (M_o) and stress drop ($\Delta\sigma$) are related to the m_b magnitude scale (used in the central United States) by the relationship shown in figure 6 [Toro et al., 1992]. This relationship assumes a moderately increasing stress drop with seismic moment, which is similar to that suggested by Nuttli et al. [1989] except that lower magnitude ($\leq$5.5 m_b) events retain a constant 100 bar stress drop. For great earthquakes ($m_b \geq 7.0$; $M_o \geq 10^{27}$ dyne-cm), the stress drop is assumed 250 bars (1 bar=10^{-1} MPa), however.

Using the above model, a synthetic time-history of the 18 June 2002 event for each of the sites was generated. Input parameters used in generating the ground motions for the event is given in Table 4. The peak ground accelerations varies from 0.0046 to 0.0220g.

Table 4

Input Parameters of the Stochastic Modeling

Input Parameters:	
Magnitude (Mw)	**4.6**
Epicentral Distance (km)	**variable**
Moment (dyne-cm)	**6.3×10^{22}**
f_{max} (Hz)	**100**
Stress Drop (bars)	**150**
Q	**680**
γ	**0.36**
PR	**0.55**
FS	**2.0**
RF	**0.71**
β (km/s)	**3.6**
ρ (kg/m^3)	**2,800**

Q = specific quality factor
γ = attenuation
RP = radiation pattern
FS = free surface effect
RF = reduction factor

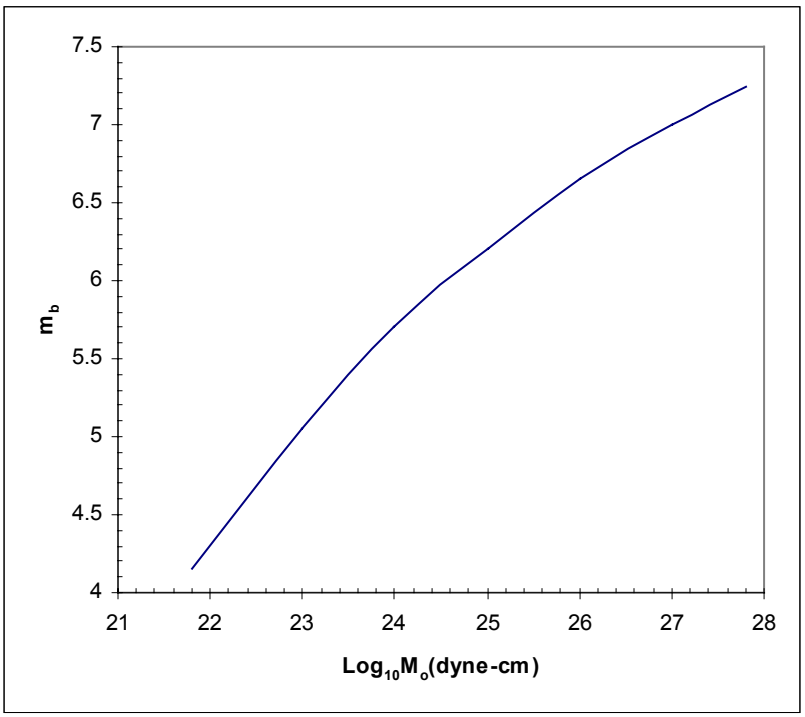

Figure 6. m_b to M_o relationship [Torro et al., 1992]

Horizontal-to-Vertical Spectral Ratio (HVSR)

Site effects are also frequently estimated by the horizontal-to-vertical spectral ratios (HVSR) of ambient noise, which is sometimes referred to as Nakamura's (1988) technique, and earthquake generated S-waves. A basic assumption in both techniques is that the vertical component of the ground motions are relatively free of near-surface site effects, whereas the horizontal components are amplified in such a way as to reflect the resonance period at the site and the extent of amplification of the ground motions at that period. Results derived from the two techniques have been mixed, however. Nonetheless, the two spectral ratio techniques are often used due to the ease in acquiring and processing the necessary data. Successful applications of Nakamura's technique has been shown by Lermo and Chavez-Garcia (1993), Chavez-Garcia et al. (1996), Seekins et al. (1996), and De Luca et al. (2005), among others. Other studies, however, have concluded that while it is possible to deduce the resonance site frequency using Nakamura's technique, the amplification factor interpreted for the site using the technique is unreliable (e.g., Field and Jacob, 1995; Lachet et al., 1996, Horike et al., 2001). Still other studies have concluded that Nakamura's technique fails either in general, or under certain conditions. For example, Riepel et al. (1998) and Paraolia et al. (2004) note that the vertical component of the ambient noise is influenced by two- and three-dimensional site complexities, and consequently if such complexities exist, the technique fundamentally fails to estimate the site response.

The ambient noise samples acquired at the midpoints of the geophone arrays used in the SH-wave seismic refraction/reflection profiling. Three 15 s windows of the ambient noise were recorded at each site with a 1 Hz, Mark Products L-4-3D seismometer and at a sampling rate of 250 sps; the repeatability observed for the records was excellent (Fig. 7). The recording system did not include a low-cut filter, but it did include an active, anti-aliasing high-cut filter that rolled off at 12 db at 15 Hz, and truncated the signal at 20 Hz. The L-4-3D was sheltered as much as possible from the wind, and obvious noise sources, such as passing traffic and people walking, were avoided.

The length of the window used to calculate the HVSR from the earthquake S-waves varied from 1 to 3.4 s. The window was visually picked so that it began shortly before the onset of the S-

wave and continued until that point on the vertical trace the signal-to-noise ratio was too judged to be too low. The three-component traces were tapered with a five percent cosine and padded at both ends for a total of 8192 points. The individual horizontal and vertical components were then individually transformed and smoothed, and the square root of the sum of the squares of the transforms of the horizontal components were divided by two times the smoothed transform of the vertical component. Two smoothing functions were used in this study, a 17-point running window, and the logarithmic window function proposed by Konno and Ohmachi (1998). Within the range of frequencies considered in this study, the results with the two smoothing functions were nearly identical.

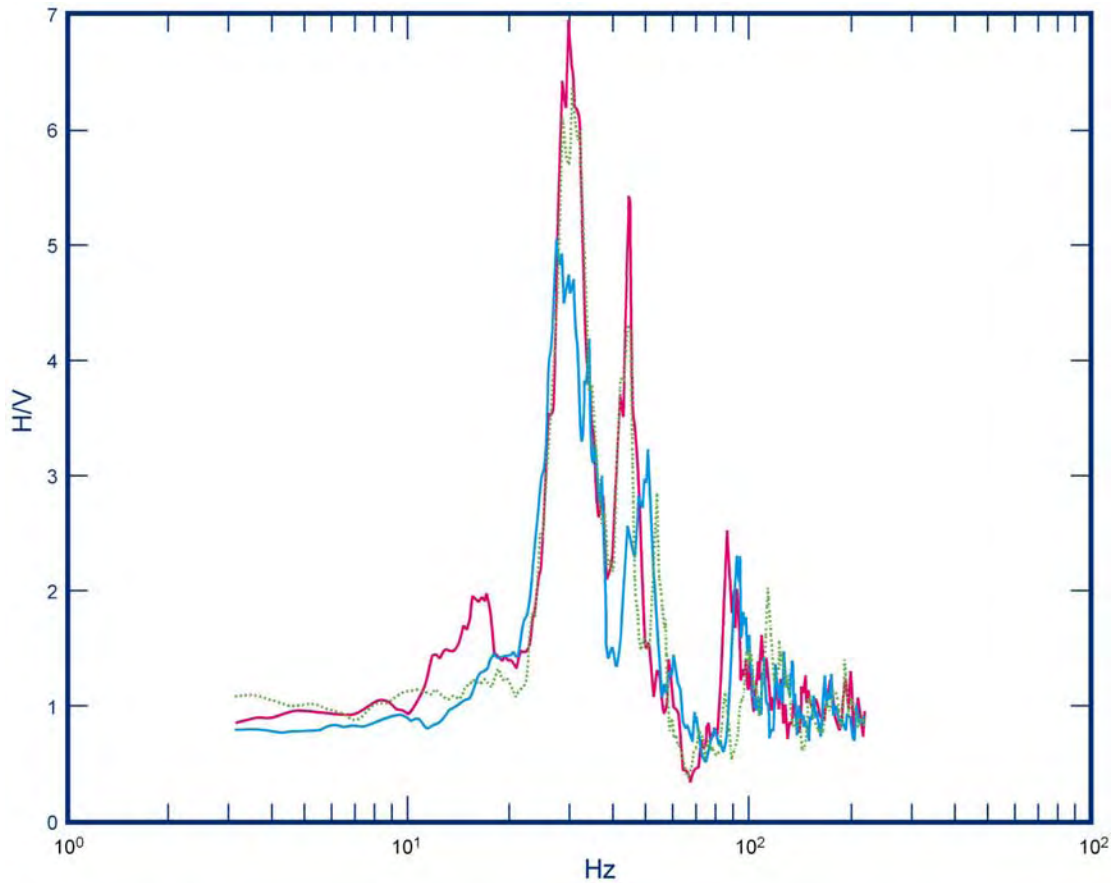

Figure 7. The repeatability of the ambient noise records is shown in this typical comparison of the three 15 s windows recorded from Site 31.

NEHRP Site Dependent Coefficients

In the lower Wabash river valley, as elsewhere in the central United States, site-specific seismic-response amplification is oftentimes defined by the properties of the upper 30 m of soils and rock at the site. Provisions within the 1997 National Earthquake Hazards Reduction Program (NEHRP) for seismic regulations of new buildings (Federal Emergency Management Agency, 1998) classify the site into one of six categories that are used to derive a local site response. The provisions and the methodology used in the central United States are a direct result of the work and recommendations by Borcherdt (1978), Borcherdt (1994) and Martin and Darby (1994) based on data that were, for the most part, acquired in California. Site-response amplification estimation from the properties of the upper 30 m of soils and rock at a site has yielded mixed results. Wald and Mori (2000) concluded that while the time-averaged shear-wave velocities of the upper 30 m of surficial soils and rock at sites in the Los Angeles region roughly correlated observed site responses, the scatter was large and the method was inadequate for predicting site amplification. Conversely, Molnar et al. (2004) concluded that the site amplification in the greater Victoria, British Columbia, area, based on shear-wave velocities, is in general agreement with the intensities observed for the 2001 Nisqually earthquake.

RESULTS

Tables 5, 6, and 7 summarize the comparison of the observed values and the calculated results of peak accelerations, the site amplification and characteristic frequency, and NEHRP site classification, respectively. The detailed results from are shown in **Appendices B and C**.

Table 5

Comparison of observed and the equivalent-linear calculated peak accelerations

Site No.	Input Value, g	Output Value, g	Observed Value, g	Observed/Output
1	0.0124	0.018	0.053	2.94
2	0.0124	0.020	0.083	4.15
3	0.0114	0.030	0.036	1.20
4	0.0130	0.030	0.033	1.10
5	0.0140	0.024	0.053	2.21
6	0.0140	0.024	0.028	1.17
7	0.0117	0.042	0.033	0.79
10	0.0046	0.013	-	-
11	0.0061	0.020	-	-
12	0.0220	0.034	0.047	1.38
13	0.0220	0.056	-	-
14	0.0163	0.038	0.119	3.13
15	0.0199	0.048	0.079	1.65
16	0.0204	0.040	0.026	0.65
17	0.0188	0.017	0.030	1.76
18	0.0171	0.018	0.028	1.56
19	0.0158	0.022	0.026	1.18
20	0.0147	0.035	0.099	2.83
21	0.0118	0.042	0.132	3.14
22	0.0118	0.035	-	-
25	0.0144	0.029	0.079	2.72
26	0.0130	0.029	0.159	5.48
30	0.0172	0.029	0.066	2.28
31	0.0101	0.027	0.059	2.19
32	0.0112	0.016	0.053	3.31
33	0.0094	0.019	-	-
34	0.0096	0.026	0.124	4.77
35	0.0096	0.030	0.122	4.07
36	0.0096	0.012	0.093	7.75
37	0.0078	0.013	-	-
38	0.0079	0.022	0.098	4.45
39	0.0061	0.017	-	-
40	0.0078	0.015	-	-
41	0.0072	0.014	-	-
42	0.0053	0.011	0.010	0.91

Table 6

Amplification (Amp) and Site Characteristic Frequencies (f_c) Observed for the Southwestern Indiana Earthquake of June 18, 2002, compared to the Amplifications and Site Frequencies (f) Estimated using the EERA and Horizontal-to-Vertical Spectral Ratios of the S-wave and Ambient Noise

Site	Location		Observed		H/V_s		H/V_N		EERA	
No.	°N	°W	Amp[2]	f_c[3]	Amp[4]	f[5]	Amp[4]	f[5]	Amp[4]	f[5]
1	37.746	88.337	2.8	7.8	11.5	**6.7**	1.6	0.6	3.0	11.4
2	37.750	88.361	3.2	9	7.3	**8.9**	1.0	**9.2**	6.3	9.0
3	37.756	88.368	3.6	12	6.7	2.1	0.8[m]	7.7	602	10.0
4	37.756	88.369	4.0	12	**4.7**[m]	5.1	0.8[m]	7.7	6.2	10.0
5	37.757	88.374	4.8	12	14.8	6.6	0.7[m]	10.4	6.4	16.0
6	37.758	88.375	4.0	12	5[m]	5.8	0.7[m]	10.4	6.4	16.0
7	37.759	88.377	4.4	5.5	6.1[m]	**6.3**	**4.0**	**6.8**	9.9/11.5	8.6/20.4
12	38.128	87.35	3.0	20	6	7.1	0.9	1.1	4.7	25.0
13	38.121	87.358	3.0	11.5	3.6/**3.1**	6.3/13.2	0.6[m]	2.0	4.7	11.8
14	38.227	87.391	10.8	19	5	**9.3**	0.9	13.2	6.3	11.0
15	38.225	87.393	8.4	19	3.1/3	5.3/15	0.8[m]	13.2	6.5	11.0
16	38.089	87.285	2.7	10	4.2[m]	**10.1**	1.3	0.9	6.3	15.6
19	38.092	87.275	2.7	10	6.9/**3.5**	7.1/**9.1**	1.3	0.9	6.3	15.6
20	38.253	87.350	8.5	15	17.7	**14.4**	2.1	0.6	7.2	19.2
21	38.365	87.365	15.3	2.1	4.3/5	14.8/17	1.2	**2.6**	10.4	2.4
25	38.285	87.364	10.2	9.1	5.1	2.8	1.1	11.7	8.2	11.8
30	38.306	87.349	8.1	5.8	3.7/3.2	2.7/14.7	4.9	**6.7**	3.9/6.3	6.8/17.6
31	38.339	87.341	5.8	3	2.7	**2.0**	2.9	**2.8**	5.7/7.6	3.4/8.8
32	38.354	87.293	12.2	22	4/3.9	2.0/**21**	0.6/1.2	1.2/3.8	3.2	18.6
33	38.352	87.283	12.8	13.3	4.2/3.5	5.0/**12.8**	0.5[m]	2.2	7.2	12.4
34	38.352	87.278	15.1	18.5	3.9	12.7	1.1[m]	2.2	7.8	20.0
35	38.354	87.279	17.1	7	5.2	**6.6**	0.7[m]	10.8	7.1/7.1	9.6/16.4
36	38.354	87.276	11.7	18.5	2.7	12.9	1.1[m]	2.2	7.1/7.1	9.6/16.4
37	38.168	86.946	2.0	11	3.9	14.0	0.7	3.7	4.2	16.8
40	38.804	87.491	4.2	11.5	2.8	**11.9**	1.9	1.1	7.1	11.6
41	38.805	87.474	2.6	6	5.5	11.8	0.6	0.6	5.3/7.0	6.2/17.8
42	38.605	87.009	4.4	12.1	2.6[m]	2.4	**3.9**	**13.6**	3.9	11.0

1. Site numbers are the same as those used in Street et al. (2005).
2. Amplifications are the ratios of the PGV's reported in Street et al. (2005) to those predicted by the Atkinson and Boore (1995) model.
3. Site characteristic frequencies at the midpoint of the geophone arrays. The values were derived by dividing the time-averaged S-wave velocity of the soils by four times the soil thickness.
4. Peak amplitude(s) in H/V spectral ratio. If there are two peaks, both are listed. If there are more than two peaks or no peak of note, then the peak value is followed by the superscript "m". Peak H/V amplitudes within a multiplicity factor of 2 of those determined by the PGV's recorded for the earthquake (column 4) are indicated by bold print.
5. Frequencies at which the peak amplitude(s) occurred. Frequencies that are within two Hz of the site characteristic frequency (column 5) are indicated by bold print.

Table 7

NEHRP V_{30} measurements and associated Site Classification

Site No.	Location °N	°W	NEHRP V_{30} (m/s)	NEHRP Site Class	NEHRP Site Coefficient
1	37.746	-88.337	706	C	1.2
2	37.751	-88.360	753	C	1.2
3	37.755	-88.360	754	C	1.2
4	37.755	-88.360	754	C	1.2
5	37.758	-88.377	850	B	1.0
6	37.758	-88.377	850	B	1.0
7	37.759	-88.379	675	C	1.2
10	37.788	-89.125	279	D	-
11	37.788	-89.130	486	C	-
12	38.128	-87.358	675	C	1.2
13	38.120	-87.356	749	C	1.2
14	38.226	-87.391	753	C	1.2
15	38.226	-87.391	753	C	1.2
16	38.090	-87.281	832	B	1.0
20	38.253	-87.350	933	B	1.0
21	38.363	-87.365	250	D	1.54
22	38.335	-87.455	580	C	1.2
25	38.284	-87.363	730	C	1.2
26	38.336	-87.445	389	C	1.2
30	38.304	-87.350	435	C	1.2
31	38.337	-87.341	314	D	1.6
32	38.353	-87.293	780	B	1.0
33	38.352	-87.282	705	C	1.2
34	38.352	-87.275	883	B	1.0
35	38.353	-87.278	690	C	1.2
36	38.352	-87.275	883	B	1.0
37	38.167	-86.945	1044	B	1.0
38	37.926	-87.708	774	B	1.0
39	38.765	-87.435	679	C	1.2
40	~38.804	-87.491	681	C	1.2
41	38.801	-87.473	580	C	1.2
42	38.605	-87.011	595	C	1.2

SUMMARY

The disparity between the observed peak parameters for the June 18, 2002, earthquake and the predicted values for the top of bedrock at blast-monitor observation sites in southern Indiana and southern Illinois is larger than would be expected based on suggested predictive relationships. Dynamic site characterization at the blast-monitor locations also suggests that the disparity is not all due to site effects. The observed PGA at 23 of the 26 sites modeled exceeded the expected values by an average factor of 2.89 (ranging between 1.10 and 7.75).

In addition, the study evaluated the ambient noise and S-wave horizontal-to-vertical methods, as well as the V_{30} classification method, as estimation techniques for ground motion site effects (>2 Hz) at the blast monitors. The goal was to determine if any of the methods were robust enough to use as a general reconnaissance tool for estimating site effects in the area. The results indicated the horizontal-to-vertical ratio of the ambient noise method is too inconsistent to use as site-specific seismic hazard tool and, like Wald and Mori (2000), the data also indicated that there is so much scatter in the V_{30} site classification scheme, that it too is unreliable for use as a site-specific seismic hazard tool. The horizontal-to-vertical ratio of the S-wave method for estimating site effects maybe useful if there are a significant number of events recorded at a site to derive a statistical average, as suggested by Chen and Atkinson (2002); however, based on the results of this single event, it too fails as a site-specific seismic hazard tool.

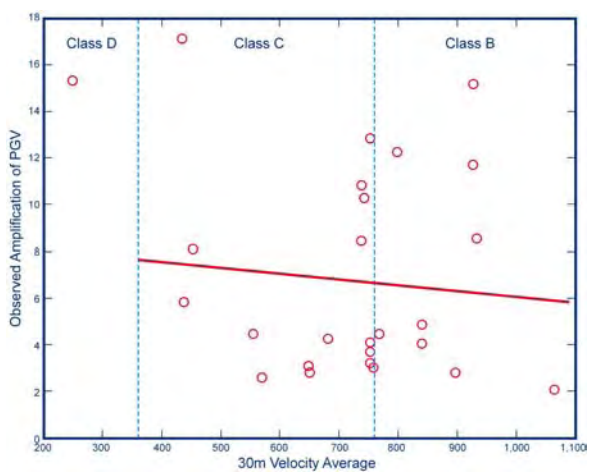

Figure 8. Plot of PGV residuals (i.e., the observed PGV's minus the Atkinson and Boore (1995) predicted PGV's). The solid line is the least squares fit for site classes C and B PVG's and V_{30} (the <u>single</u> Site Class D observation was not included). The relationship indicates that PGV decreases with increasing V_{30}, but the data scatter indicates significant uncertainty.

BIBLIOGRAPHY

Abrahamson, N. (1995). Rock should be the reference condition, Proceedings of National Earthquake Ground Motion Mapping Workshop, Applied Technology Council, ATC-35-2.

Aki, K. (1988). Local site effects on strong motion, in Earthquake Engineering and Soil Dynamics II, vol. 20, Geotechnical Special Publication, J. V. Thun (editor), American Society of Civil Engineers, New York, 103-155.

Anderson, J. G, Y. Lee, Y. Zeng, and S. Day (1996). Control of strong motion by the upper 30 meters, *Bull. Seism. Soc. Am.* 86. 1749-1759.

Atkinson, G.M. and D. M. Boore (1995). Ground-motion relations for eastern North America, *Bulletin of the Seismological Society of America*. 85, 17-30.

Bardet, J.P., K. Ichii, and C.H. Lin (2000). EERA – A computer program for equivalent-linear earthquake site response analyses for layered soil deposits, at http://gees.usc.edu/GEES/, 40 p.

Boore, D.M. (1983). Stochastic simulation of high-frequency ground motions based on seismological models of radiated spectra, *Bull. Seism. Soc. Am*., 73, 1865–1894.

Borcherdt, R. D. (1994). Estimates of site-dependent response spectra for design (methodology and justification), Earthquake Spectra, 10, 617-653.

Borcherdt, R. D., J. F. Gibbs, and T. E. Fumal (1978). Progress on ground motion predictions for the San Francisco Bay region, Calif., in Proceedings, Second International Conference on Microzonation - Safer Construction Research, App. 2,1, 13-25.

Brune, J.N. (1970). Tectonic stress and spectra of seismic shear waves from earthquakes, *Jour. Geophy. Res.*, 75, 4997–5009.

Brune, J.N. (1971). Correction, *Jour. Geophy. Res.*, 76, 5002.

Chavez-Garcia, F. J., L. R. Sanchez, and D. Hatzfed (1996). Topographic site effects and HVSR: A comparison between observation and theory, Bull. Seism. Soc. Am., 86, 1559-1573.

Chen, S.-Z., and G. M. Atkinson (2002). Global comparisons of earthquake source spectra, Bull. Seism. Soc. Am. 92, 885-895.

Cooley, J. W. and Tukey, J. W. (1965). An Algorithm for the Machine Calculations of Complex Fourier Series, *Mathematics of Computation*, 19, p. 297-301.

Coutel, F., and P. Mora (1998). Simulation-based comparison of four site response estimation techniques, Bull. Seism. Soc. Am. 88, 30-42.

De Luca, G., S. Marcucci, G. Milana, and T. San (2005). Evidence of low-frequency amplification in the city of LAquila, central Italy, through a multi disciplinary approach including strong- and weak-motion data, ambient noise, and numerical modeling. Bull. Seism. Soc. Am. 95, 1469-1481.

Federal Emergency Management Agency (1998). *NEHRP Recommended Provisions for Seismic Regulations for New Buildings and Other Structures*.

Field, E.H., and K. H. Jacob (1995). A comparison and test of site response estimation techniques, including three that are non-reference-site dependent, Bull. Seism. Soc. Am. 85, 1127-1143.

Field, E. H., P. A. Johnson, I.A. Beresnev, and Y. Zeng (1997). Nonlinear ground-motion amplification by sediment during the 1994 Northridge earthquake, Nature, 390, 599-602.

Hartzell, S., A. Leeds, A. Frankel, and J. Michael (1996). Site response for urban Los Angeles using aftershocks of the Northridge earthquake, Bull. Seism. Soc. Am.86, S168-S192.

Hartzell, S., E. Cranswick, A. Frankel, D. Carver, and M. Meremonte (1997). Variability of site response in the Los Angeles urban area, Bull. Seism. Soc. Am. 87, 1377-1400.

Horike, M., B. Zhao, and H. Kawase (2001). Comparison of site response characteristics inferred from microtremors and earthquake shear waves, Bull. Seism. Soc. Am. 91, 1526-1536.

Idriss, I. M. (1990). Response of Soft Soil Sites during Earthquakes*, Proceedings, Memorial Symposium to honor Professor Harry Bolton Seed*, Berkeley, California, Vol. II, May.

Idriss, I. M. and Seed, H. B. (1968). Seismic Response of Horizontal Soil Layers, *Journal of the Soil Mechanics and Foundations Division*, ASCE, 94, p.1003-1031.

Idriss, I. M. and Sun, J. I. (1992). User's Manual for SHAKE91, *Center for Geotechnical Modeling, Department of Civil Engineering*, University of California, Davis.

Joyner, W. B. (1995). Soil is the most appropriate reference site condition, Proceedings of National Earthquake Ground Motion Mapping Workshop, Applied Technology Council, ATC-35-2, 27-31.

Konno, K., and T. Ohmachi (1998). Ground-motion characteristics estimated from spectral ratio between horizontal and vertical components of microtremor, Bull. Seism. Soc. Am. 88, 228-241.

Kramer, S. L. (1996). *Geotechnical Earthquake Engineering*, Prentice Hall, Upper Saddle River, New Jersey, pp. 254-280.

Lachet, C., D. Hatzfelr, P.-Y. Bard, N. Theodulidis, C. Papaioannou, and A. Savvaidis (1996). Site effects and microzonation in the city of Thessaloniki (Greece) Comparison of different approaches, Bull. Seism. Soc. Am. 86, 1692-1703.

Lermo, J., and F. J. Chavez-Garcia (1993). Site effects evaluation using spectral ratios with one station, Bull. Seism. Soc. Am. 83, 1574-1594.

Lysmer, J., Seed, H. B. and Schnabel, P. B. (1971). Influence of Base–Rock Characteristics on Ground Response, *Bulletin of the Seismological Society of America*, 61, p. 1213-1232.

Martin, G. R., and R. Dobry (1994). Earthquake site response and seismic code provisions, NCEER Bulletin, 8, 1-6.

Molnar, S., J. F. Cassidy, and S. E. Dosso (2004). Comparing intensity variation of the 2001 Nisuqally earthquake with geology in Victoria, British Columbia, Bull. Seism. Soc. Am. 94, 2229-2238.

Munson, P.J., C.A. Munson, N.K. Bleuer, and M.D. Labitzke (1992). Distribution and dating of prehistoric earthquake liquefaction in the Wabash Valley of the central U.S., *Seismological Research Letters* 63, 337-342.

Munson, P.J., S.F. Obermeier, C.A. Munson, and E.R. Hajic (1997). Liquefaction evidence for Holocene and latest Pleistocene seismicity in the southern halves of Indiana and Illinois: A preliminary overview, *Seismological Research Letters* 68, 521-536.

Nakamura, Y. (1989). A method for dynamic characteristics estimation of subsurface using microtremor on the ground surface, Q. Rept. Railway Tech. Res. Inst. 30(1), 25-33.

Nuttli, O.W. (1973). Seismic wave attenuation and magnitude relations for eastern North America, *Journal of Geophysical Research* 78, 876-885.

Nuttli, O.W., and R.B. Herrmann (1978). Credible earthquakes in the central United States. In *State-of-the-Art for Assessing Earthquake Hazards in the United States*, Vicksburg, Miss., U.S. Army Corps of Engineers Geotechnical Lab Report 12, 99 p.

Nuttli, O.W., and R.B. Herrmann (1984). Ground motion of Mississippi Valley earthquakes, *Journal of Technical Topics in Civil Engineering, American Society of Civil Engineering* 110, 54-69.

Obermeier, S.F., N.K. Bleuer, C.A. Munson, P.J. Munson, W.S. Martin, K.M. McWilliams, D.A. Tabaczynski, J.K. Odum, M. Rubin, and D.L. Eggert (1991). Evidence of strong earthquake shaking in the lower Wabash Valley from prehistoric liquefaction features, *Science* 251, 1061-1063.

Obermeier, S.F., P.J. Munson, C.A. Munson, J.R. Martin, A.D. Frankel, T.L. Youd, and E.C. Pond (1992). Liquefaction evidence from strong Holocene earthquake(s) in the Wabash Valley of Indiana-Illinois, *Seismological Research Letters* 63, 611-623.

O'Connor, J.M. and B.R. Ellingwood (1992). Site-dependent models of earthquake ground motion, *Earthquake Engineering and Structural Dynamics*, 21, 573–589.

Ohtsuki, A., and K.Harumi (1983). Effect of topography and subsurface inhomogeneities on seismic SV waves, Earthquake Eng. Struct. Dyn. 11, 441-462.

Parolai, D., D. Bindi, M. Baumbach, H. Grosser, C. Milkereit, S. Karakisa, and Z (2004). Comparison of different site response techniques using aftershocks of the 1999 Izmit earthquake, Bulletin of the Seismological Society of America 94, 1096-1108.
Pond, E.C., and J.R. Martin (1997). Estimated magnitudes and accelerations associated with prehistoric earthquakes in the Wabash Valley region of the central United States, *Seismological Research Letters* 68, 611-623.

Reiter, L. (1990). *Earthquake Hazard Analysis: Issues and Insights*, Columbia University Press, New York, 254 p.

Riepel, J., P. Y. Bard, D. Hatzfeld, C. Papaioannou, and S. Nechtschein (1998). Detailed evaluation of site-response estimation methods across and along the sedimentary valley of Vovi (EURO-SEISTEST), Bull Seism. Soc. Am. 88, 488-502.

Rimrock Geophysics, Inc. (1995). SIPT2 version 4.1 (and other programs), 56 pp.

Satoh, T., H. Kawase, and S. Matsushima (2001). Differences between site characteristics obtained from microtremors, S-waves, P-waves, and codas, Bull. Seism. Soc. Am. 91, 313-334.

Schnabel, P. B., Lysmer, J., and Seed, H. B. (1972). SHAKE: A Computer Program for Earthquake Response Analysis of Horizontally Layered Sites, *Report No. UCB/EERC-72/12*, Earthquake Engineering Research Center, University of California, Berkeley, 102p.

Seed, H. B. and Idriss, I. M. (1970). Soil Moduli and Damping Factors for Dynamic Response Analysis, Report No. UCB/EERC-70/10, Earthquake Engineering Research Center, University of California, Berkeley, 48p.

Seed, H. B., Wong, R. T., Idriss, I. M. and Tokimatsu, K. (1986). Moduli and Damping factors for Dynamic Analyses of Cohesionless Soils, *Journal of the Geotechnical Engineering Division*, ASCE, 11 2, No. GTI 1, p.1016-1032.

Seekins, L. C., L. Wennerberg, L. Margheriti, H.-P. Liu (1996). Site amplifications at five locations in San Francisco, California: a comparison of S-waves, codas, and microtremor, Bull. Seism. Soc. Am. 86, 627-635.

Seismic Image Software, Ltd. (1995). VISTA7.0 notes.

Street, R., J. Wiegand, E. W. Woolery, and P. Hart (2005). Ground-motion parameters of the southwestern Indiana earthquake of 18 June 2002 and the disparity between the observed and predicted values, Seismological Research Letters, 76, 512-530.

Toro, G.R., N.A. Abrahamson, and J.F. Schneider (1997). Model of strong ground motions from earthquakes in central and eastern North America: Best estimates and uncertainties, *Seismological Research Letters* 68, 41-57.

Wald, L. A., and J. Mori (2000). Evaluation of methods for estimating linear site-response amplifications in the Los Angeles region, Bulletin of the Seismological Society of America, 90, S32-S42.

Wheeler, R.L., and C.H. Cramer (2002). Updated seismic hazard in the southern Illinois Basin: Geological and geophysical foundations for use in the 2002 USGS national seismic-hazard maps, *Seismological Research Letters* 73, 776-791.

Yuncha, Z. A., and F. Luz (2000). On the horizontal-to-vertical spectral ratio in sedimentary basins, Bull. Seism. Soc. Am. 90, 1101-1106

Zhang, M., R. Street, J. Harris, and V.P. Drnevich (1993). A note on the influence of site conditions on ground motion values observed for the southeastern Illinois earthquake of June 10, 1987, *Seismological Research Letters* 64, 149-156.

APPENDIX A

Site S-wave velocity model

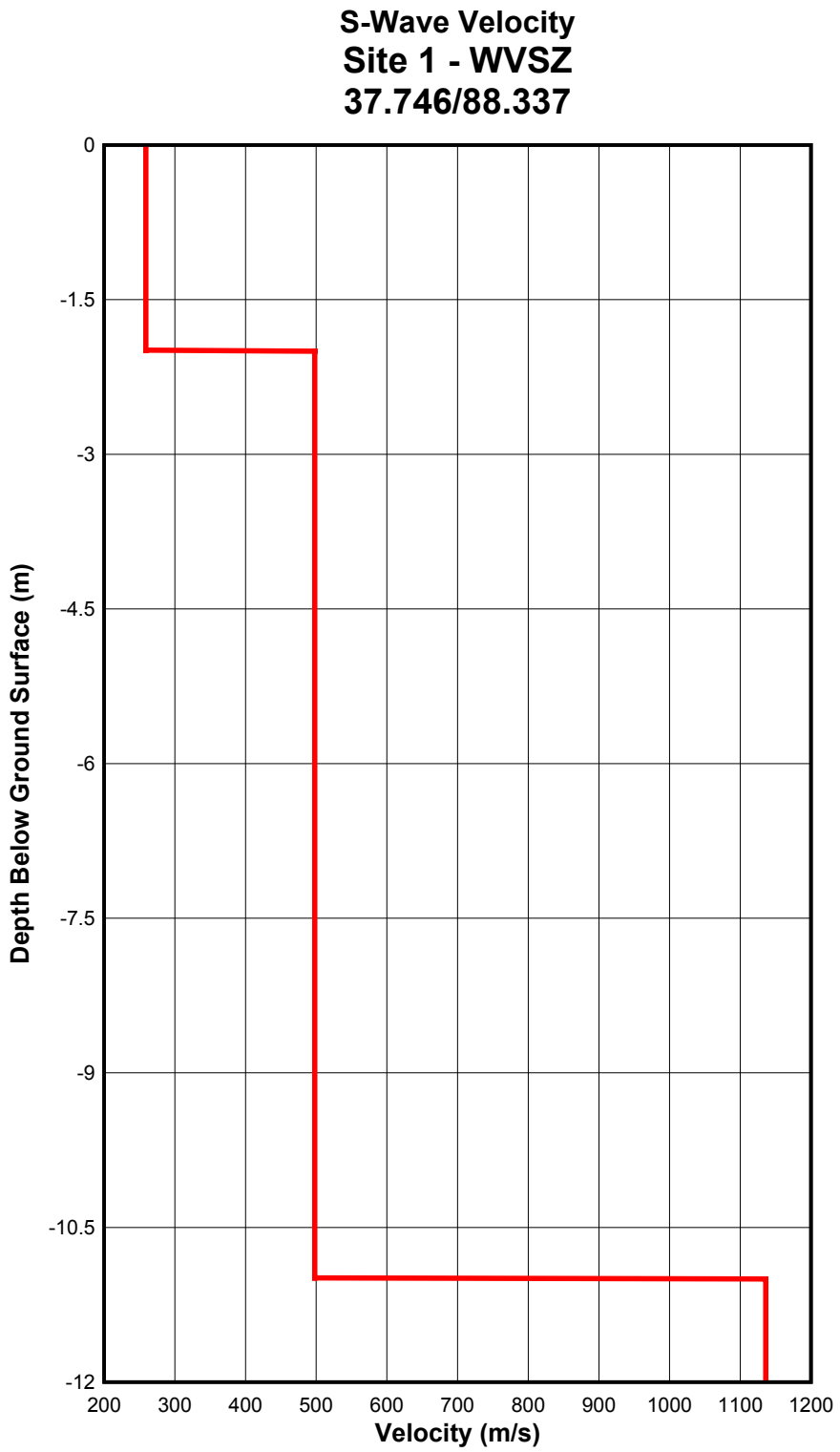
S-Wave Velocity
Site 1 - WVSZ
37.746/88.337
Depth Below Ground Surface (m)
0
-1.5
-3
-4.5
-6
-7.5
-9
-10.5
-12
200
300
400
500
600
700
800
900
1000
1100
1200
Velocity (m/s)

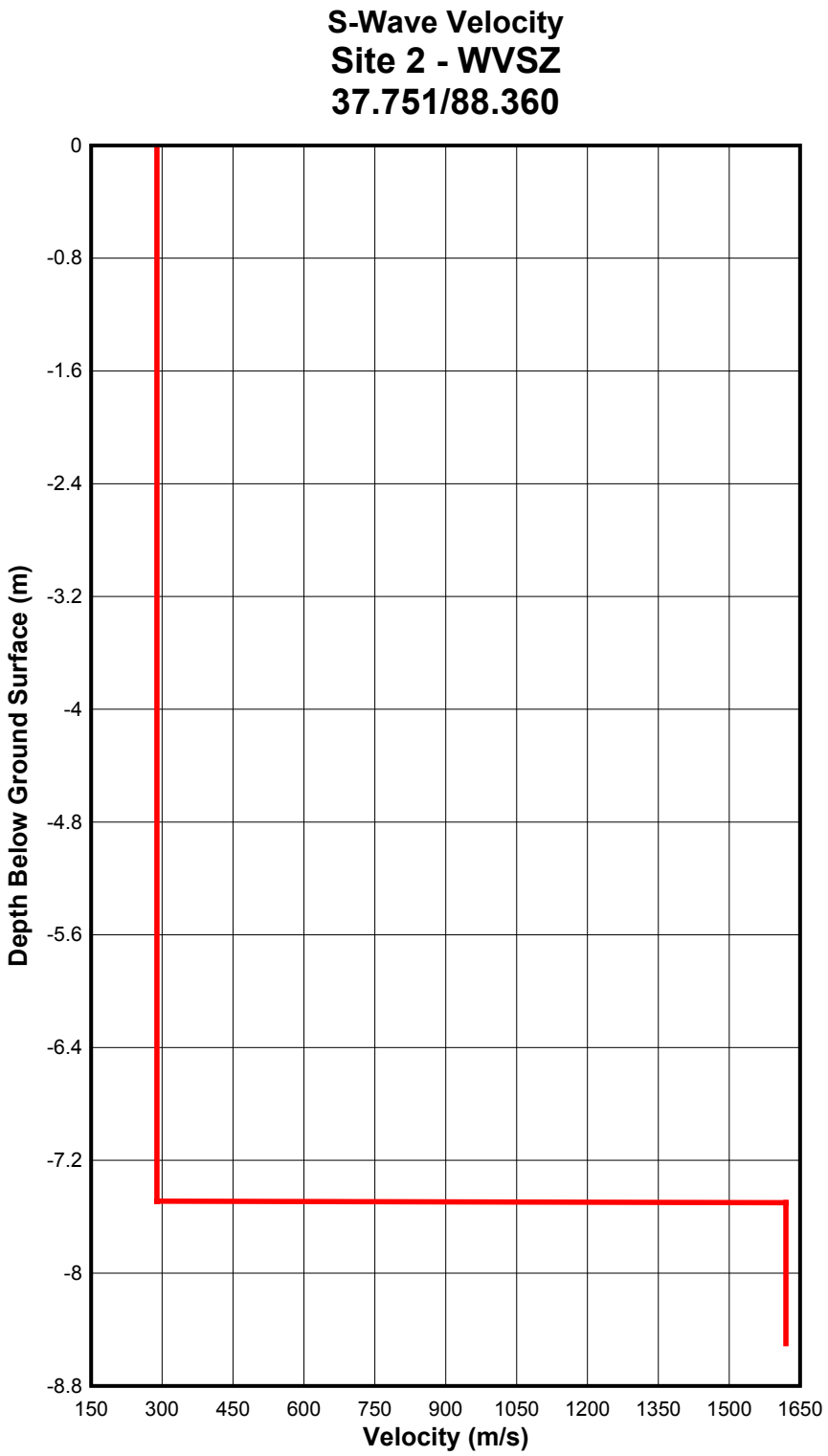
S-Wave Velocity
Site 2 - WVSZ
37.751/88.360
Depth Below Ground Surface (m)
0
-0.8
-1.6
-2.4
-3.2
-4
-4.8
-5.6
-6.4
-7.2
-8
-8.8
150
300
450
600
750
900
1050
1200
1350
1500
1650
Velocity (m/s)

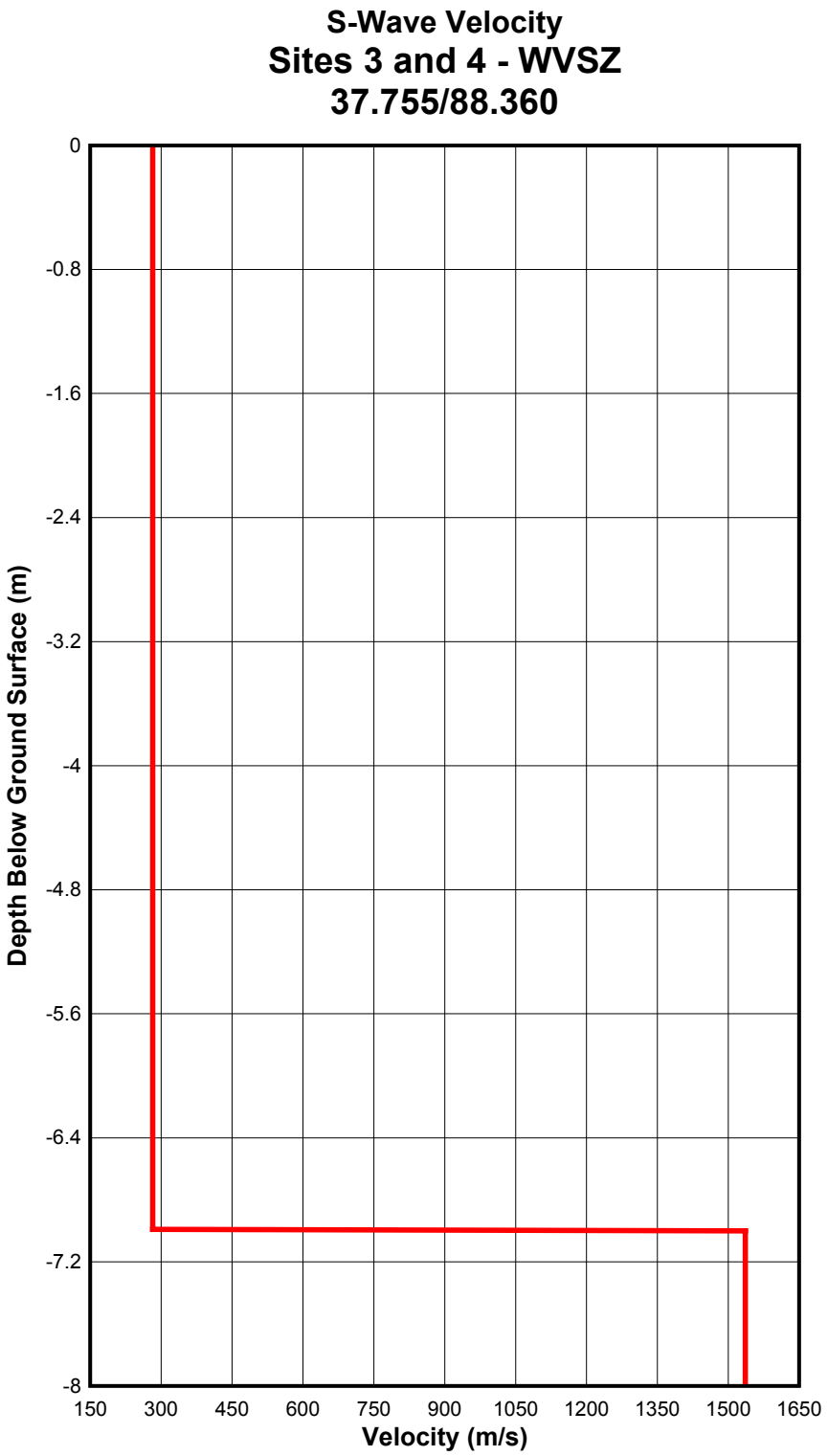
S-Wave Velocity
Sites 3 and 4 - WVSZ
37.755/88.360
Depth Below Ground Surface (m)
0
-0.8
-1.6
-2.4
-3.2
-4
-4.8
-5.6
-6.4
-7.2
-8
150
300
450
600
750
900
1050
1200
1350
1500
1650
Velocity (m/s)

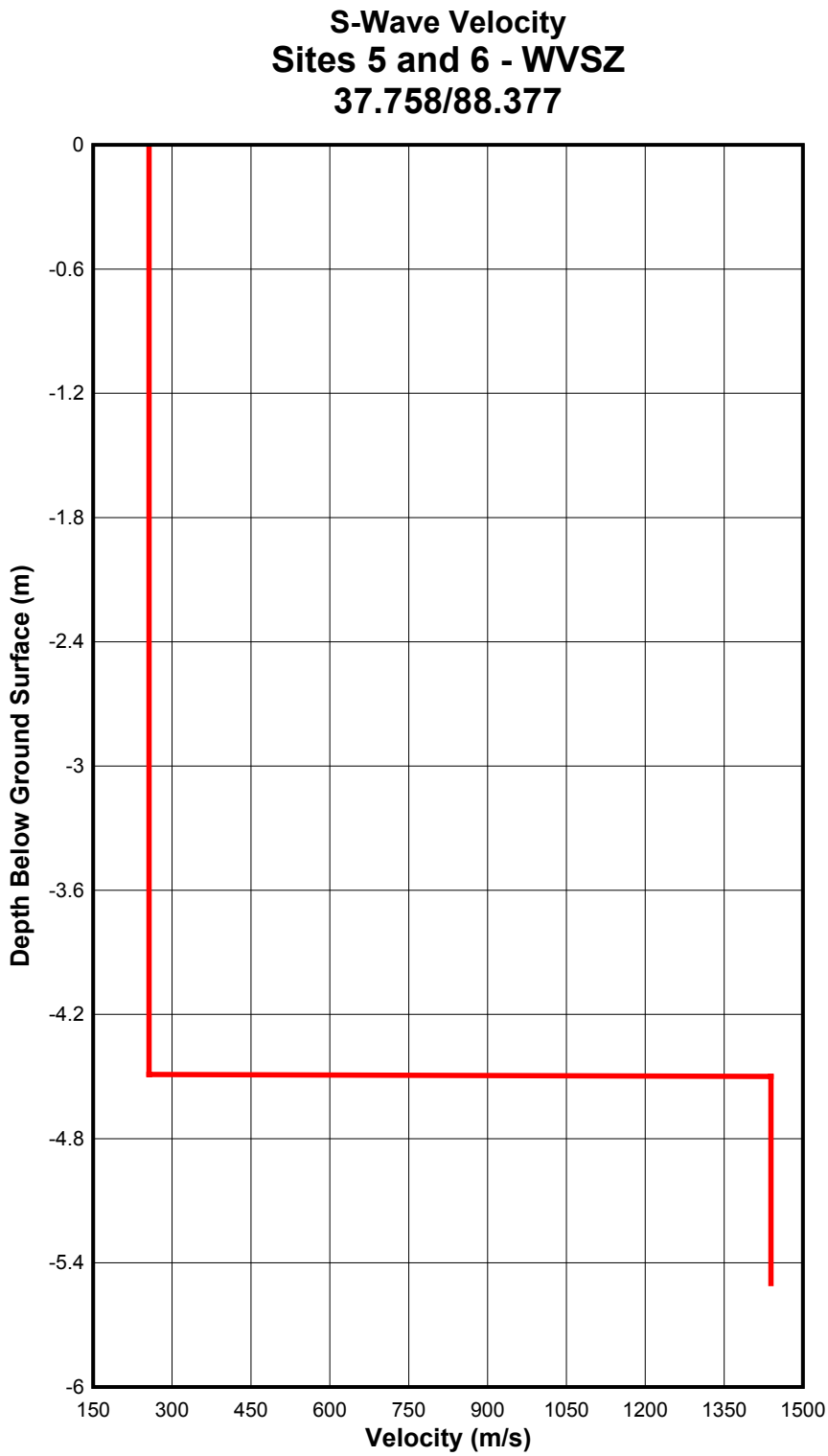
S-Wave Velocity
Sites 5 and 6 - WVSZ
37.758/88.377
Depth Below Ground Surface (m)
0
-0.6
-1.2
-1.8
-2.4
-3
-3.6
-4.2
-4.8
-5.4
-6
150
300
450
600
750
900
1050
1200
1350
1500
Velocity (m/s)

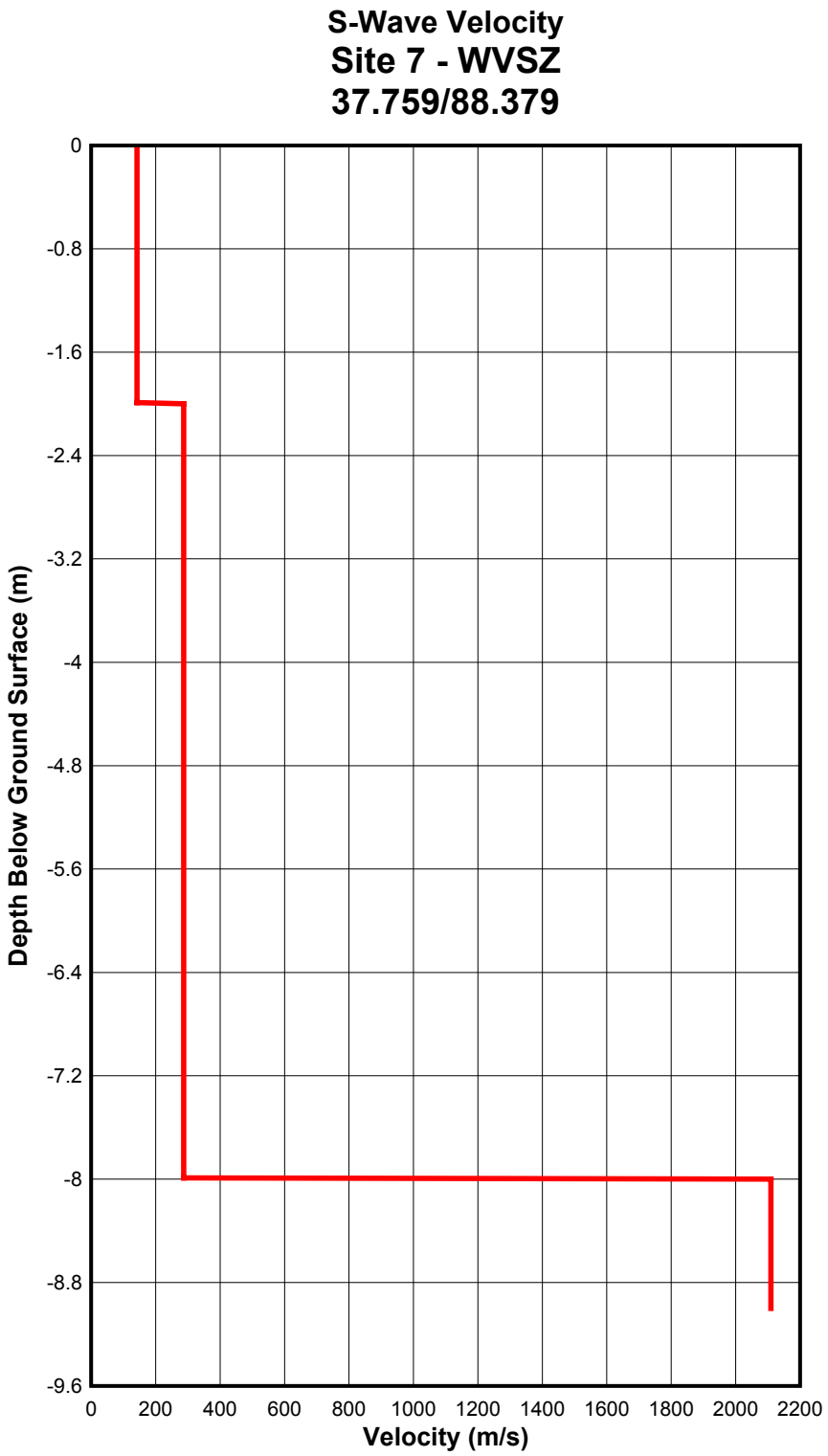
S-Wave Velocity
Site 7 - WVSZ
37.759/88.379
Depth Below Ground Surface (m)
0
-0.8
-1.6
-2.4
-3.2
-4
-4.8
-5.6
-6.4
-7.2
-8
-8.8
-9.6
0
200
400
600
800
1000
1200
1400
1600
1800
2000
2200
Velocity (m/s)

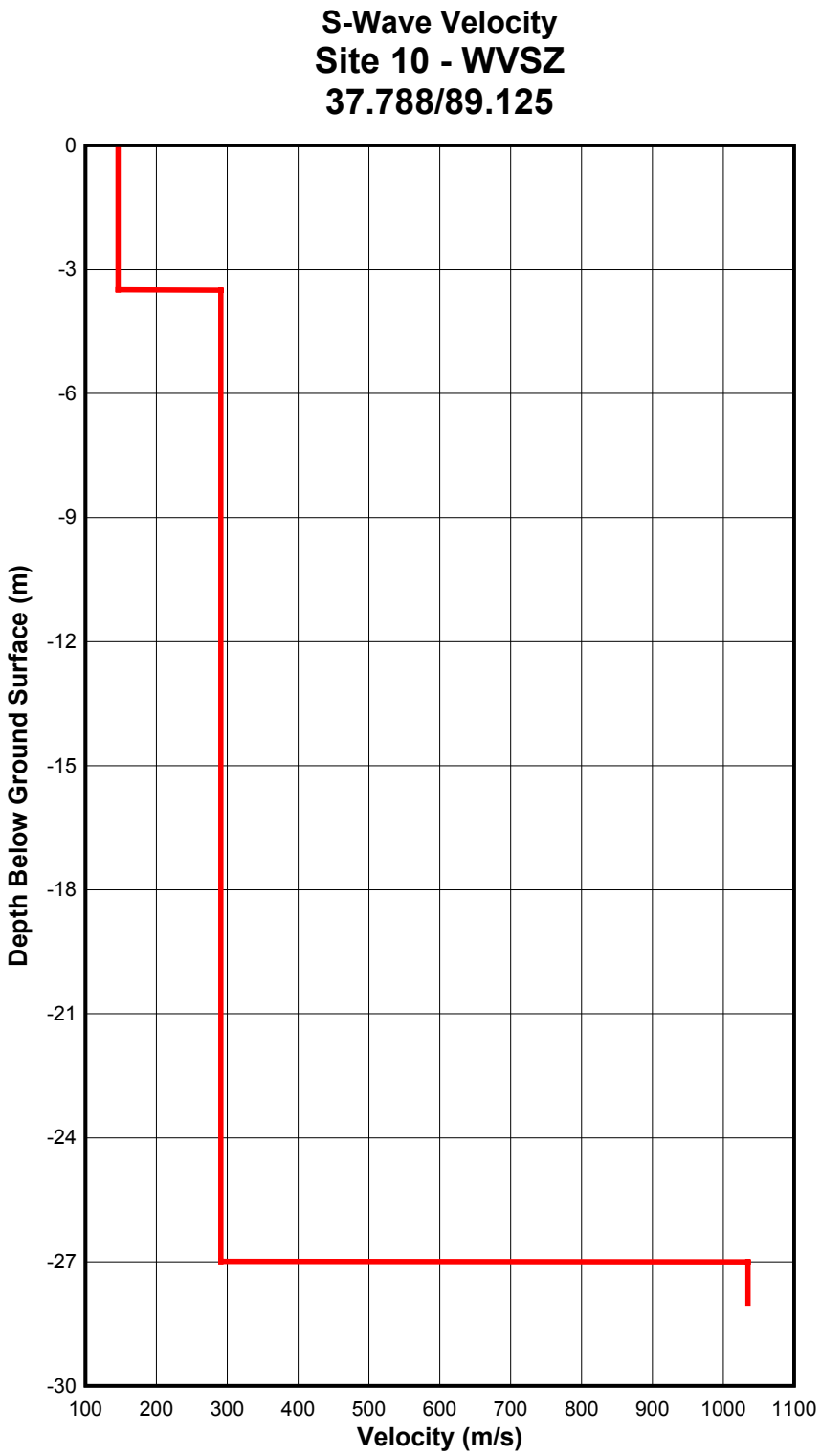
S-Wave Velocity
Site 10 - WVSZ
37.788/89.125
Depth Below Ground Surface (m)
0
-3
-6
-9
-12
-15
-18
-21
-24
-27
-30
100
200
300
400
500
600
700
800
900
1000
1100
Velocity (m/s)

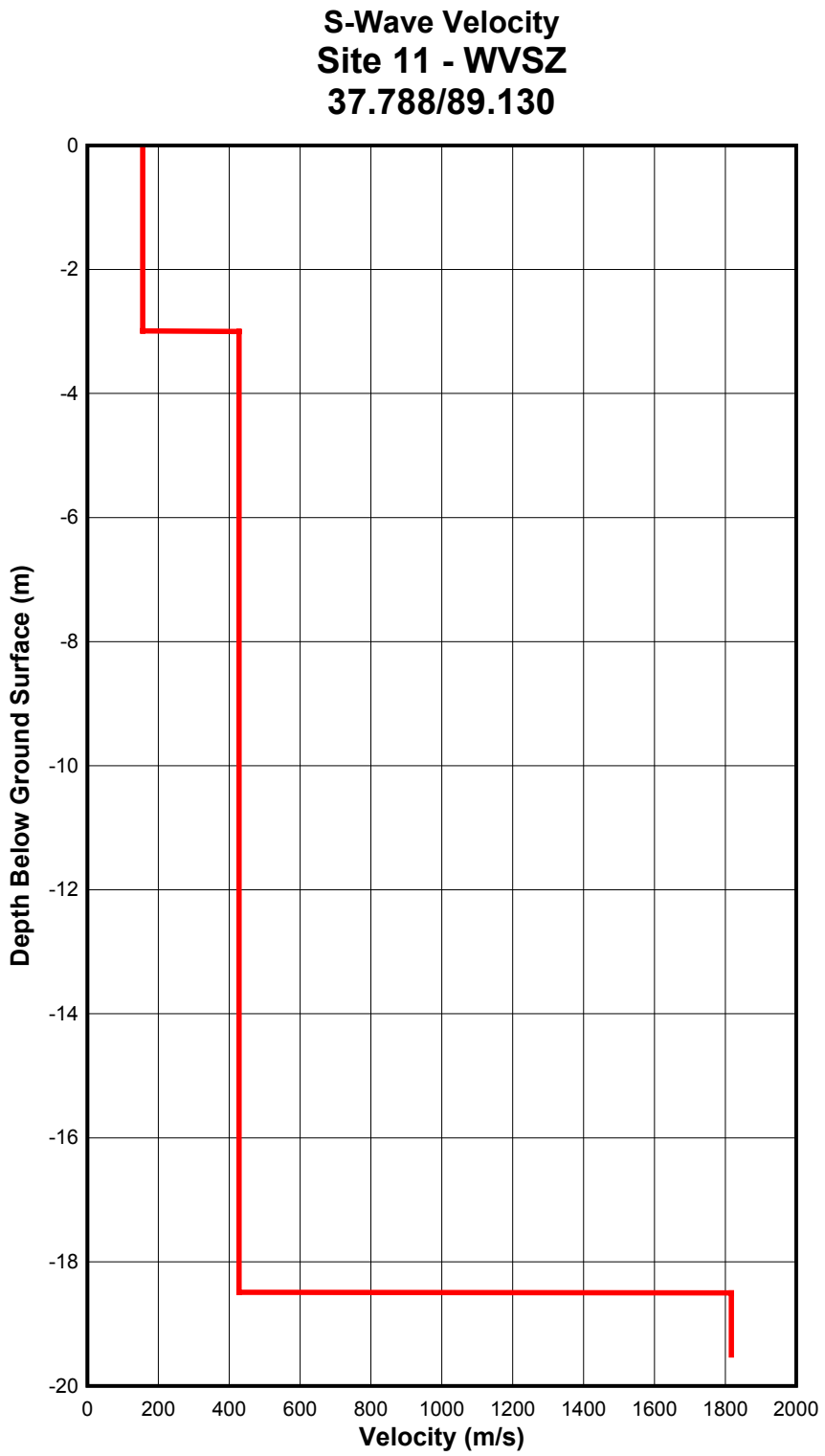
S-Wave Velocity
Site 11 - WVSZ
37.788/89.130
Depth Below Ground Surface (m)
0
-2
-4
-6
-8
-10
-12
-14
-16
-18
-20
0
200
400
600
800
1000
1200
1400
1600
1800
2000
Velocity (m/s)

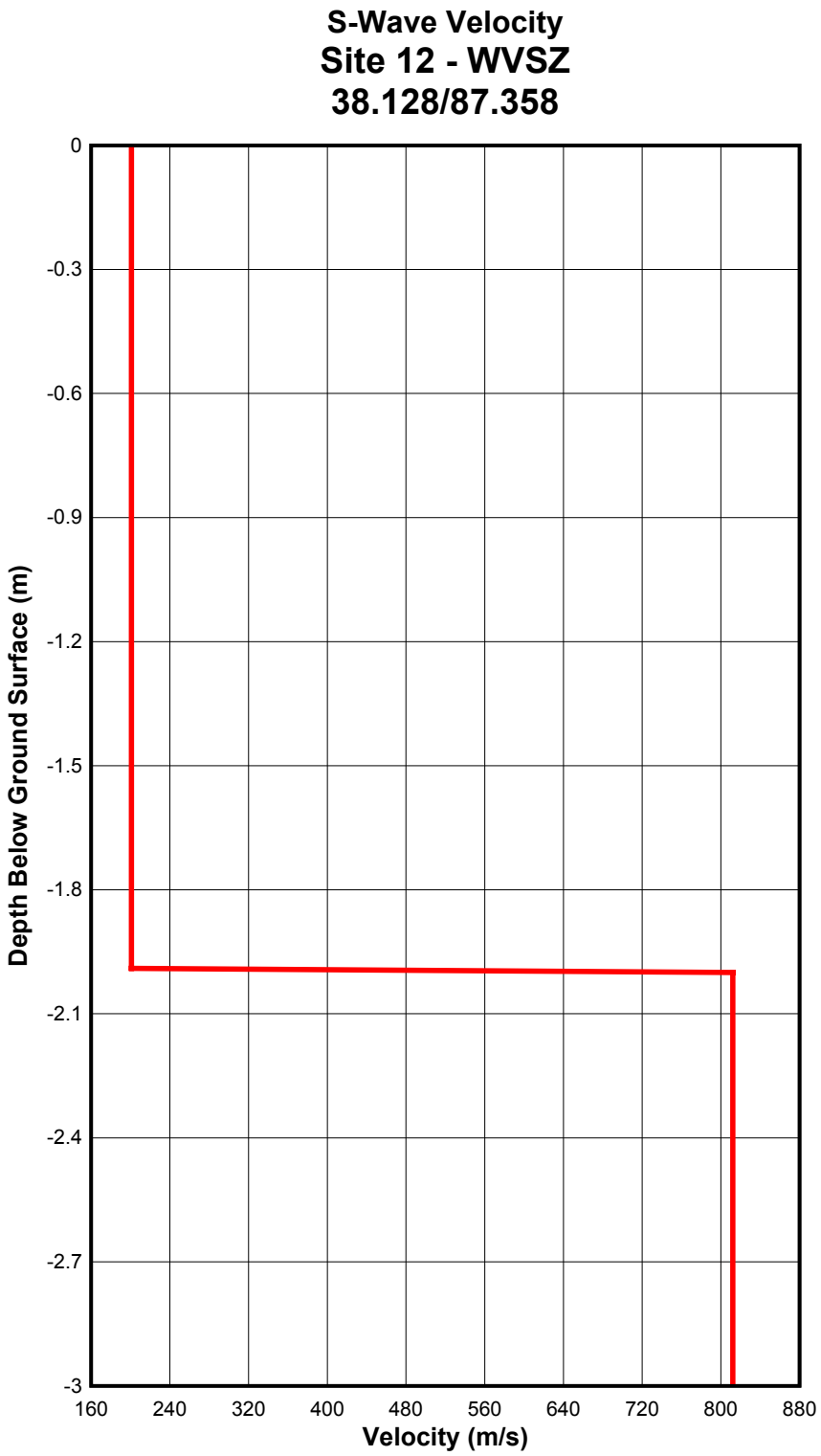
S-Wave Velocity
Site 12 - WVSZ
38.128/87.358
Depth Below Ground Surface (m)
0
-0.3
-0.6
-0.9
-1.2
-1.5
-1.8
-2.1
-2.4
-2.7
-3
160
240
320
400
480
560
640
720
800
880
Velocity (m/s)

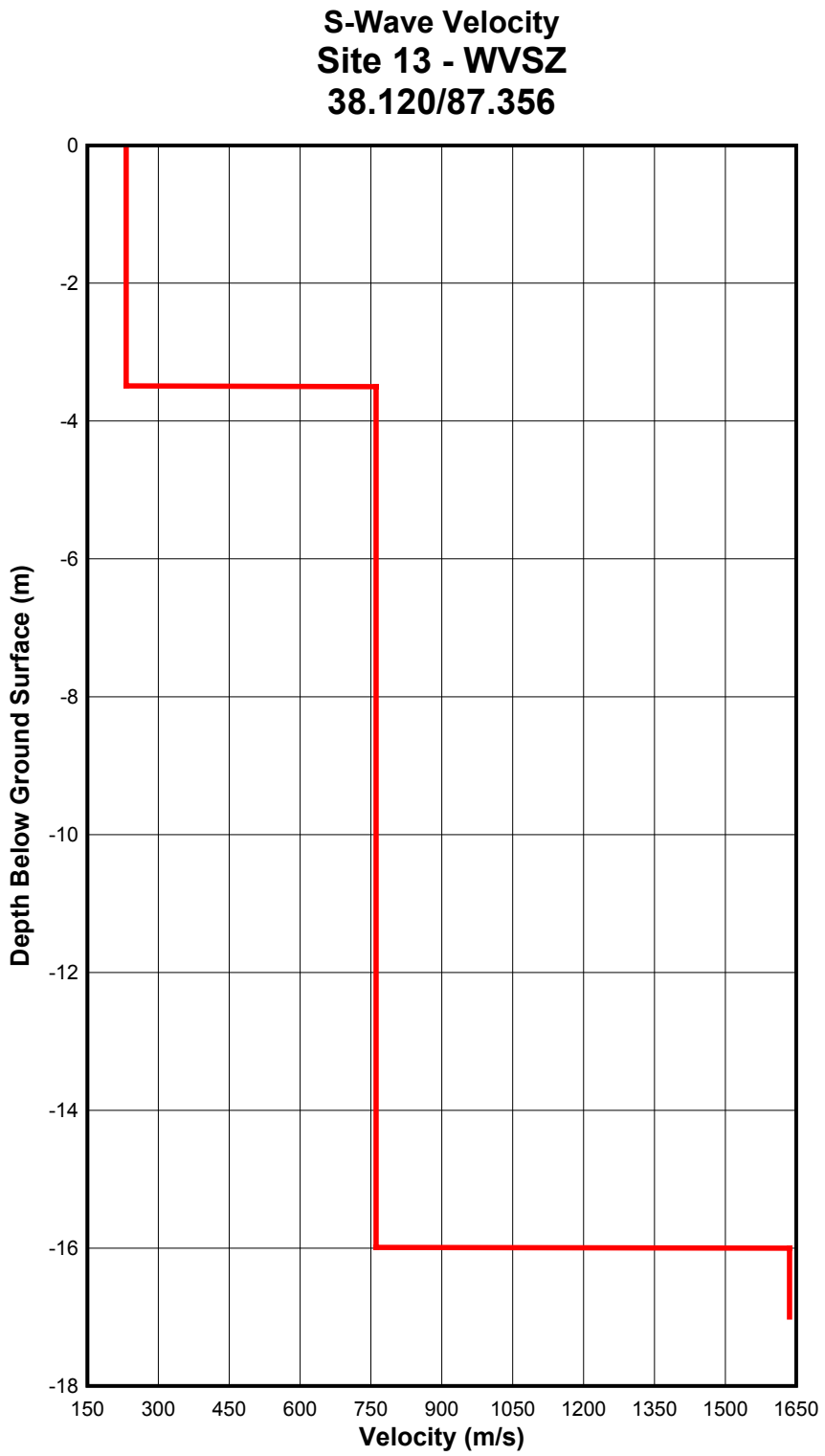
S-Wave Velocity
Site 13 - WVSZ
38.120/87.356
Depth Below Ground Surface (m)
0
-2
-4
-6
-8
-10
-12
-14
-16
-18
150
300
450
600
750
900
1050
1200
1350
1500
1650
Velocity (m/s)

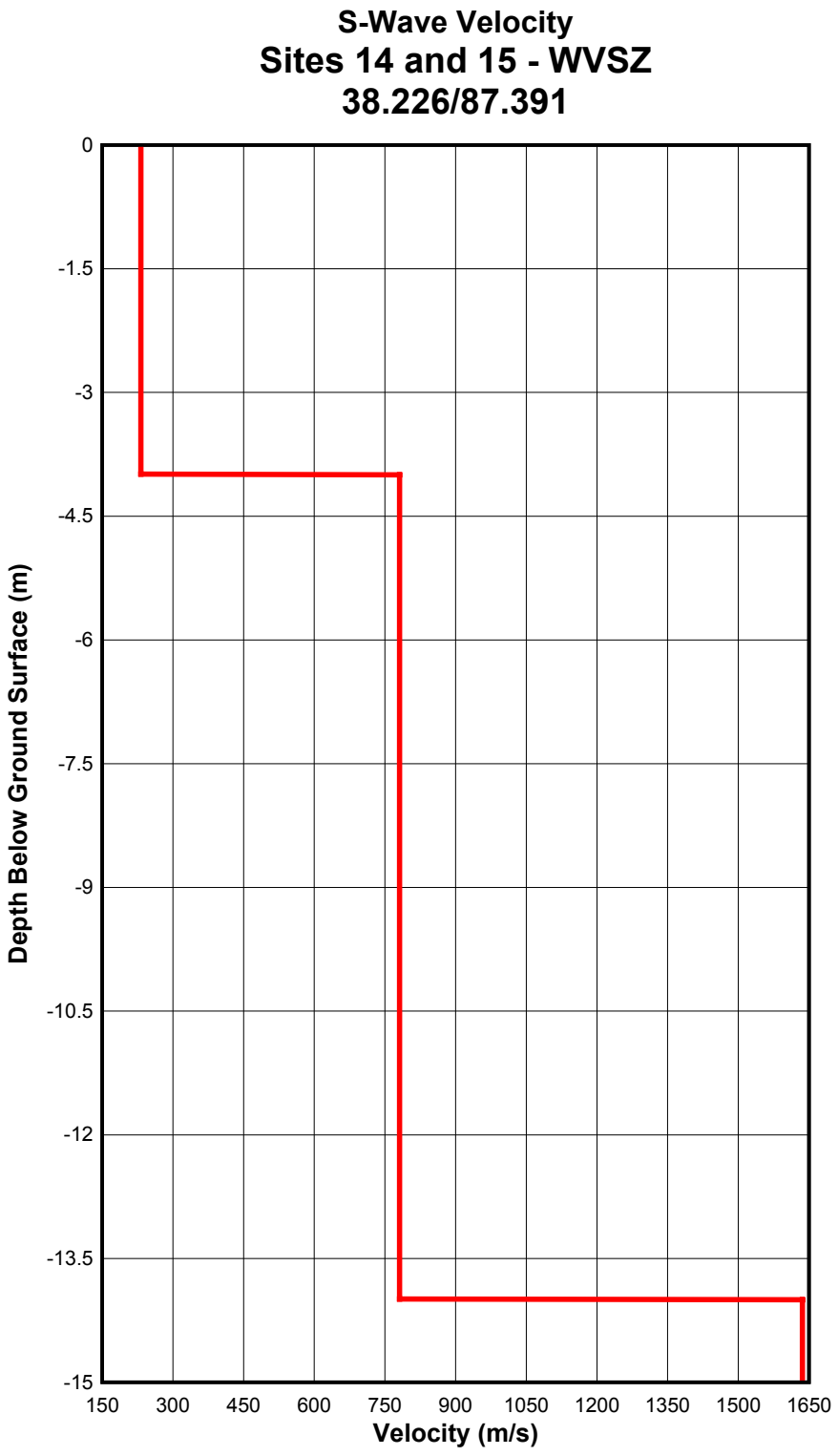
S-Wave Velocity
Sites 14 and 15 - WVSZ
38.226/87.391
Depth Below Ground Surface (m)
0
-1.5
-3
-4.5
-6
-7.5
-9
-10.5
-12
-13.5
-15
150
300
450
600
750
900
1050
1200
1350
1500
1650
Velocity (m/s)

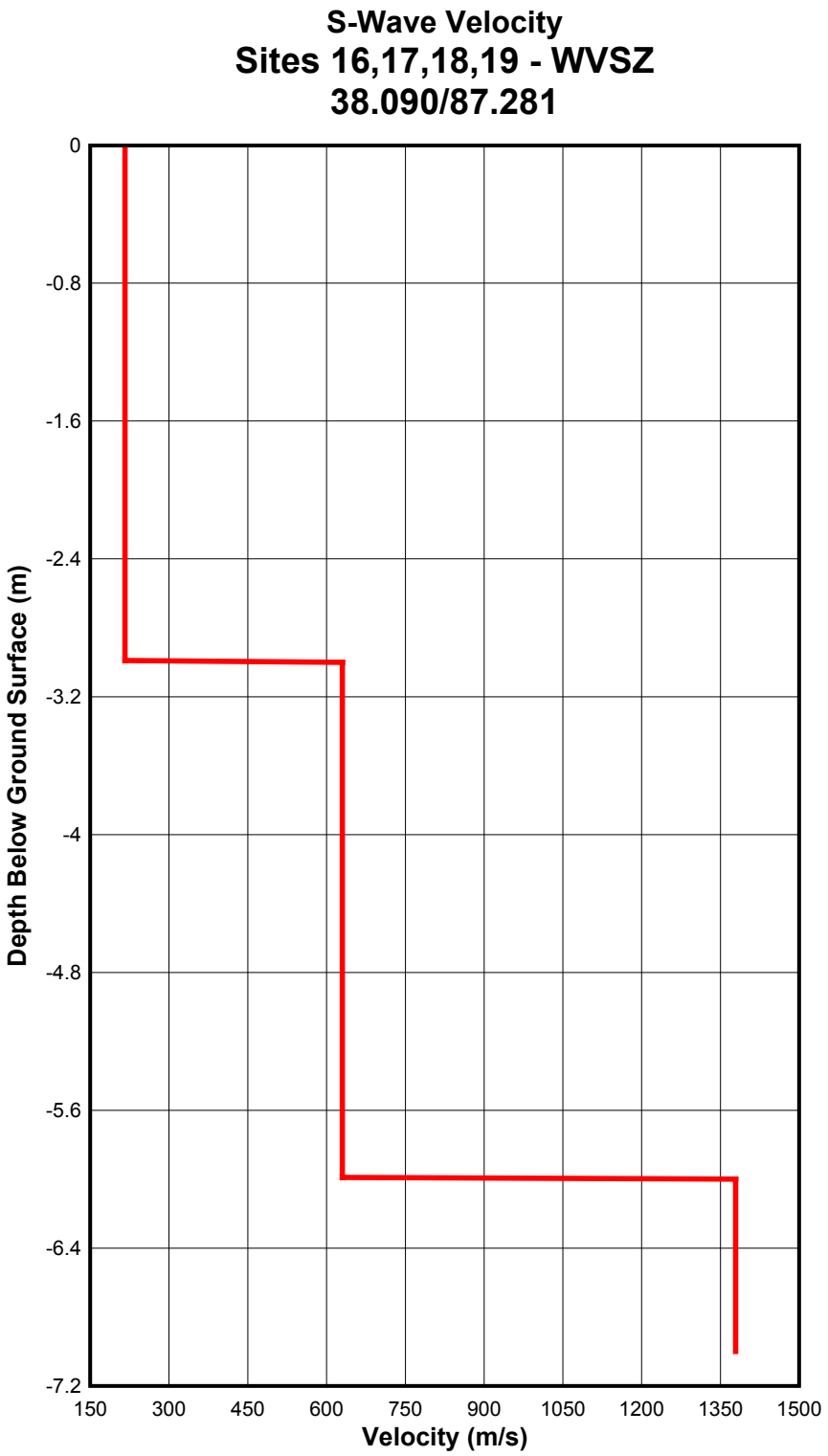
S-Wave Velocity
Sites 16,17,18,19 - WVSZ
38.090/87.281
Depth Below Ground Surface (m)
0
-0.8
-1.6
-2.4
-3.2
-4
-4.8
-5.6
-6.4
-7.2
150
300
450
600
750
900
1050
1200
1350
1500
Velocity (m/s)

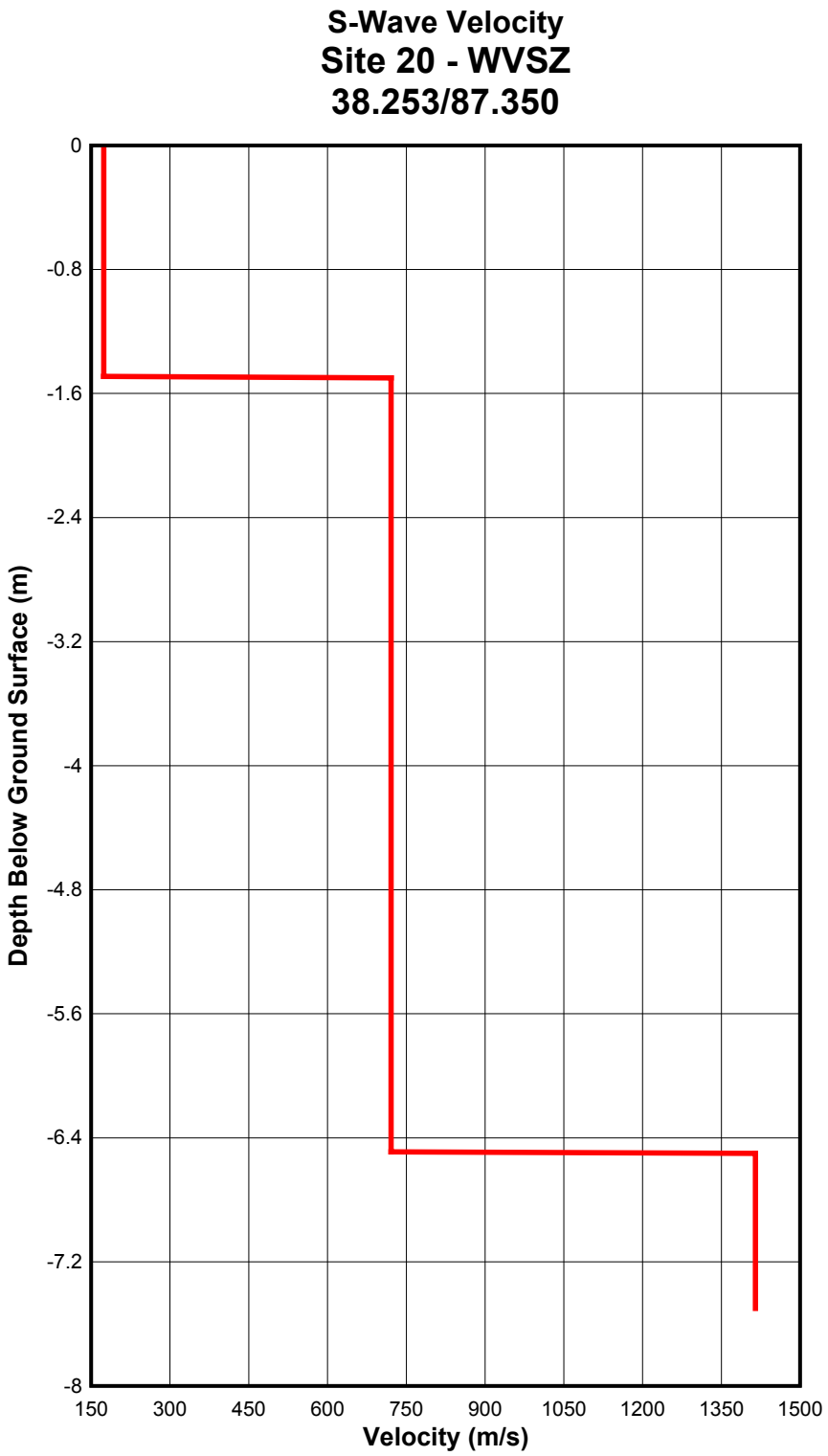
S-Wave Velocity
Site 20 - WVSZ
38.253/87.350
Depth Below Ground Surface (m)
0
-0.8
-1.6
-2.4
-3.2
-4
-4.8
-5.6
-6.4
-7.2
-8
150
300
450
600
750
900
1050
1200
1350
1500
Velocity (m/s)

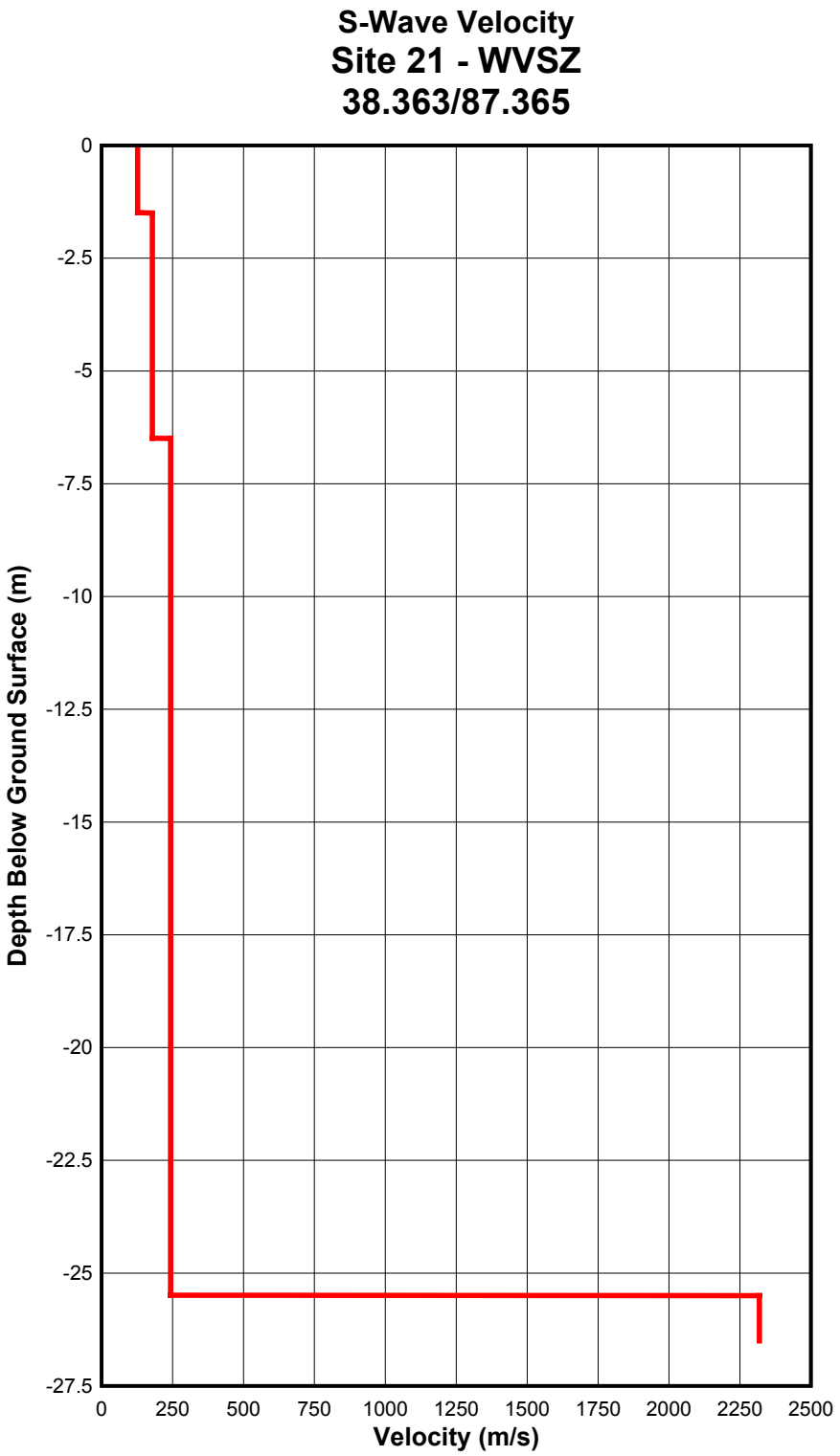
S-Wave Velocity
Site 21 - WVSZ
38.363/87.365
Depth Below Ground Surface (m)
0
-2.5
-5
-7.5
-10
-12.5
-15
-17.5
-20
-22.5
-25
-27.5
0
250
500
750
1000
1250
1500
1750
2000
2250
2500
Velocity (m/s)

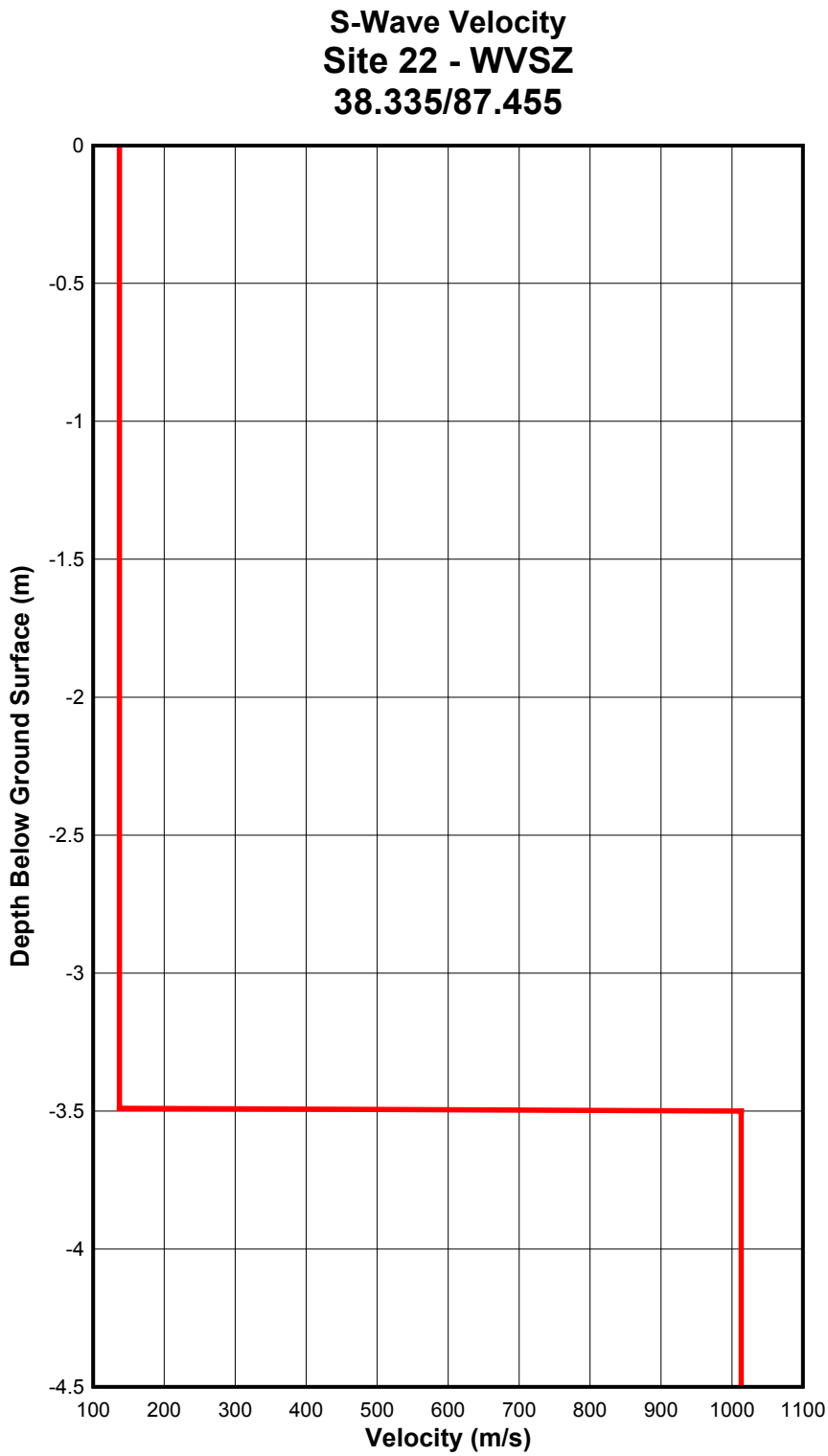
S-Wave Velocity
Site 22 - WVSZ
38.335/87.455
Depth Below Ground Surface (m)
0
-0.5
-1
-1.5
-2
-2.5
-3
-3.5
-4
-4.5
100
200
300
400
500
600
700
800
900
1000
1100
Velocity (m/s)

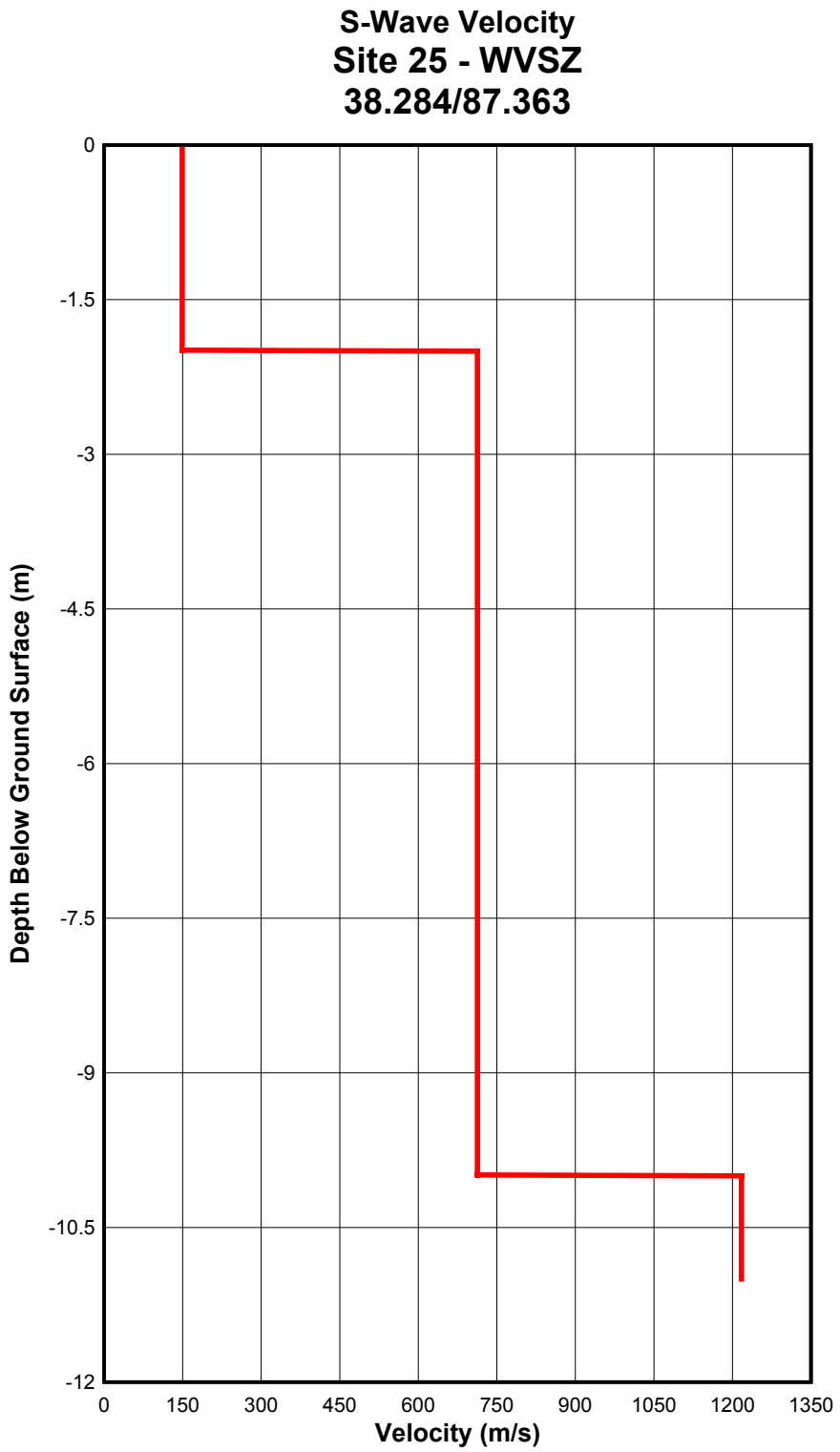
S-Wave Velocity
Site 25 - WVSZ
38.284/87.363
Depth Below Ground Surface (m)
0
-1.5
-3
-4.5
-6
-7.5
-9
-10.5
-12
0
150
300
450
600
750
900
1050
1200
1350
Velocity (m/s)

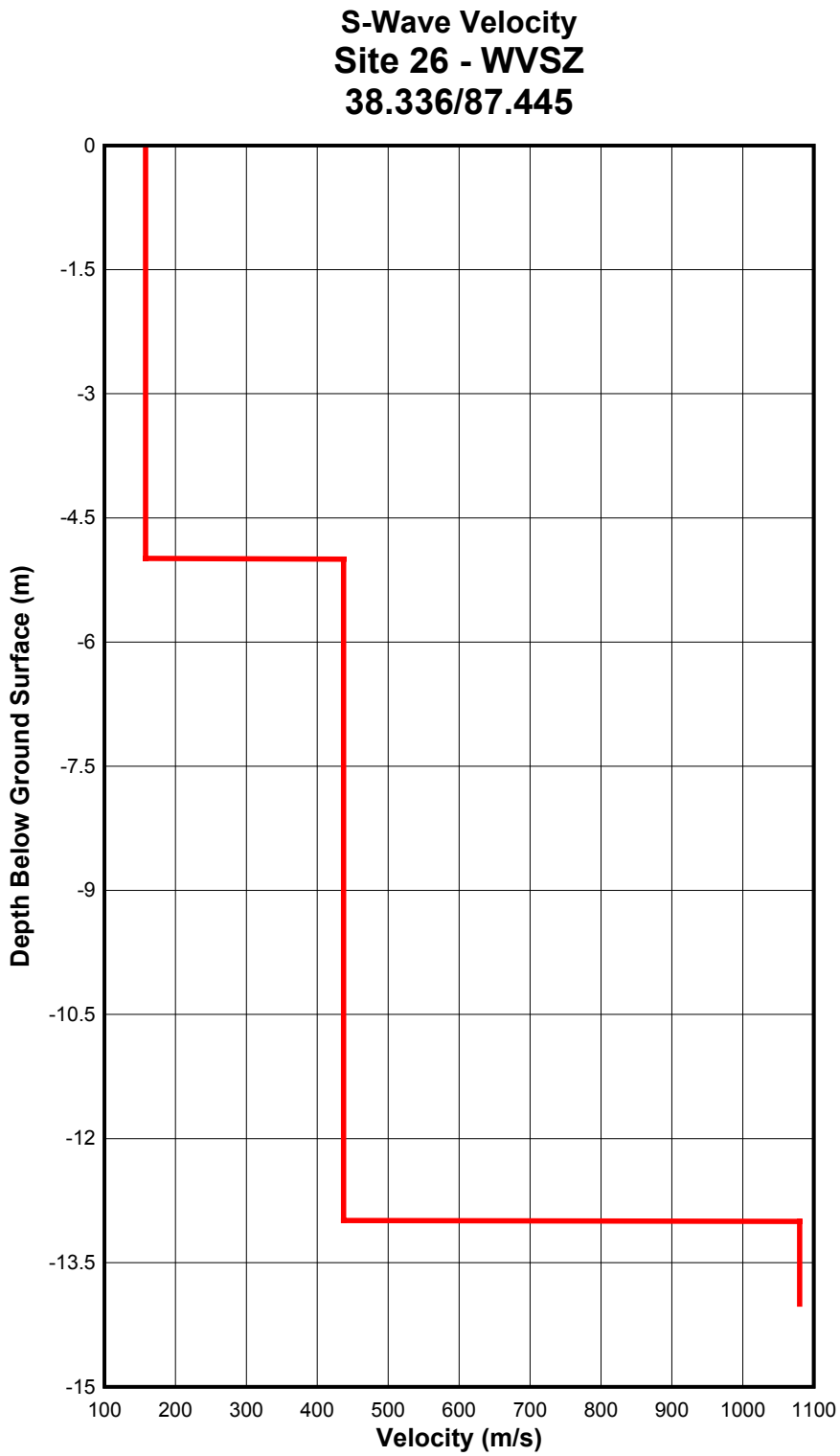
S-Wave Velocity
Site 26 - WVSZ
38.336/87.445
Depth Below Ground Surface (m)
0
-1.5
-3
-4.5
-6
-7.5
-9
-10.5
-12
-13.5
-15
100
200
300
400
500
600
700
800
900
1000
1100
Velocity (m/s)

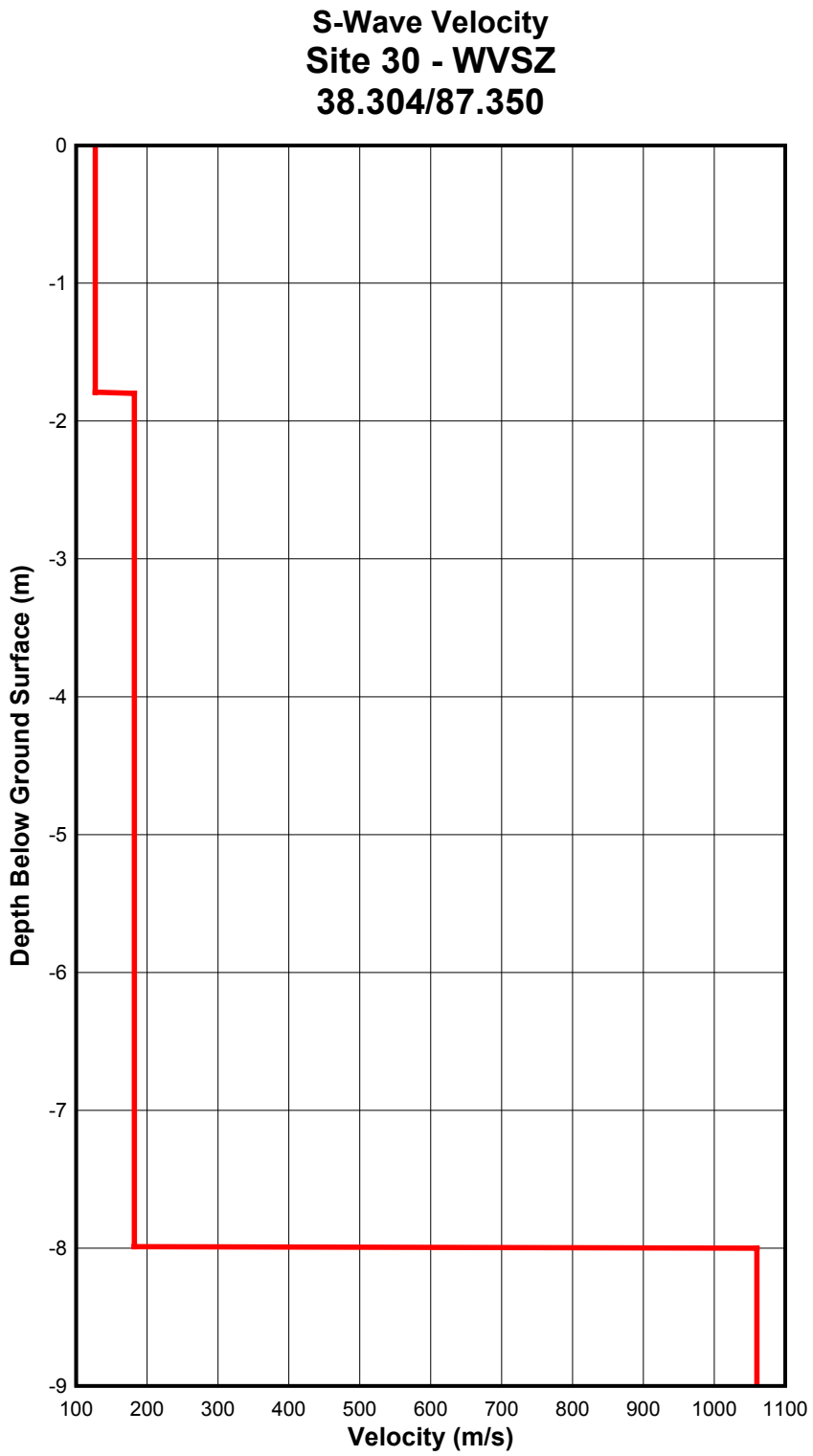
S-Wave Velocity
Site 30 - WVSZ
38.304/87.350
Depth Below Ground Surface (m)
0
-1
-2
-3
-4
-5
-6
-7
-8
-9
100
200
300
400
500
600
700
800
900
1000
1100
Velocity (m/s)

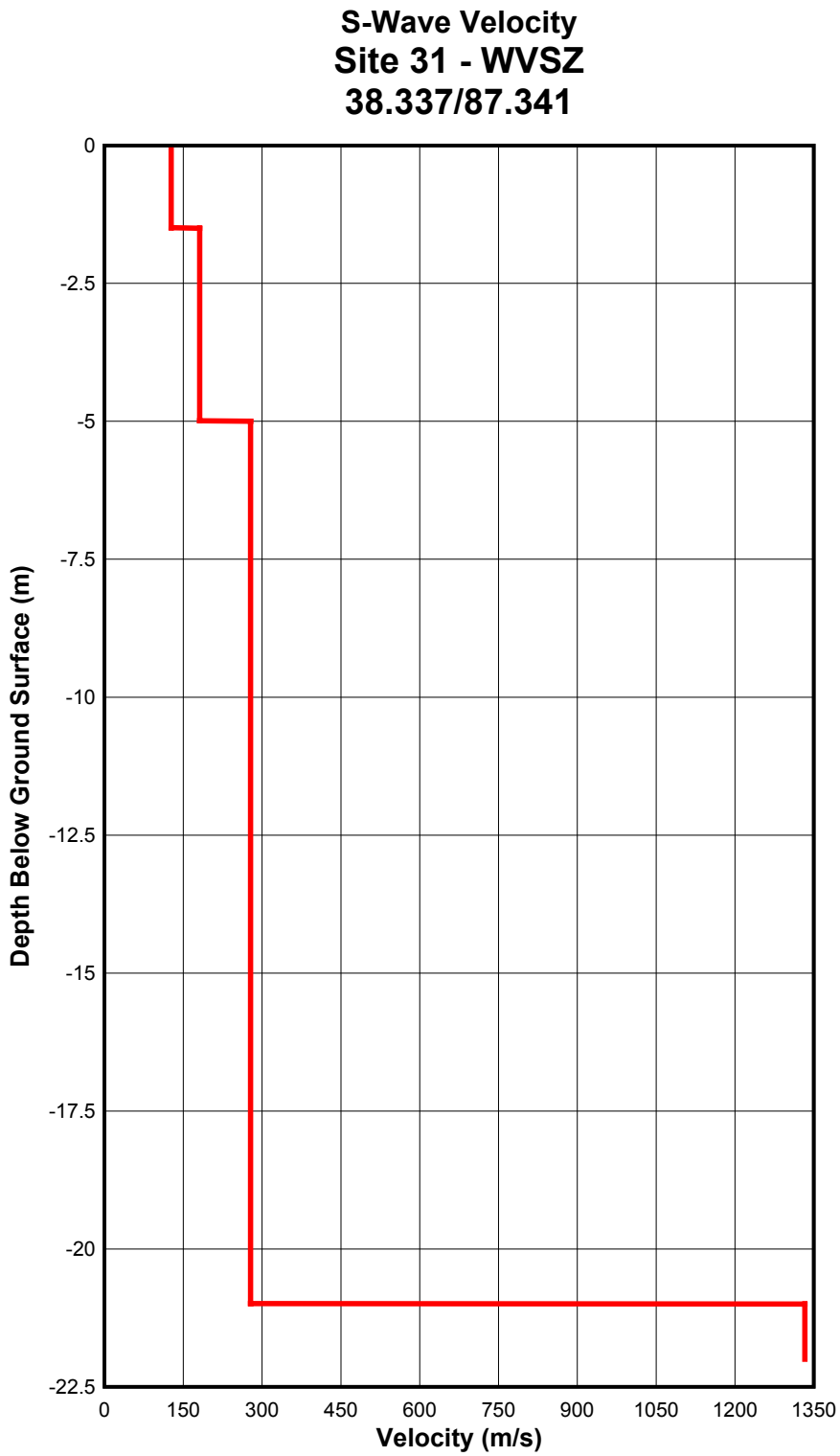
S-Wave Velocity
Site 31 - WVSZ
38.337/87.341
Depth Below Ground Surface (m)
0
-2.5
-5
-7.5
-10
-12.5
-15
-17.5
-20
-22.5
0
150
300
450
600
750
900
1050
1200
1350
Velocity (m/s)

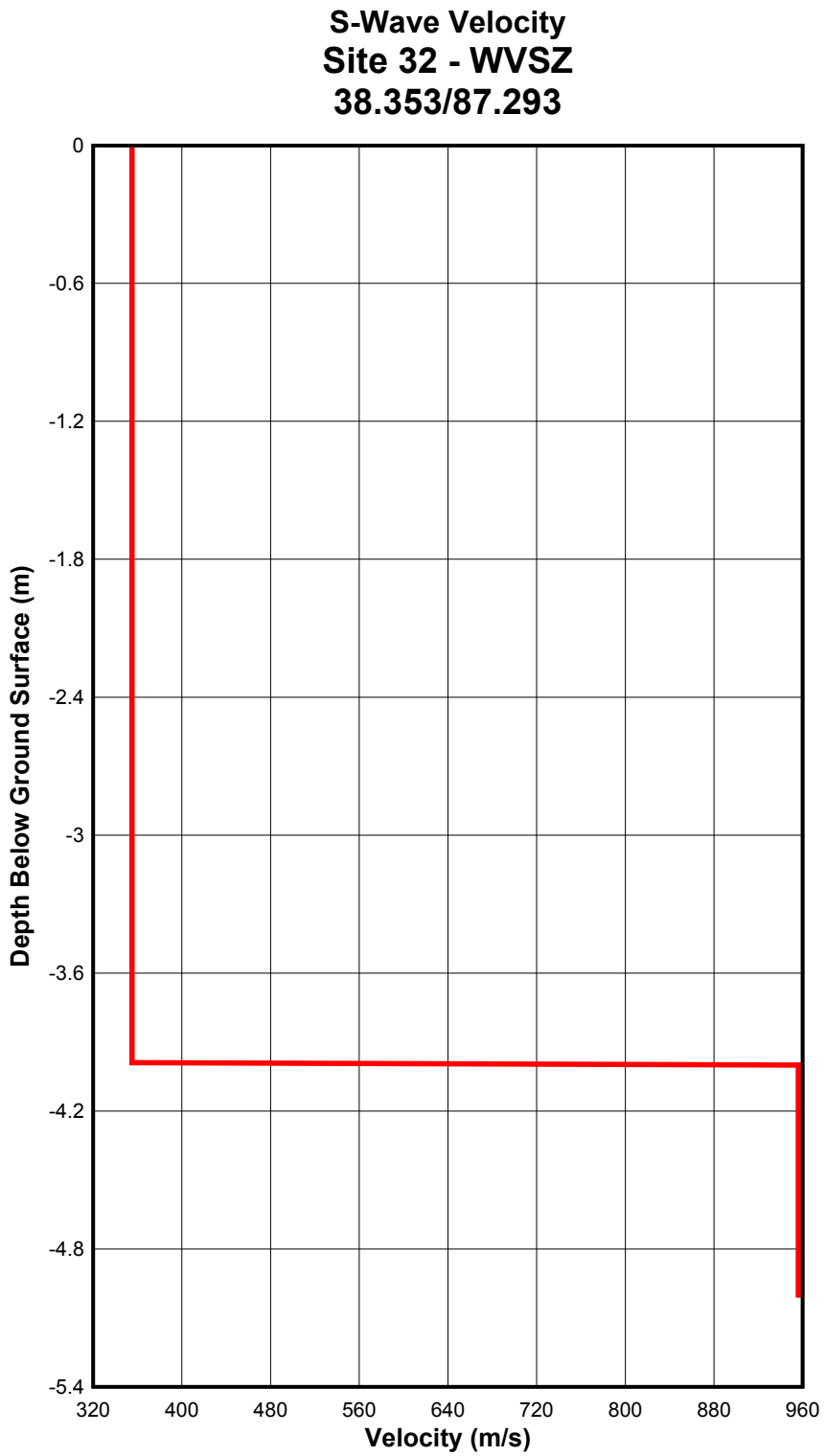
S-Wave Velocity
Site 32 - WVSZ
38.353/87.293
Depth Below Ground Surface (m)
0
-0.6
-1.2
-1.8
-2.4
-3
-3.6
-4.2
-4.8
-5.4
320
400
480
560
640
720
800
880
960
Velocity (m/s)

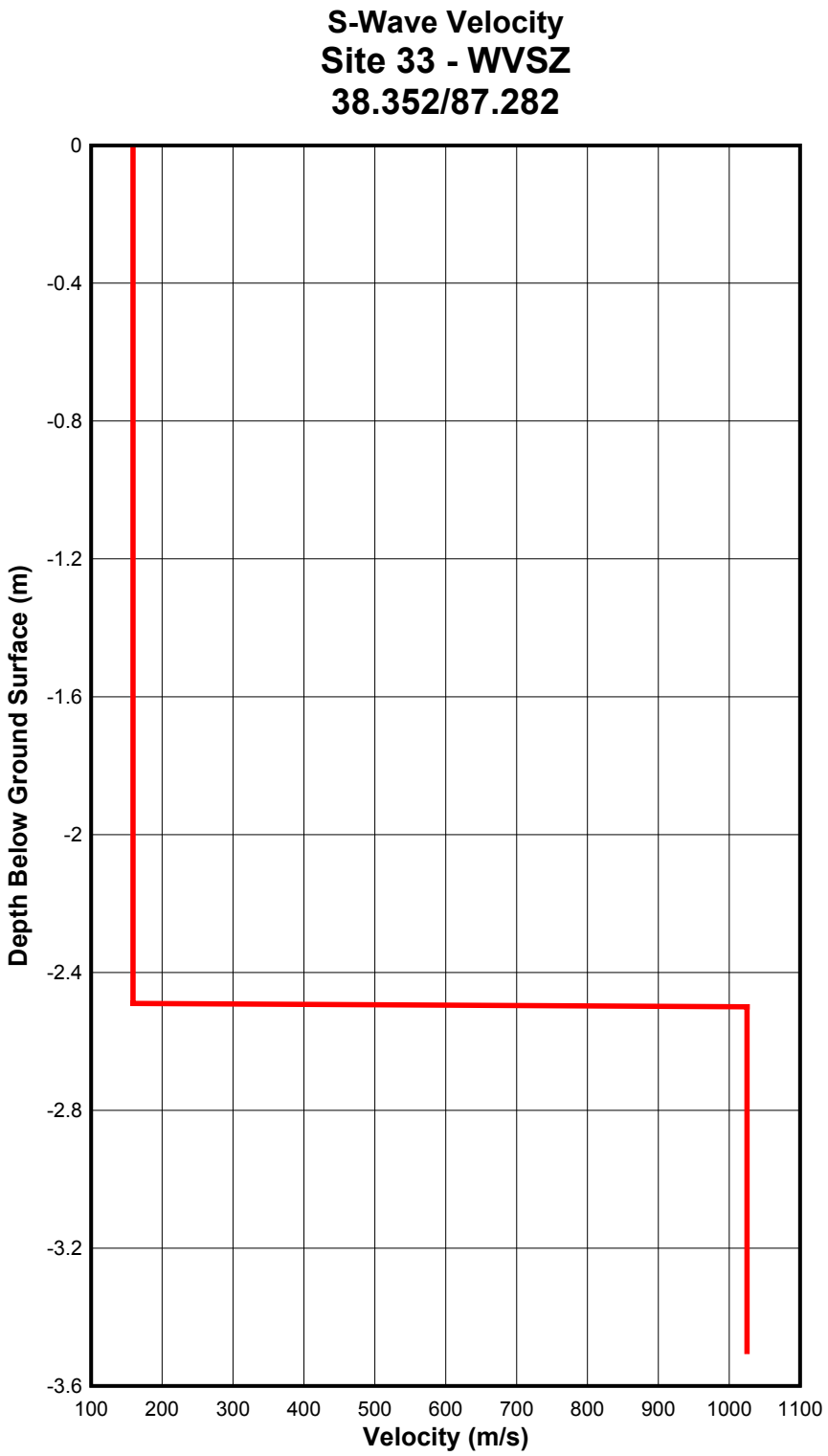
S-Wave Velocity
Site 33 - WVSZ
38.352/87.282
Depth Below Ground Surface (m)
0
-0.4
-0.8
-1.2
-1.6
-2
-2.4
-2.8
-3.2
-3.6
100
200
300
400
500
600
700
800
900
1000
1100
Velocity (m/s)

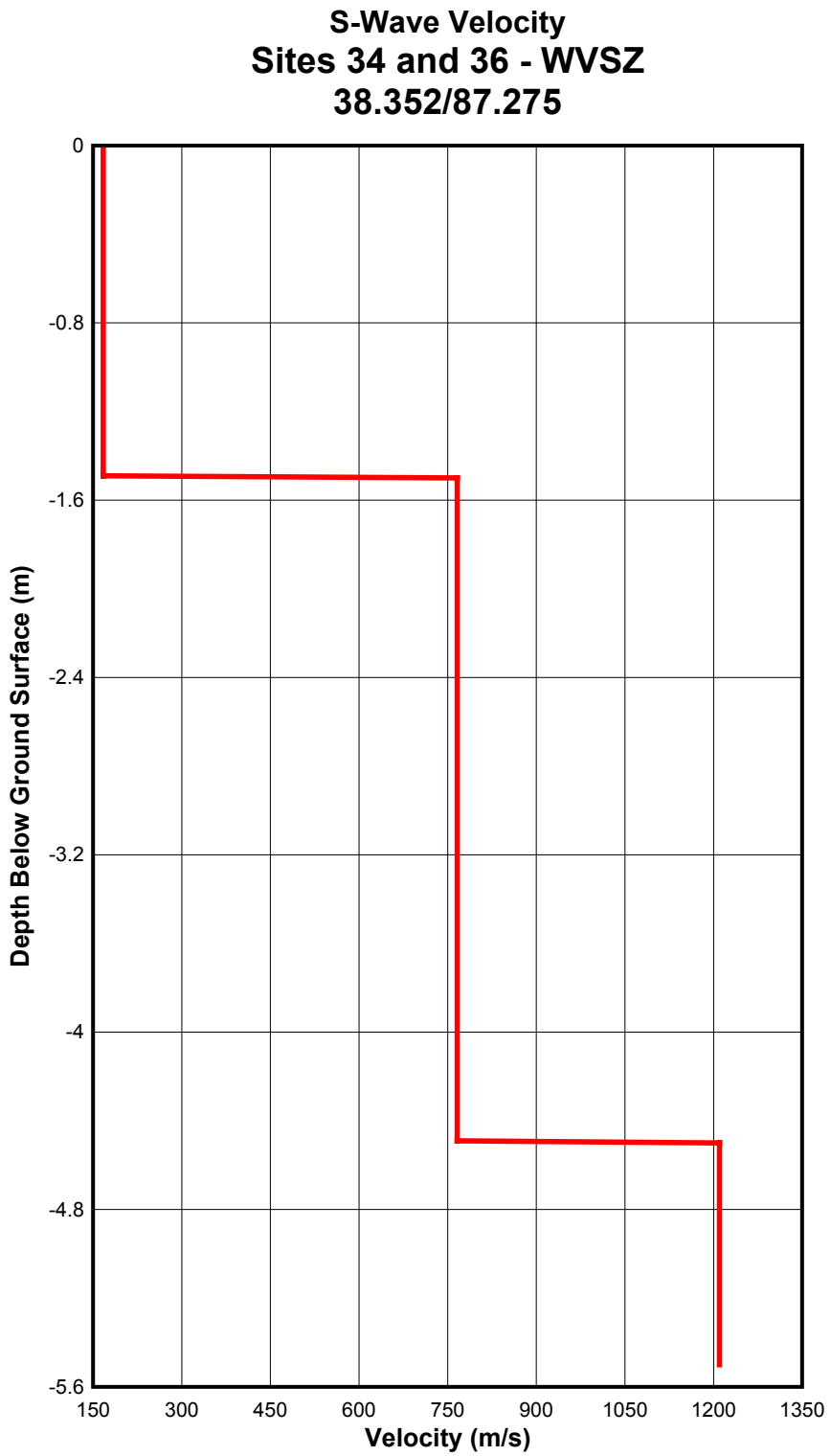
S-Wave Velocity
Sites 34 and 36 - WVSZ
38.352/87.275
Depth Below Ground Surface (m)
0
-0.8
-1.6
-2.4
-3.2
-4
-4.8
-5.6
150
300
450
600
750
900
1050
1200
1350
Velocity (m/s)

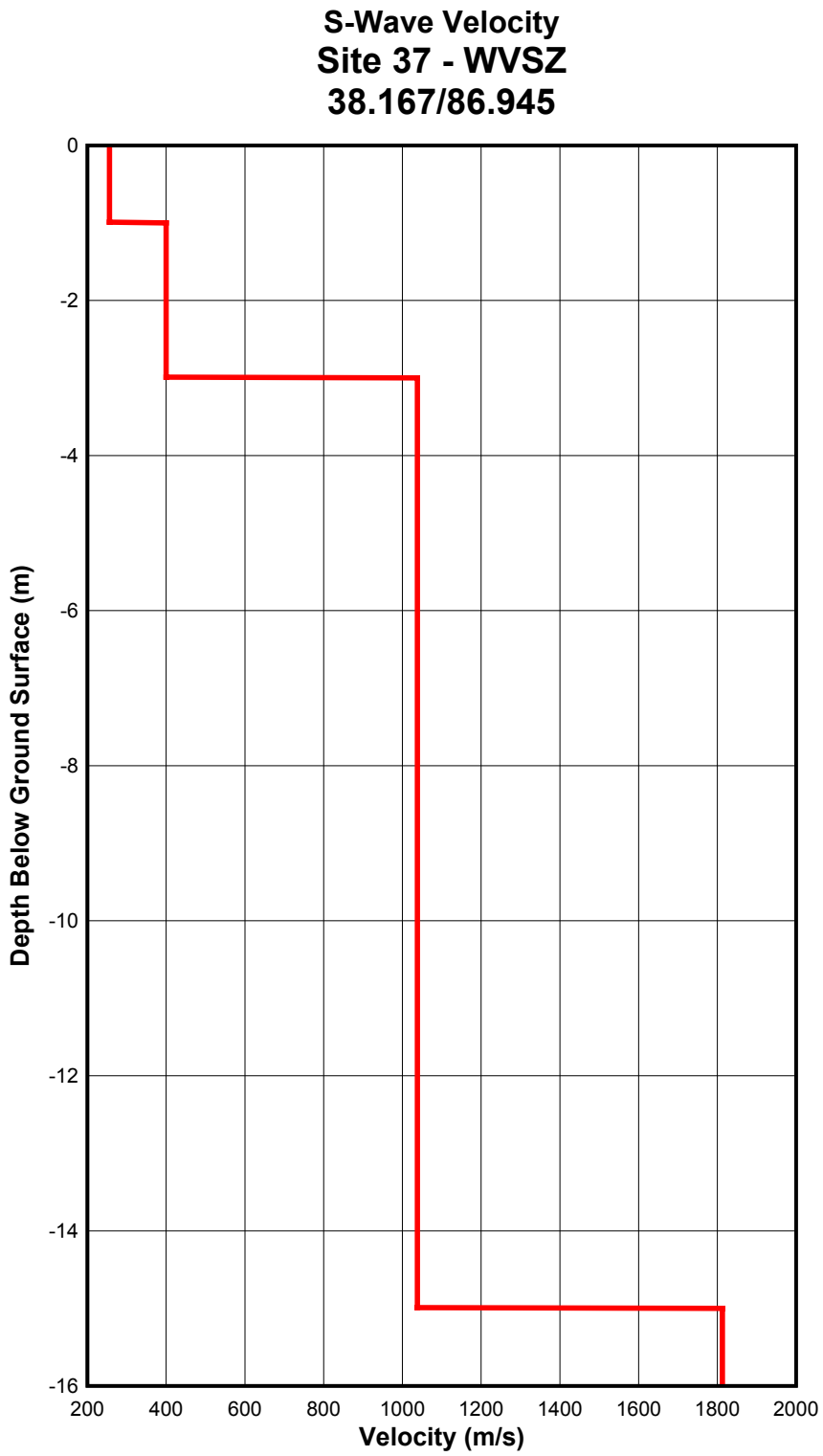
S-Wave Velocity
Site 37 - WVSZ
38.167/86.945
Depth Below Ground Surface (m)
0
-2
-4
-6
-8
-10
-12
-14
-16
200
400
600
800
1000
1200
1400
1600
1800
2000
Velocity (m/s)

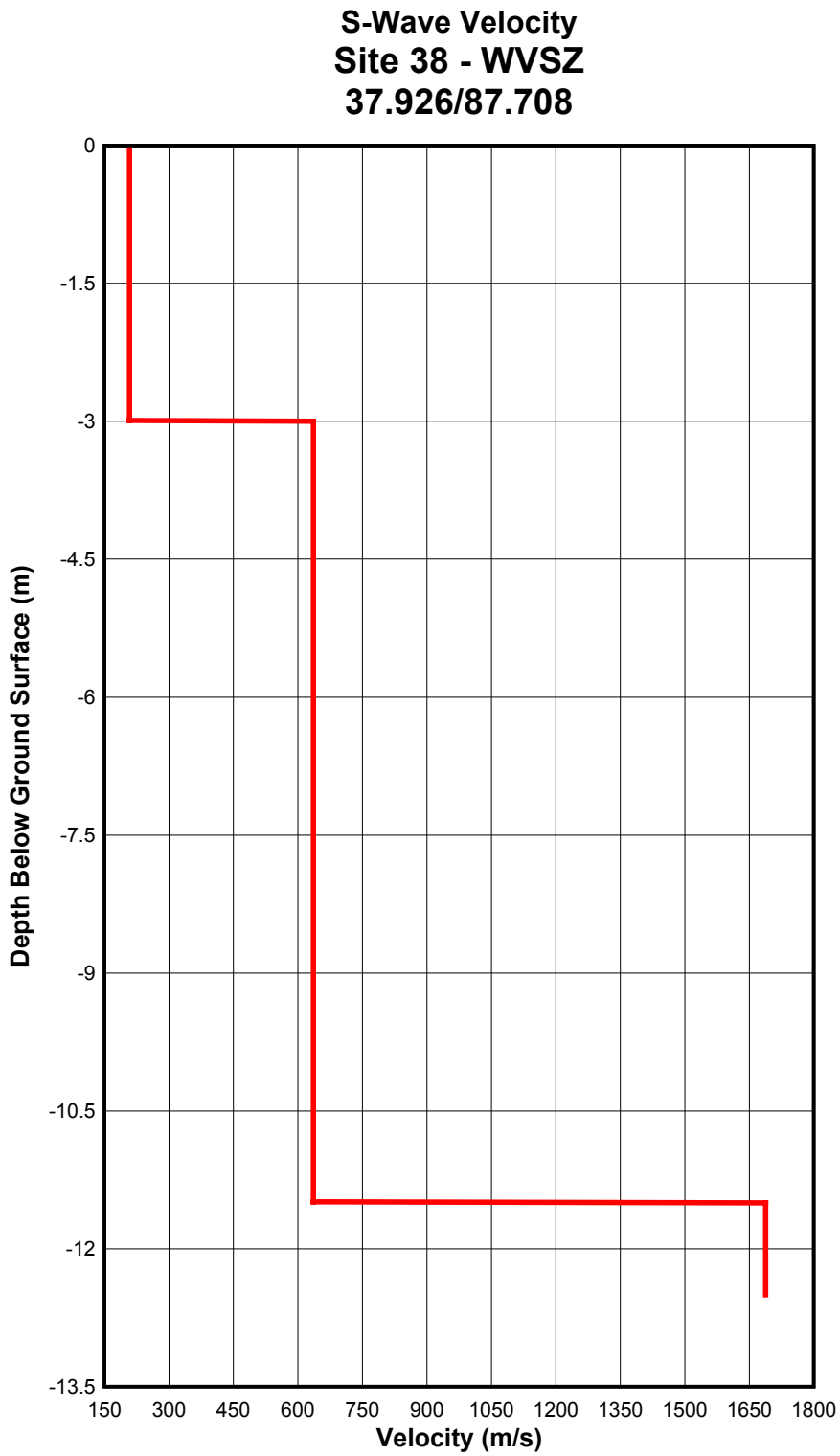
S-Wave Velocity
Site 38 - WVSZ
37.926/87.708
Depth Below Ground Surface (m)
0
-1.5
-3
-4.5
-6
-7.5
-9
-10.5
-12
-13.5
150
300
450
600
750
900
1050
1200
1350
1500
1650
1800
Velocity (m/s)

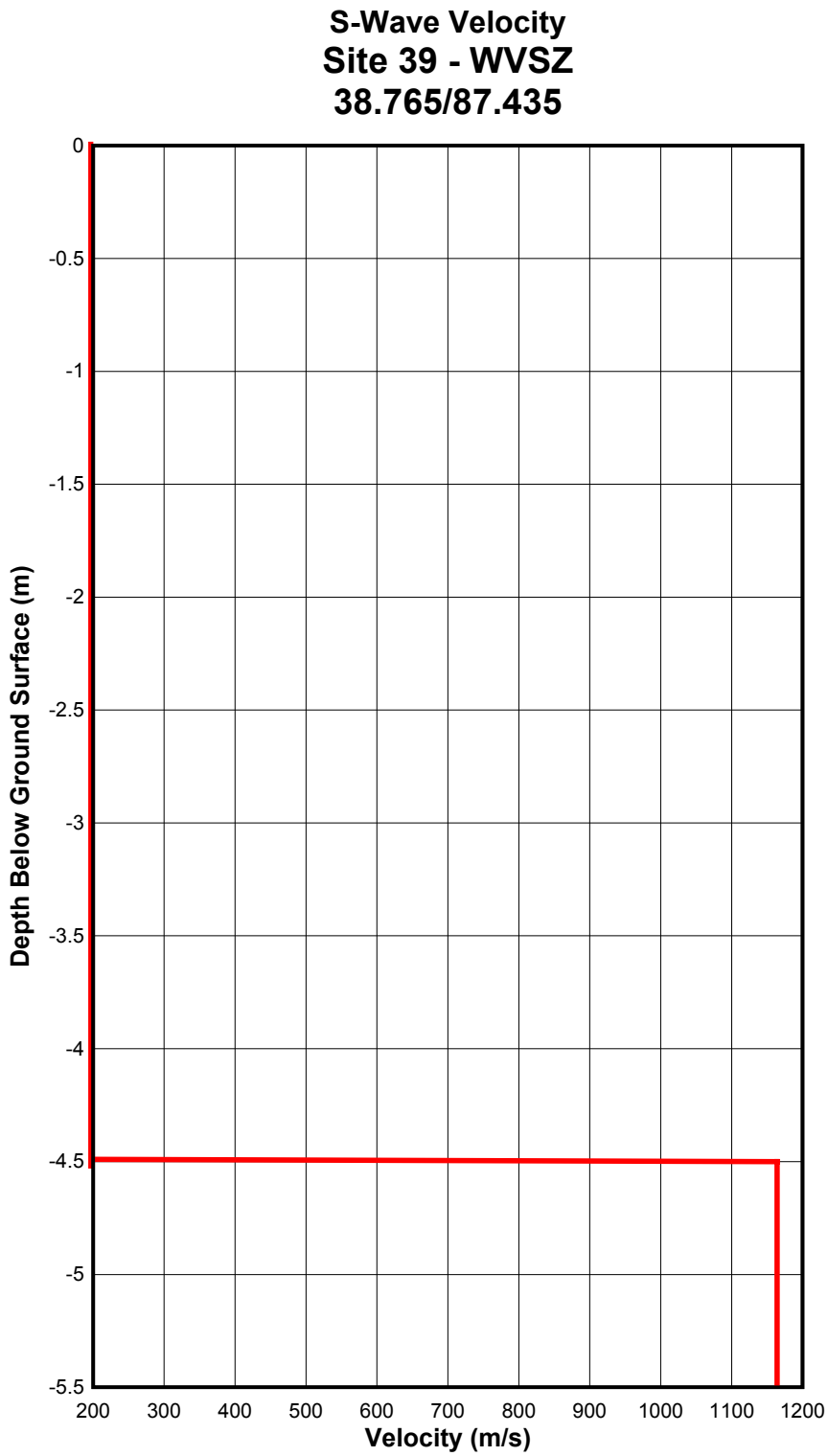
S-Wave Velocity
Site 39 - WVSZ
38.765/87.435
Depth Below Ground Surface (m)
0
-0.5
-1
-1.5
-2
-2.5
-3
-3.5
-4
-4.5
-5
-5.5
200
300
400
500
600
700
800
900
1000
1100
1200
Velocity (m/s)

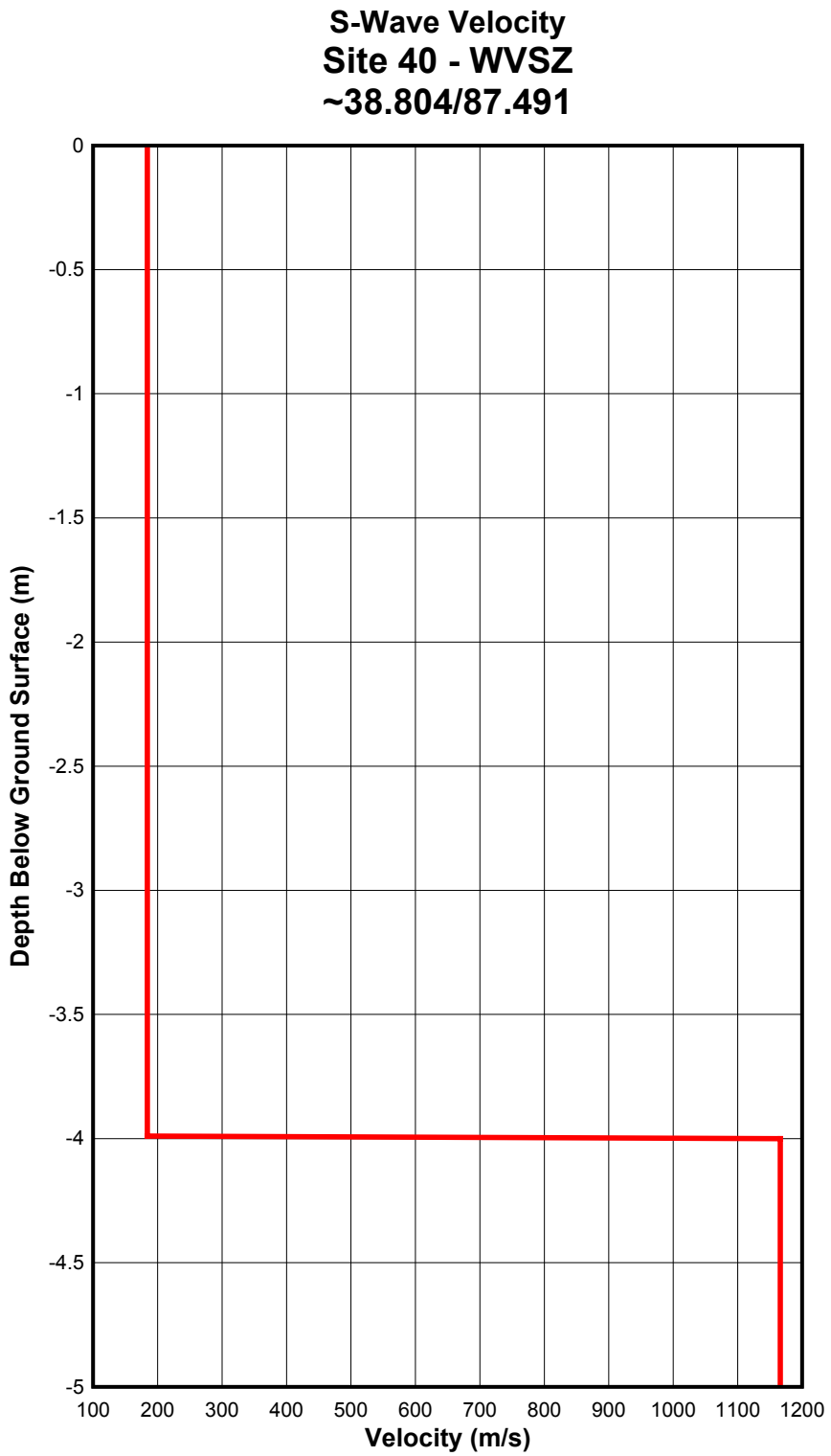
S-Wave Velocity
Site 40 - WVSZ
~38.804/87.491
Depth Below Ground Surface (m)
0
-0.5
-1
-1.5
-2
-2.5
-3
-3.5
-4
-4.5
-5
100
200
300
400
500
600
700
800
900
1000
1100
1200
Velocity (m/s)

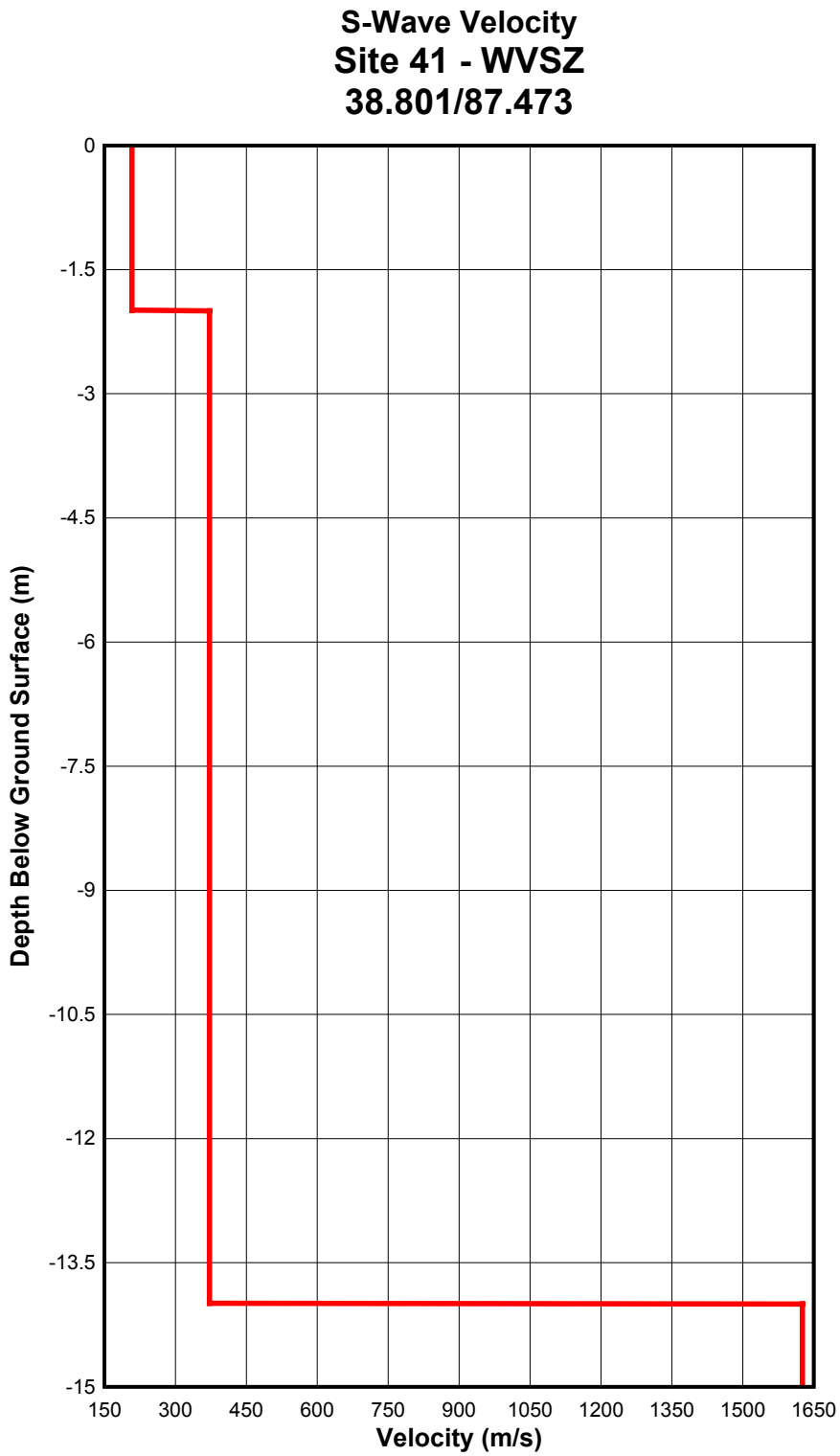
S-Wave Velocity
Site 41 - WVSZ
38.801/87.473
Depth Below Ground Surface (m)
0
-1.5
-3
-4.5
-6
-7.5
-9
-10.5
-12
-13.5
-15
150
300
450
600
750
900
1050
1200
1350
1500
1650
Velocity (m/s)

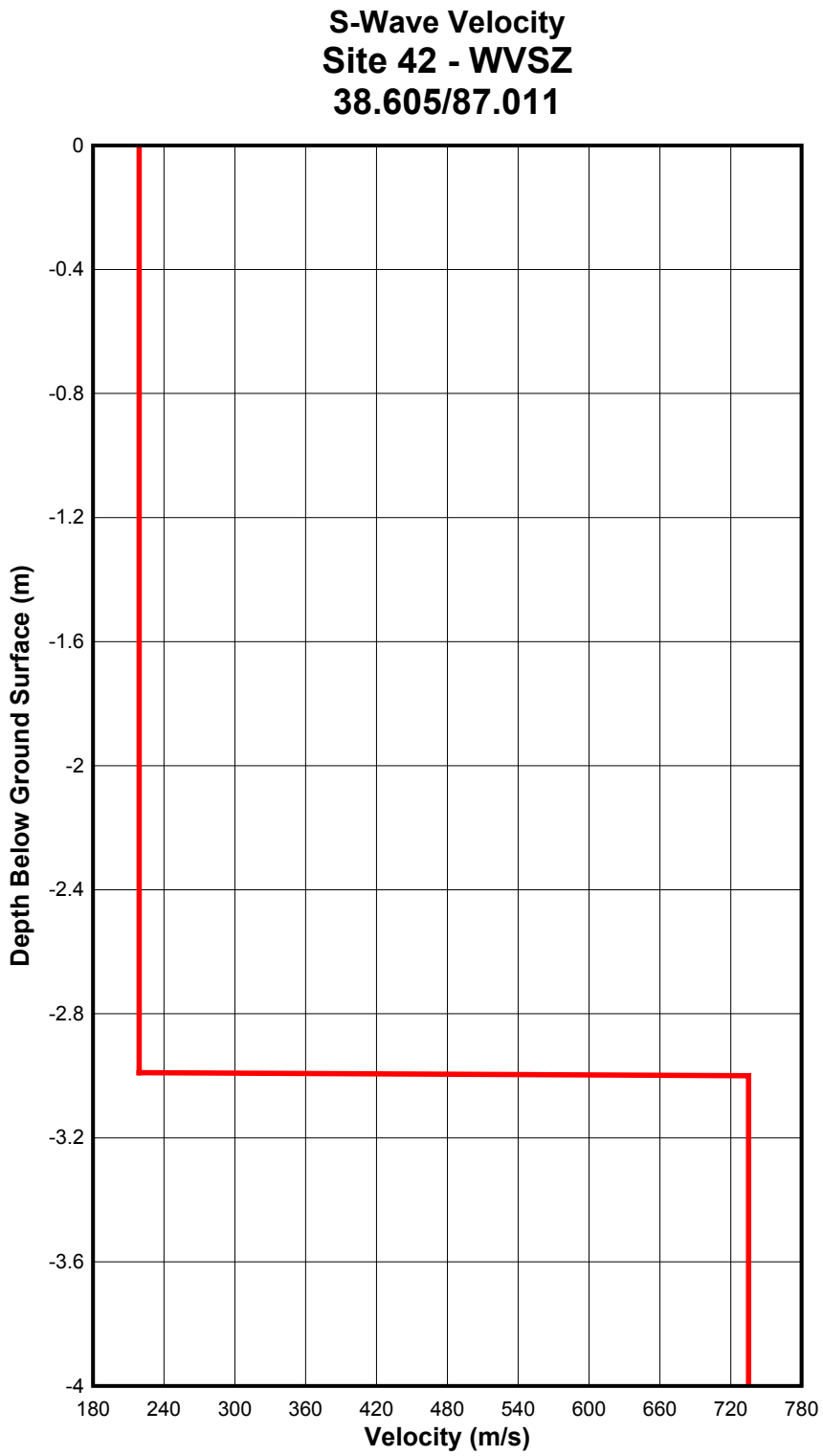
S-Wave Velocity
Site 42 - WVSZ
38.605/87.011
Depth Below Ground Surface (m)
0
-0.4
-0.8
-1.2
-1.6
-2
-2.4
-2.8
-3.2
-3.6
-4
180
240
300
360
420
480
540
600
660
720
780
Velocity (m/s)

APPENDIX B

Modeled Site Response (EERA):

Amplitude Ratio

Fourier Spectra (<10 Hz)

5% Response Spectra

Site 1

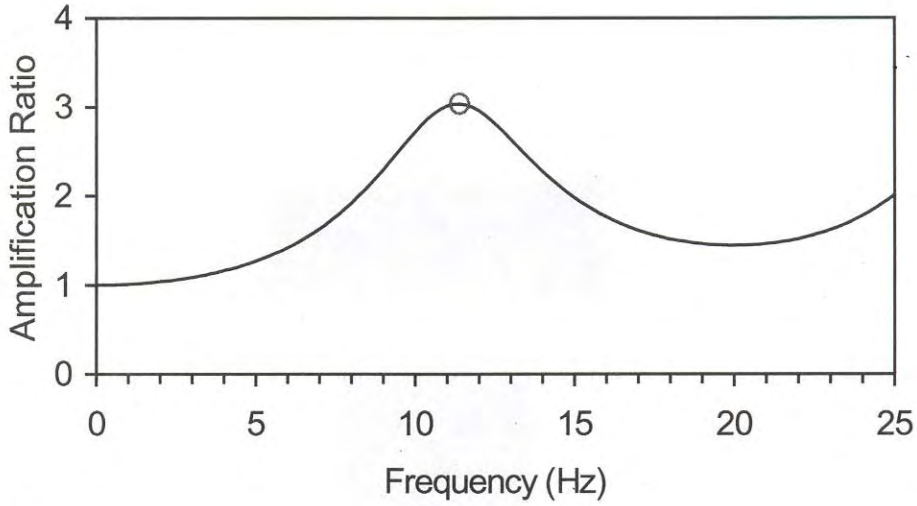
Amplification Ratio
0
1
2
3
4
0
5
10
15
20
25
Frequency (Hz)

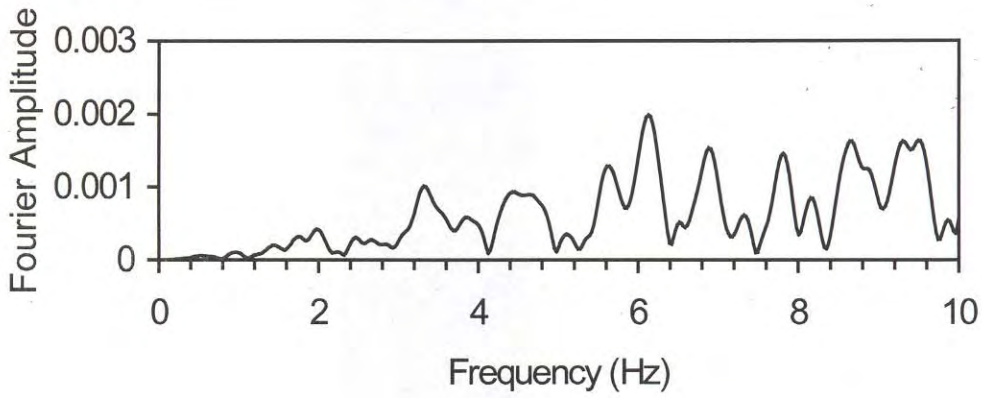
Fourier Amplitude
0
0.001
0.002
0.003
0
2
4
6
8
10
Frequency (Hz)

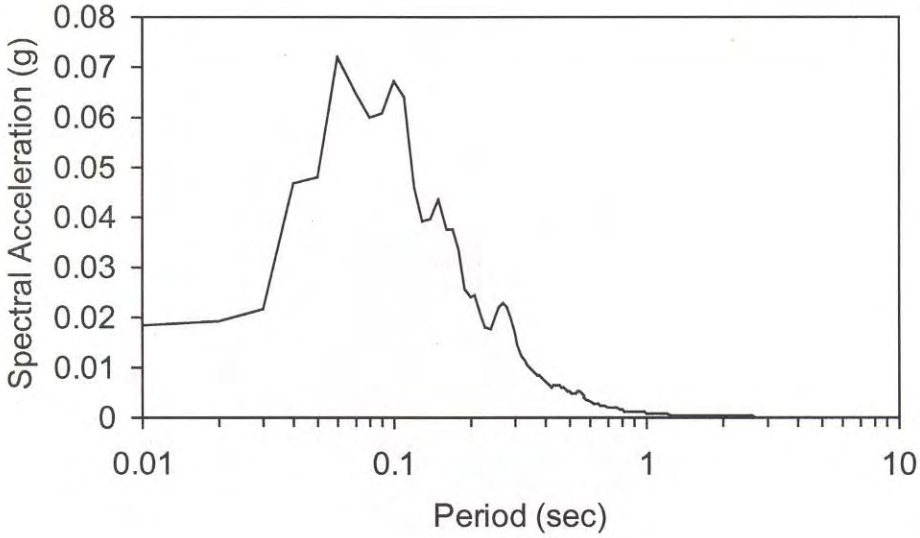
Spectral Acceleration (g)
0
0.01
0.02
0.03
0.04
0.05
0.06
0.07
0.08
0.01
0.1
1
10
Period (sec)

Site 2

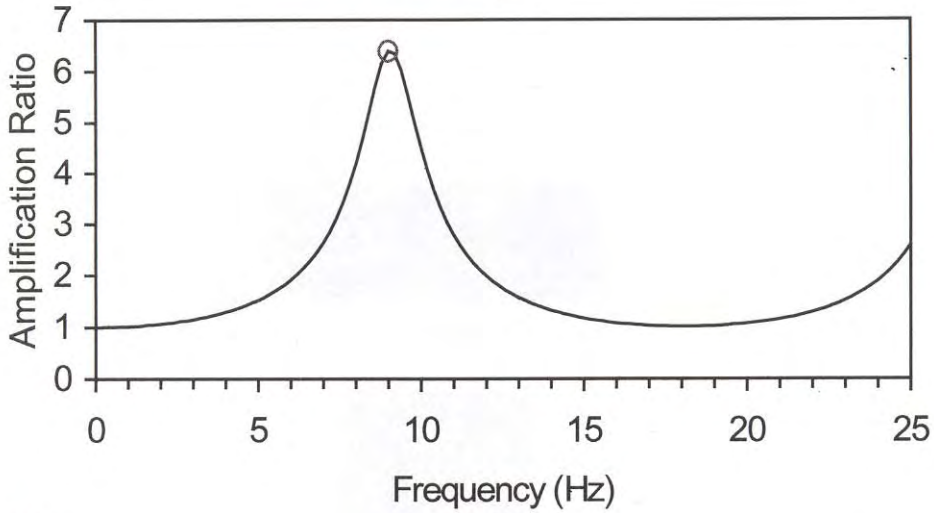
Amplification Ratio
0
1
2
3
4
5
6
7
0
5
10
15
20
25
Frequency (Hz)

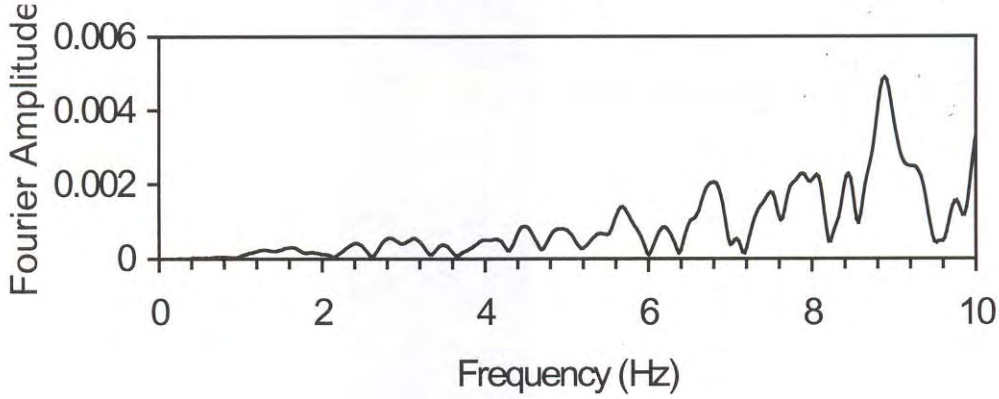
Fourier Amplitude
0
0.002
0.004
0.006
0
2
4
6
8
10
Frequency (Hz)

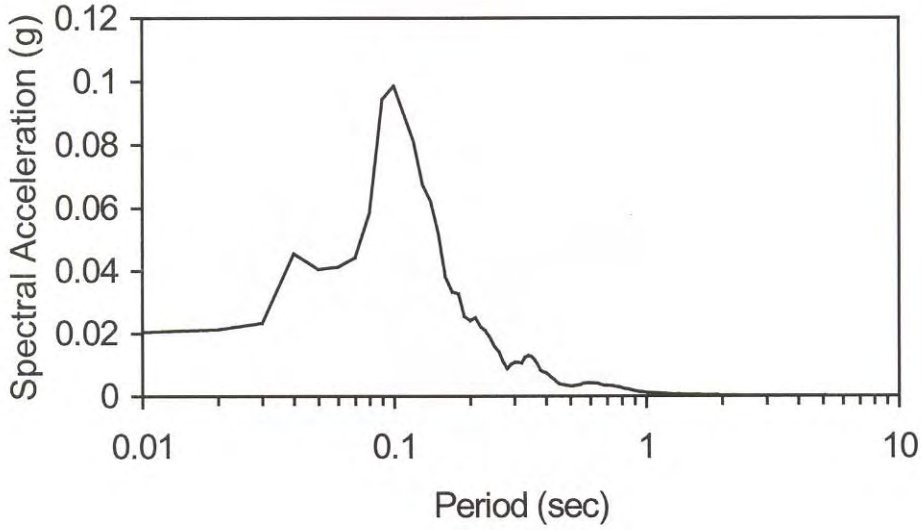
Spectral Acceleration (g)
0
0.02
0.04
0.06
0.08
0.1
0.12
0.01
0.1
1
10
Period (sec)

Site 3

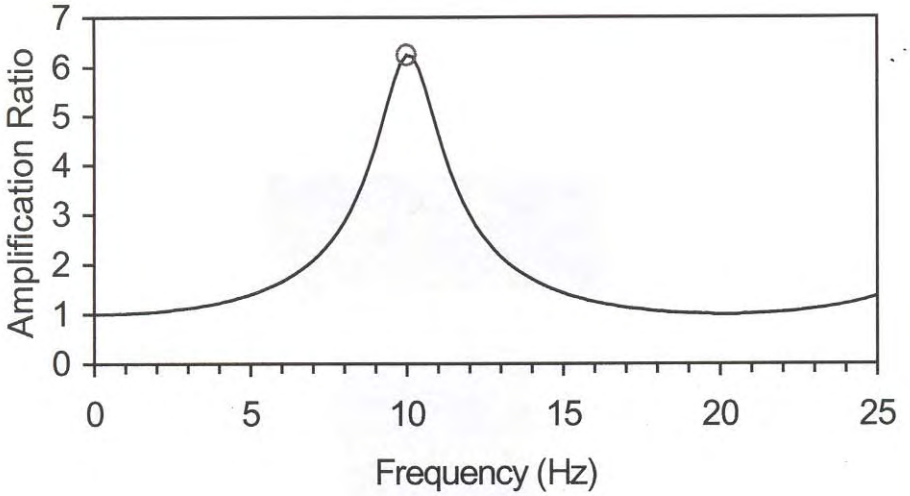
Amplification Ratio
0
1
2
3
4
5
6
7
0
5
10
15
20
25
Frequency (Hz)

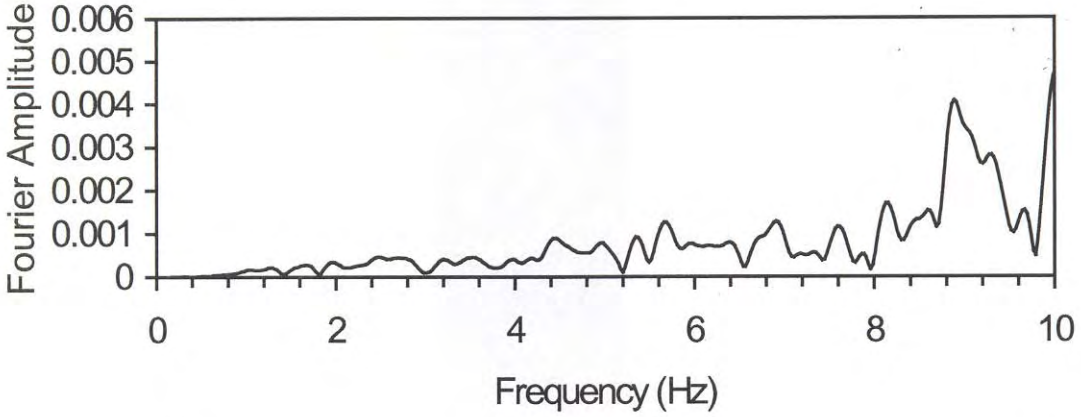
Fourier Amplitude
0
0.001
0.002
0.003
0.004
0.005
0.006
0
2
4
6
8
10
Frequency (Hz)

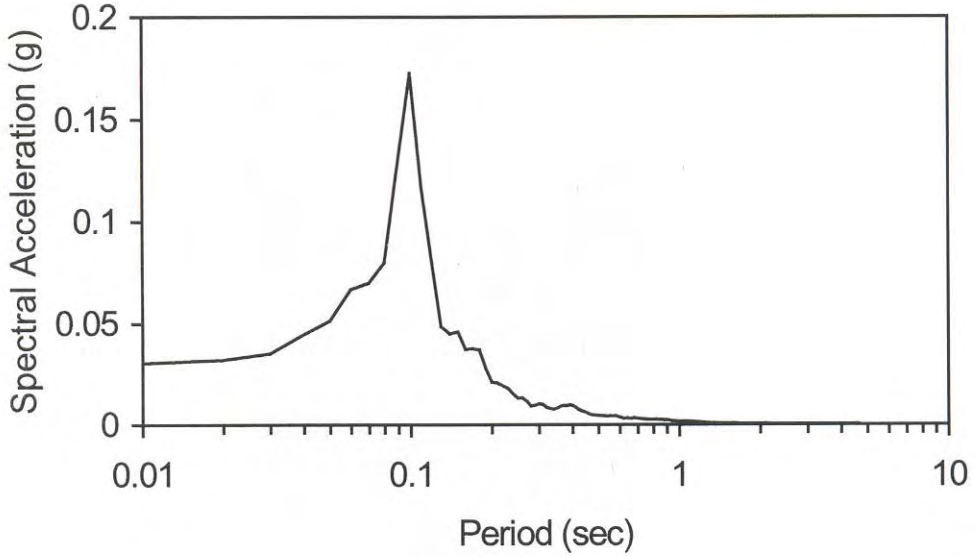
Spectral Acceleration (g)
0
0.05
0.1
0.15
0.2
0.01
0.1
1
10
Period (sec)

Site 5

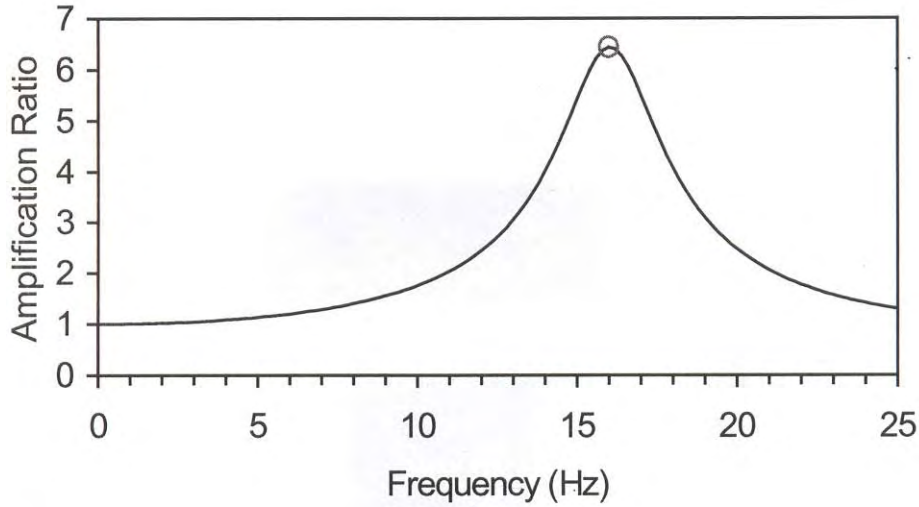
Amplification Ratio
0
1
2
3
4
5
6
7
0
5
10
15
20
25
Frequency (Hz)

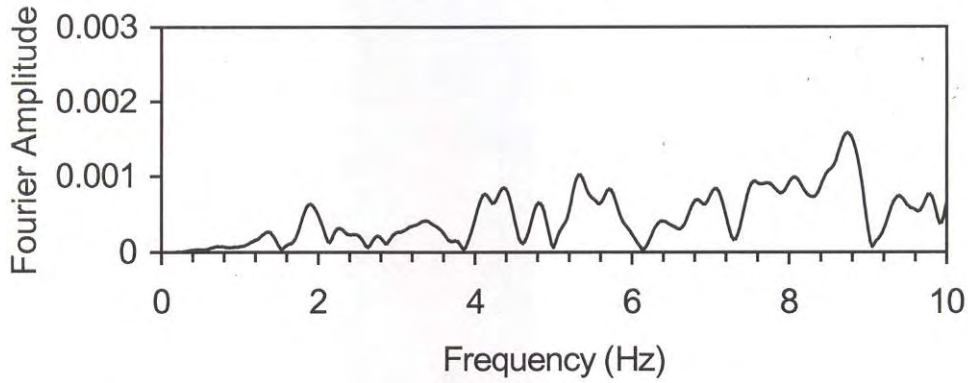
Fourier Amplitude
0
0.001
0.002
0.003
0
2
4
6
8
10
Frequency (Hz)

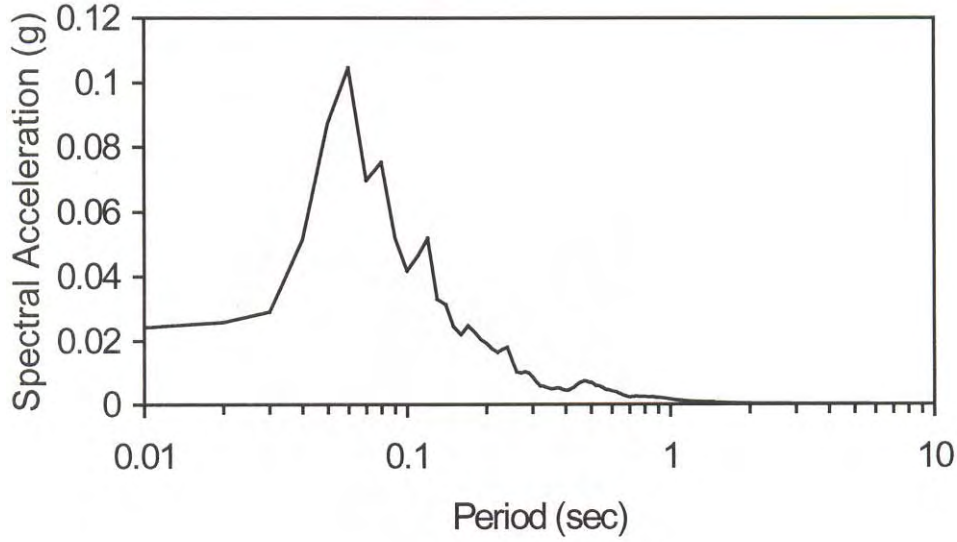
Spectral Acceleration (g)
0
0.02
0.04
0.06
0.08
0.1
0.12
0.01
0.1
1
10
Period (sec)

Site 7

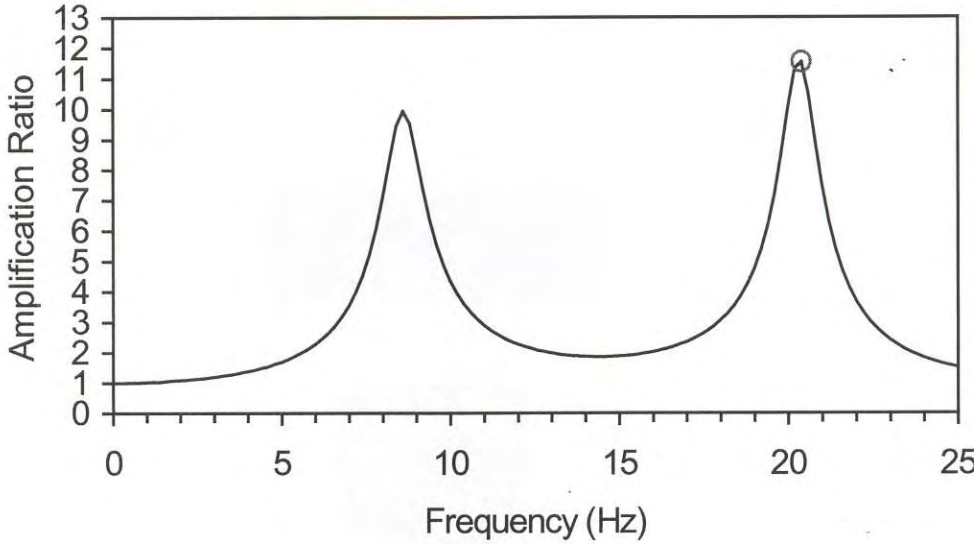
Amplification Ratio
13
12
11
10
9
8
7
6
5
4
3
2
1
0
0
5
10
15
20
25
Frequency (Hz)

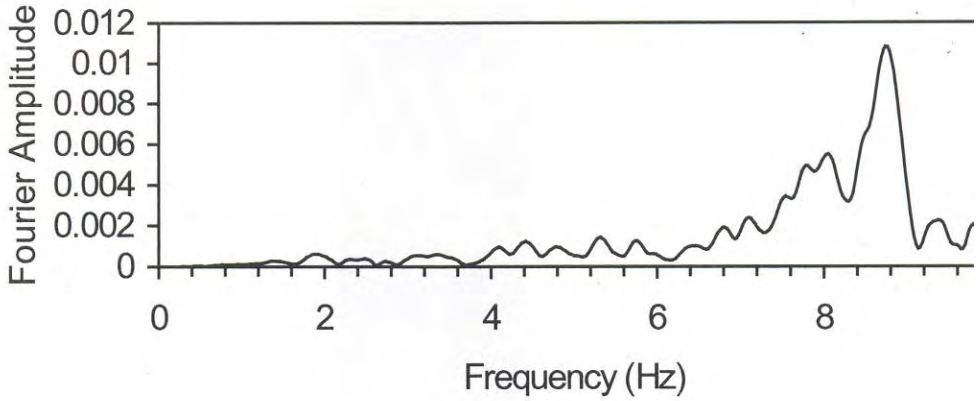
Fourier Amplitude
0.012
0.01
0.008
0.006
0.004
0.002
0
0
2
4
6
8
Frequency (Hz)

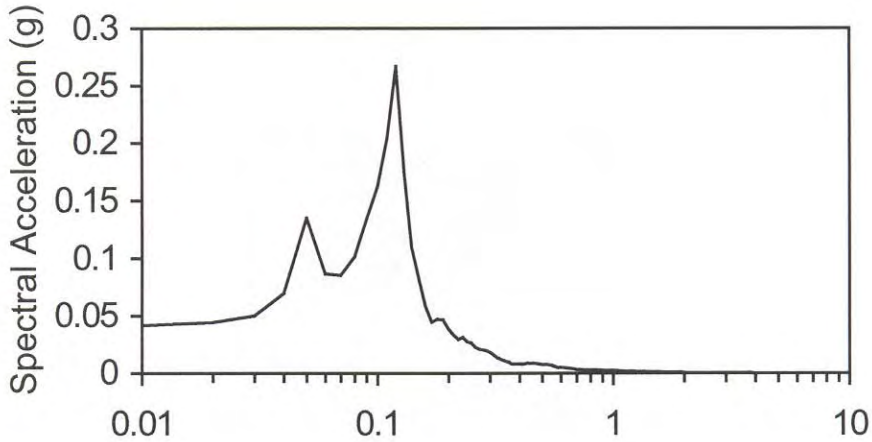
Spectral Acceleration (g)
0.3
0.25
0.2
0.15
0.1
0.05
0
0.01
0.1
1
10

Site 10

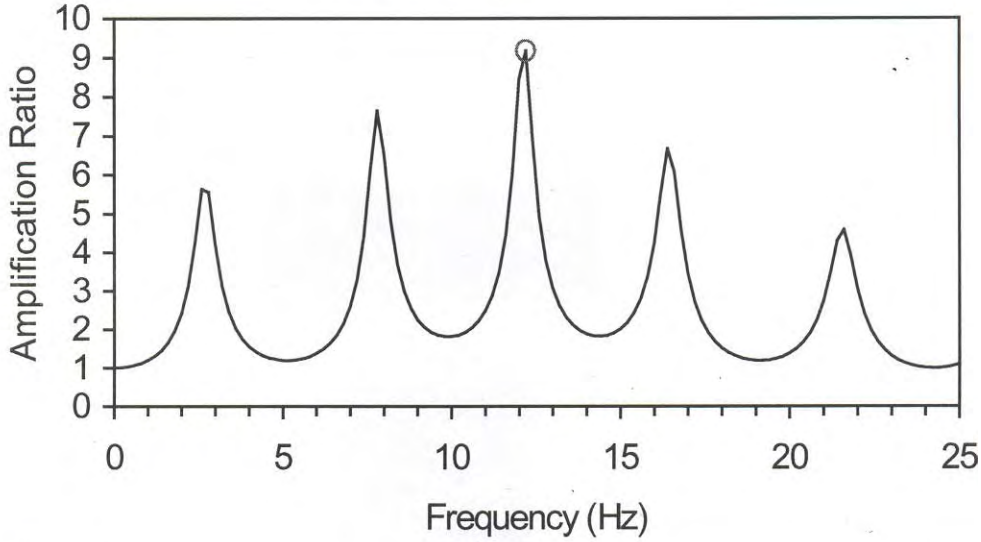
Amplification Ratio
0
1
2
3
4
5
6
7
8
9
10
0
5
10
15
20
25
Frequency (Hz)

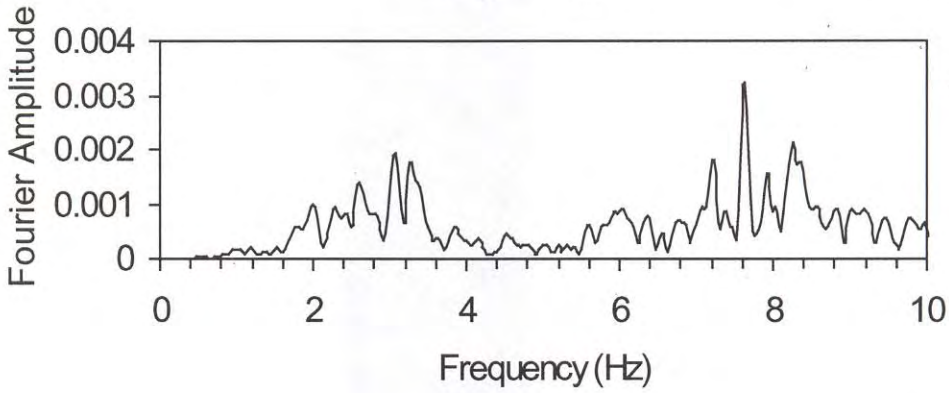
Fourier Amplitude
0
0.001
0.002
0.003
0.004
0
2
4
6
8
10
Frequency (Hz)

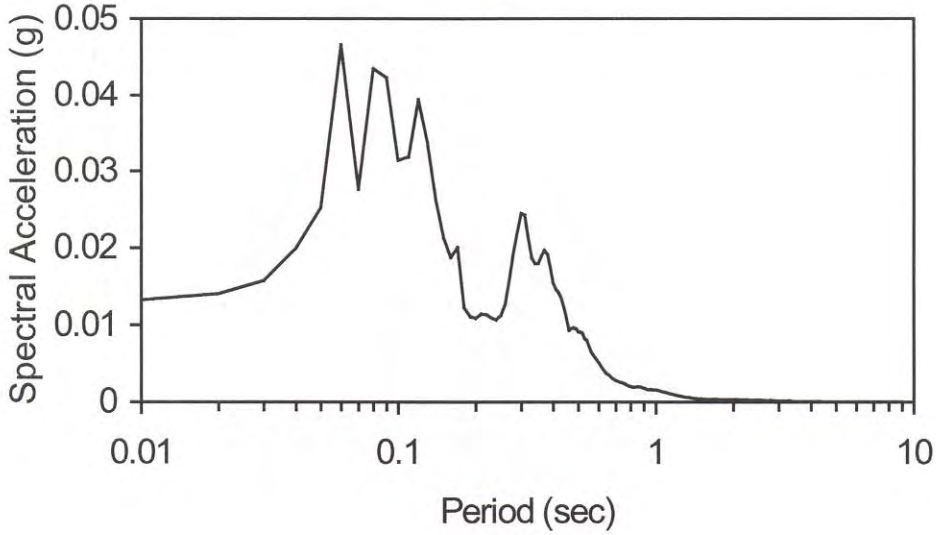
Spectral Acceleration (g)
0
0.01
0.02
0.03
0.04
0.05
0.01
0.1
1
10
Period (sec)

Site 11

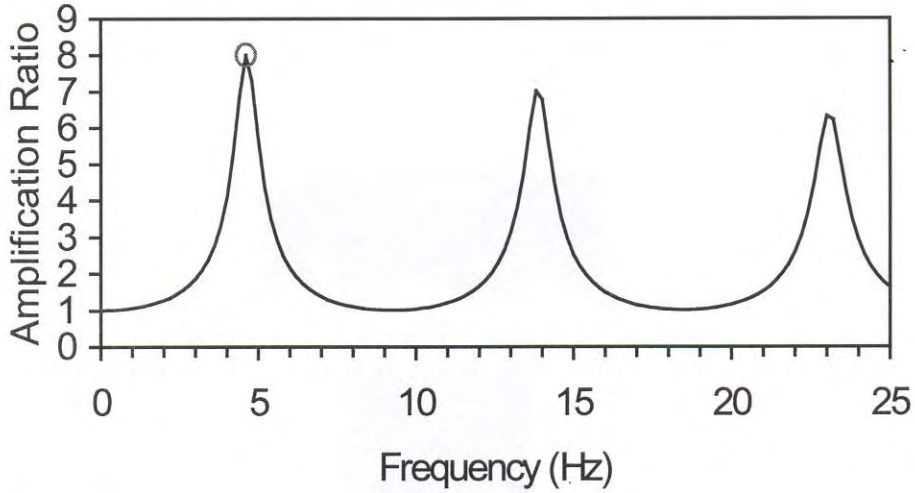
Amplification Ratio
0
1
2
3
4
5
6
7
8
9
0
5
10
15
20
25
Frequency (Hz)

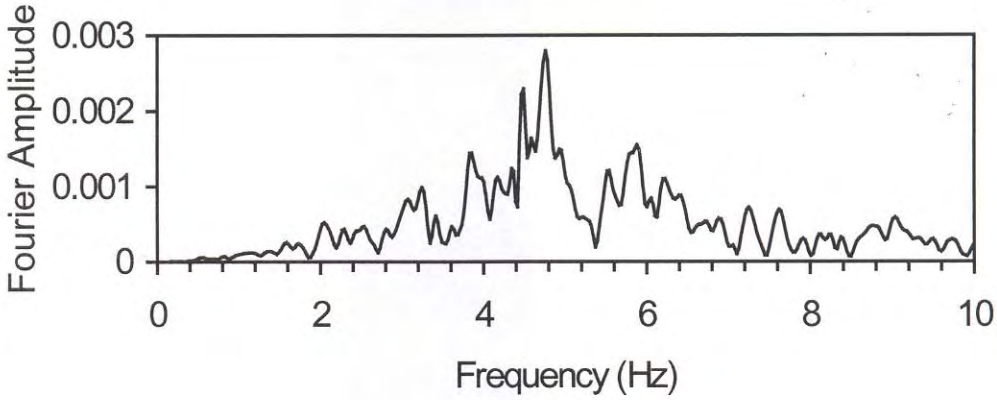
Fourier Amplitude
0
0.001
0.002
0.003
0
2
4
6
8
10
Frequency (Hz)

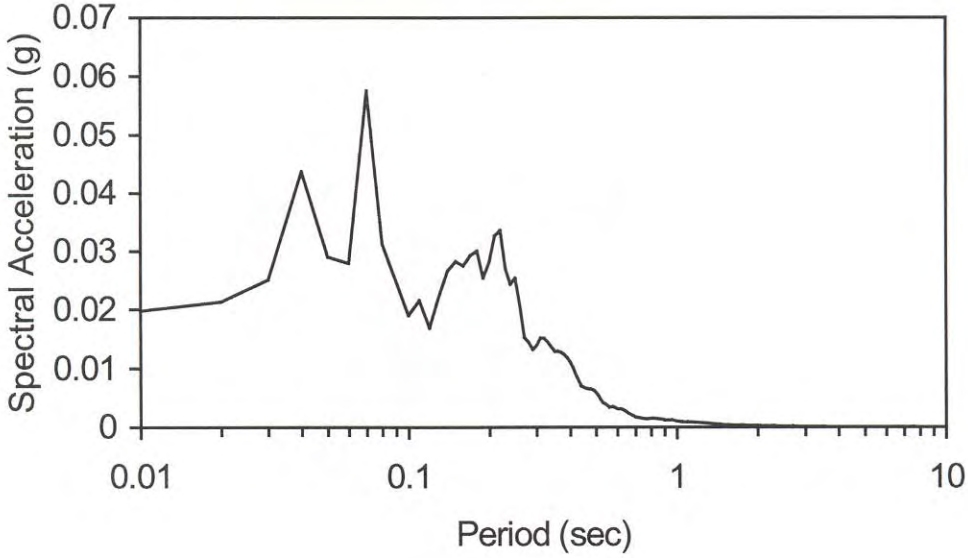
Spectral Acceleration (g)
0
0.01
0.02
0.03
0.04
0.05
0.06
0.07
0.01
0.1
1
10
Period (sec)

Site 12

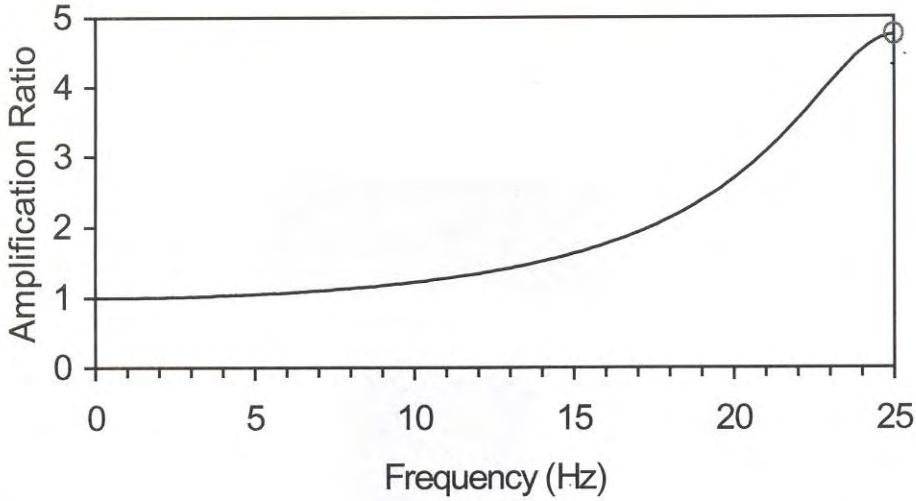
Amplification Ratio
0
1
2
3
4
5
0
5
10
15
20
25
Frequency (Hz)

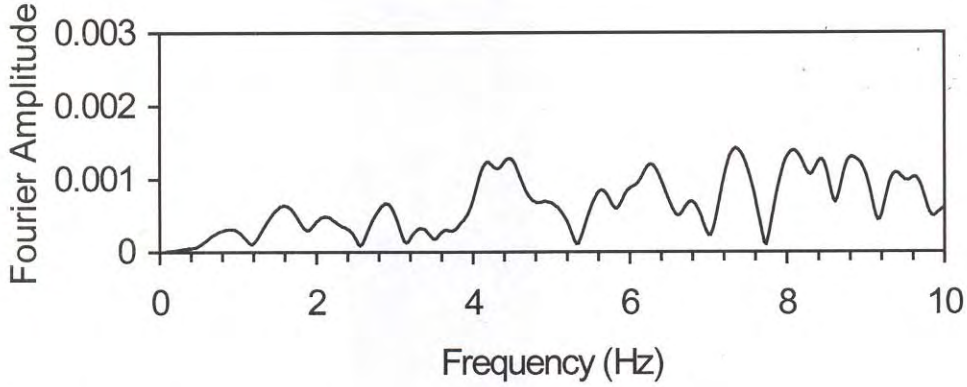
Fourier Amplitude
0
0.001
0.002
0.003
0
2
4
6
8
10
Frequency (Hz)

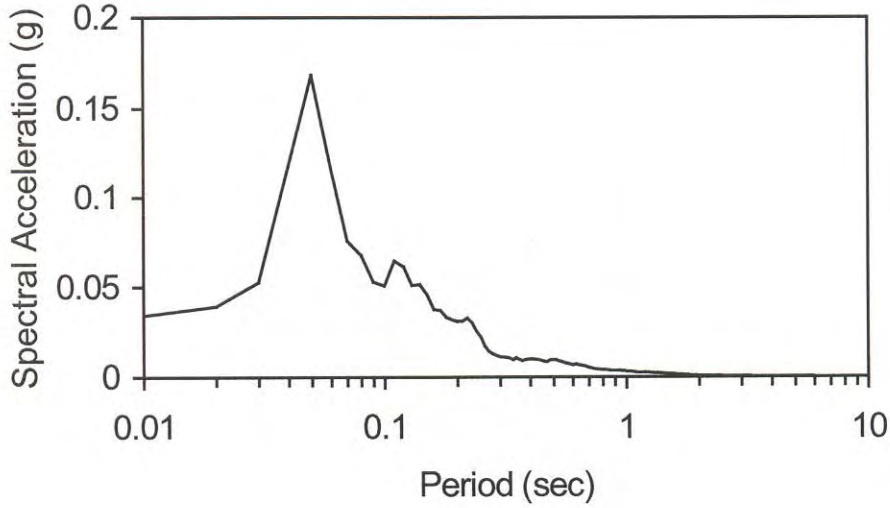
Spectral Acceleration (g)
0
0.05
0.1
0.15
0.2
0.01
0.1
1
10
Period (sec)

Site 13

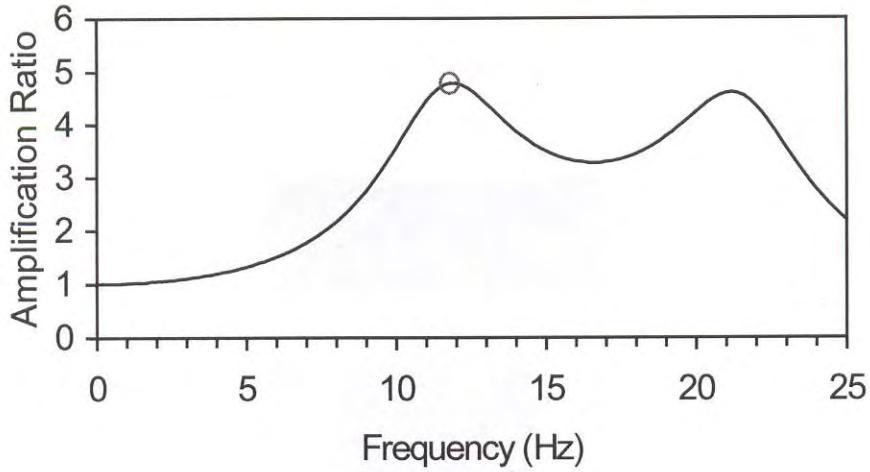
Amplification Ratio
0
1
2
3
4
5
6
0
5
10
15
20
25
Frequency (Hz)

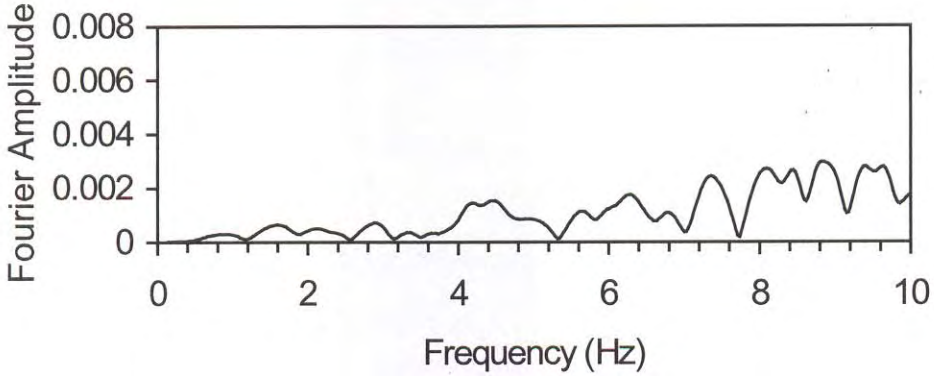
Fourier Amplitude
0
0.002
0.004
0.006
0.008
0
2
4
6
8
10
Frequency (Hz)

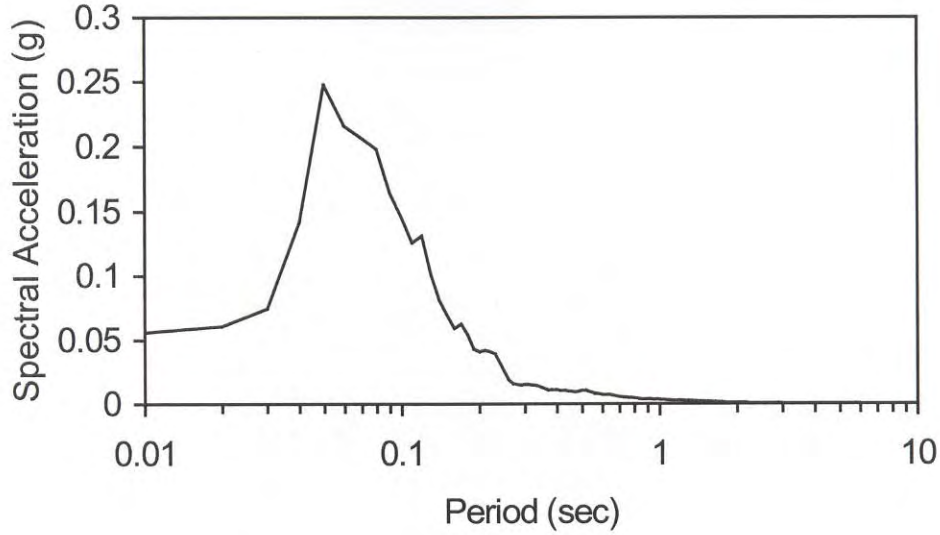
Spectral Acceleration (g)
0
0.05
0.1
0.15
0.2
0.25
0.3
0.01
0.1
1
10
Period (sec)

Site 14

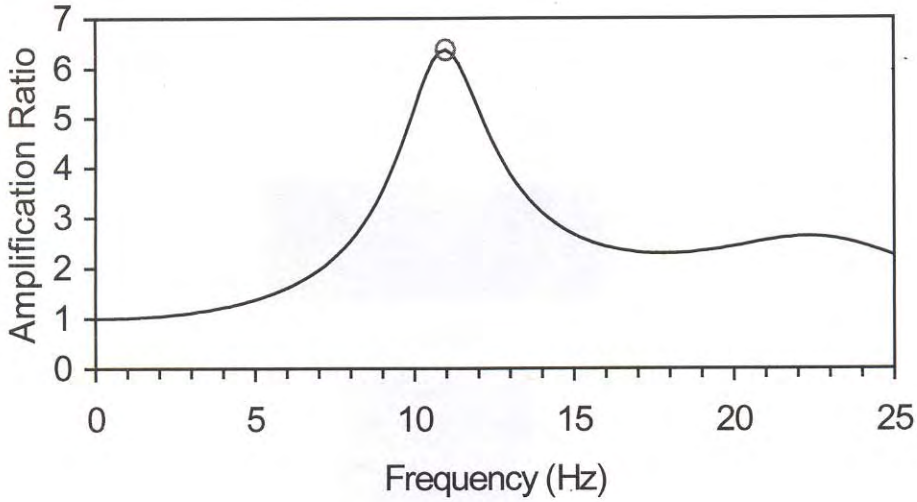
Amplification Ratio
0
1
2
3
4
5
6
7
0
5
10
15
20
25
Frequency (Hz)

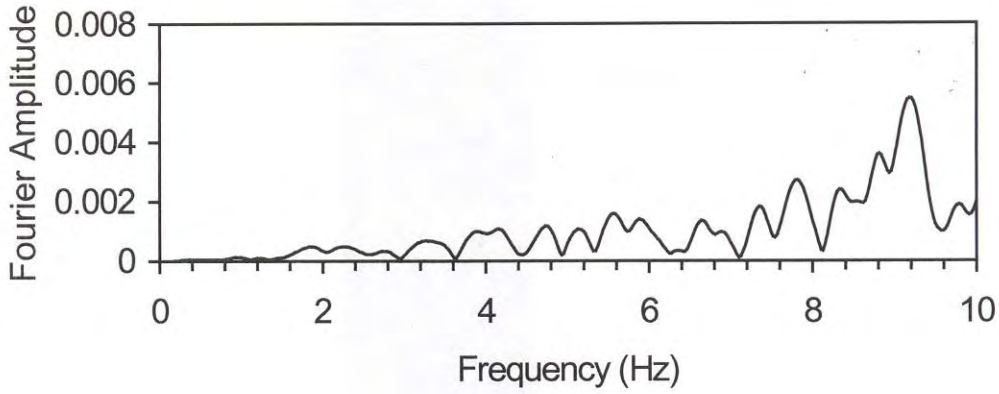
Fourier Amplitude
0
0.002
0.004
0.006
0.008
0
2
4
6
8
10
Frequency (Hz)

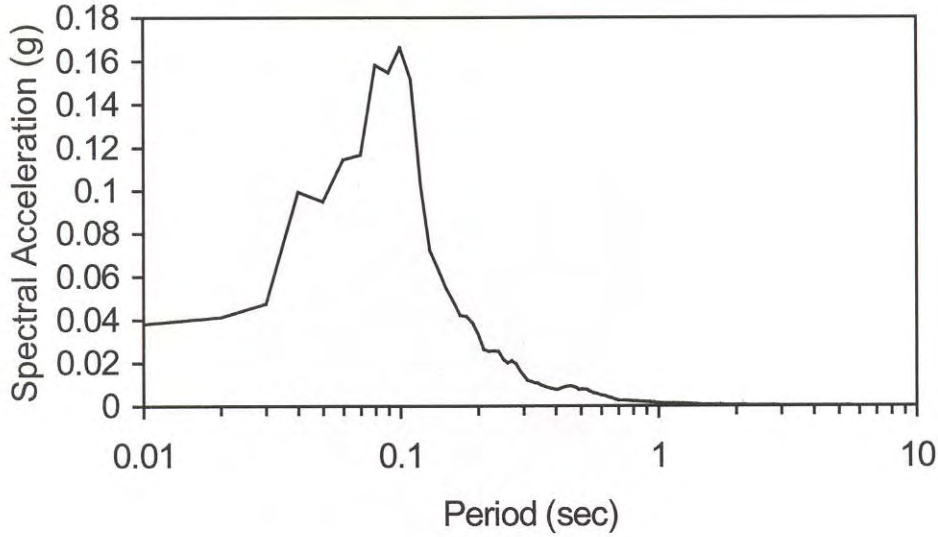
Spectral Acceleration (g)
0
0.02
0.04
0.06
0.08
0.1
0.12
0.14
0.16
0.18
0.01
0.1
1
10
Period (sec)

Site 16

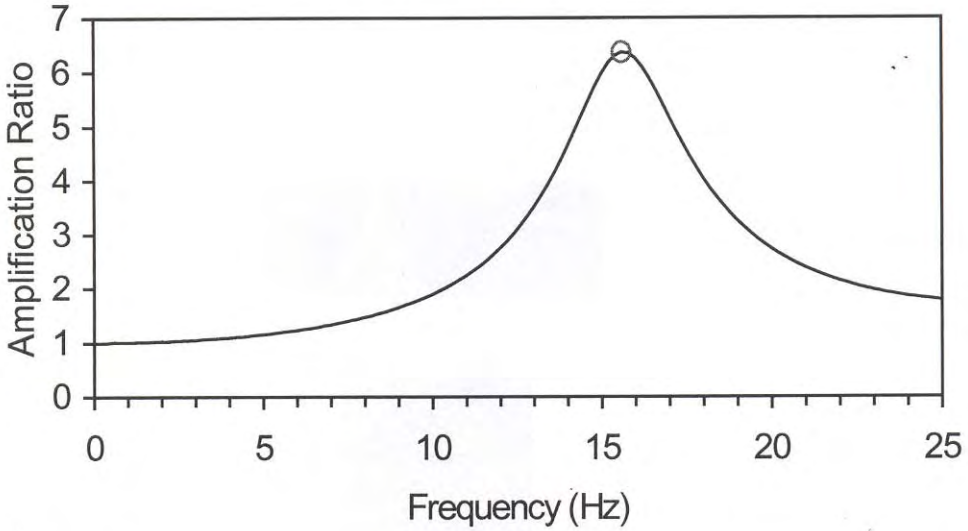
Amplification Ratio
0
1
2
3
4
5
6
7
0
5
10
15
20
25
Frequency (Hz)

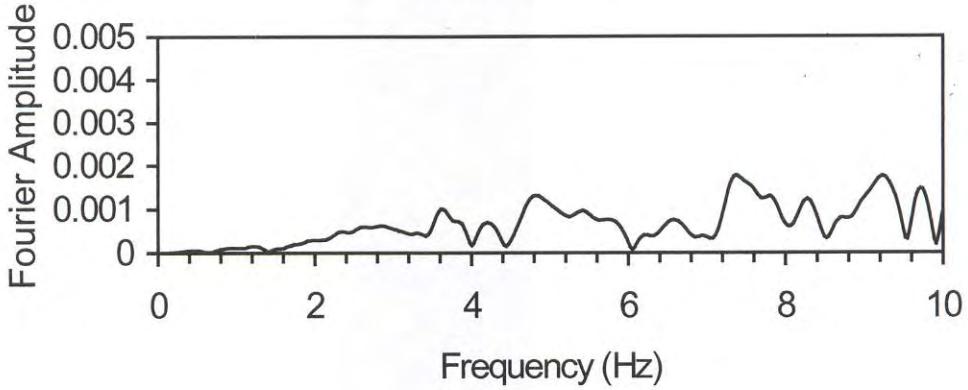
Fourier Amplitude
0
0.001
0.002
0.003
0.004
0.005
0
2
4
6
8
10
Frequency (Hz)

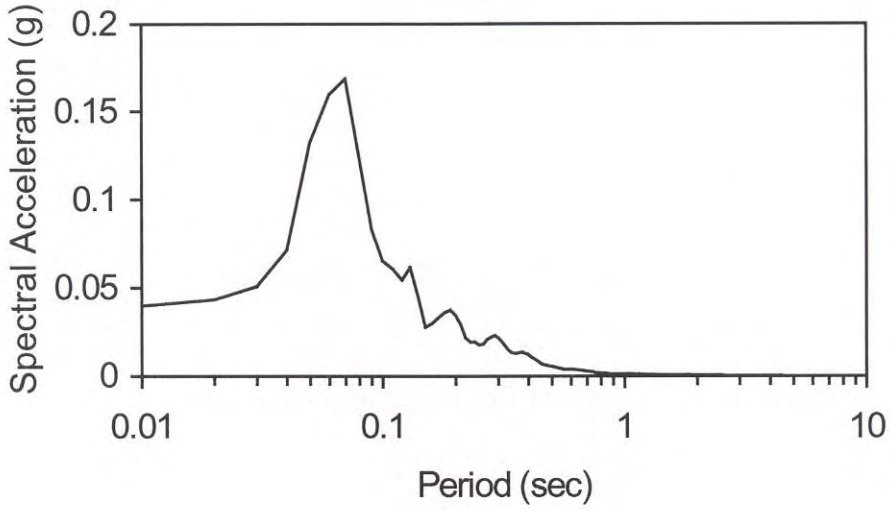
Spectral Acceleration (g)
0
0.05
0.1
0.15
0.2
0.01
0.1
1
10
Period (sec)

Site 20

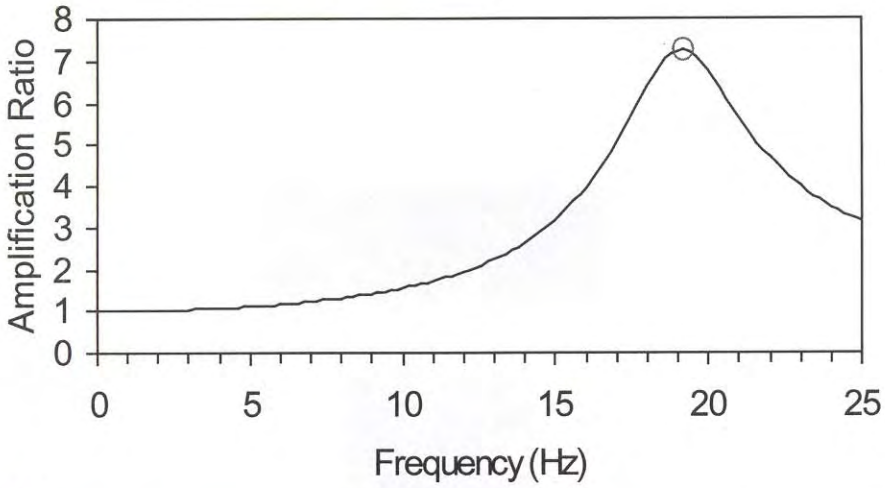
Amplification Ratio
0
1
2
3
4
5
6
7
8
0
5
10
15
20
25
Frequency (Hz)

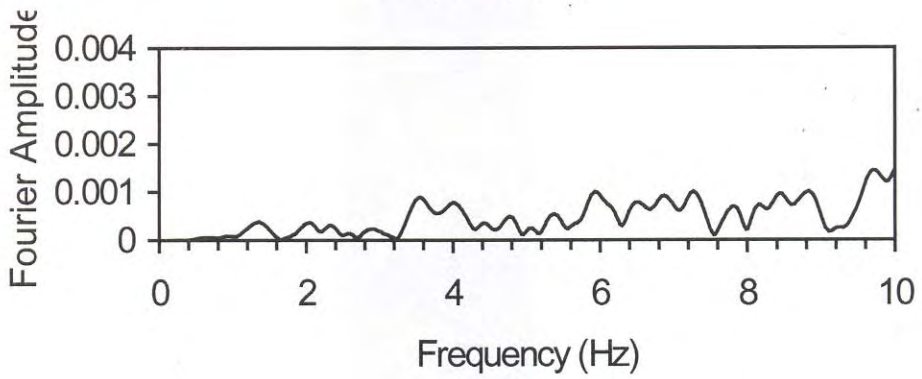
Fourier Amplitude
0
0.001
0.002
0.003
0.004
0
2
4
6
8
10
Frequency (Hz)

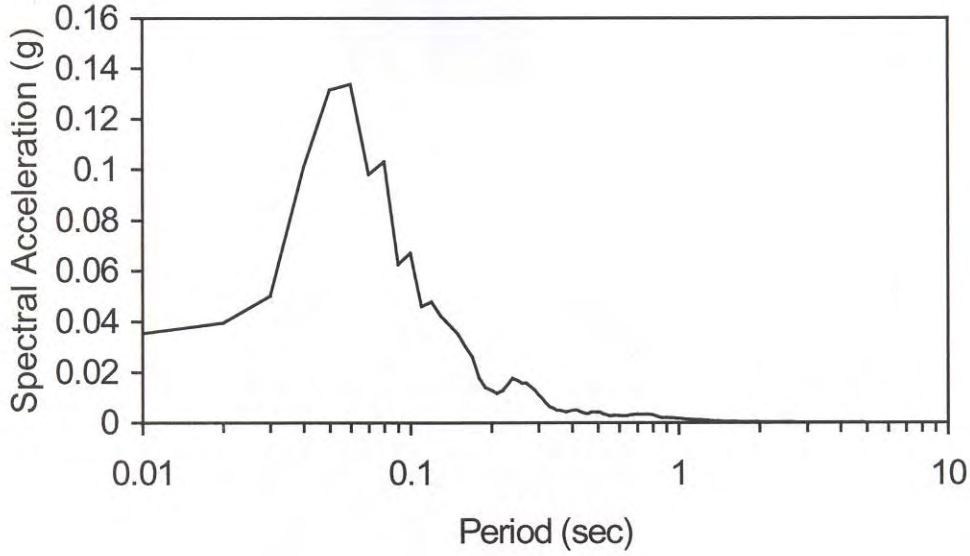
Spectral Acceleration (g)
0
0.02
0.04
0.06
0.08
0.1
0.12
0.14
0.16
0.01
0.1
1
10
Period (sec)

Site 21

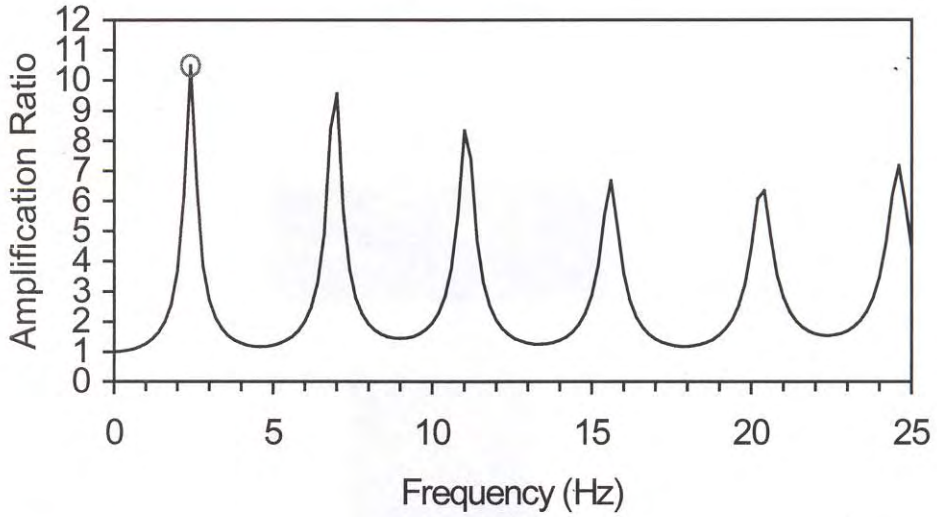
Amplification Ratio
0
1
2
3
4
5
6
7
8
9
10
11
12
0
5
10
15
20
25
Frequency (Hz)

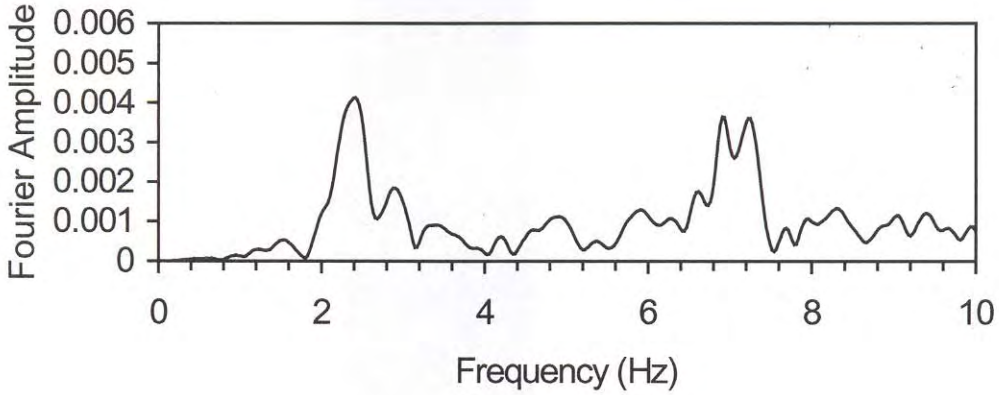
Fourier Amplitude
0
0.001
0.002
0.003
0.004
0.005
0.006
0
2
4
6
8
10
Frequency (Hz)

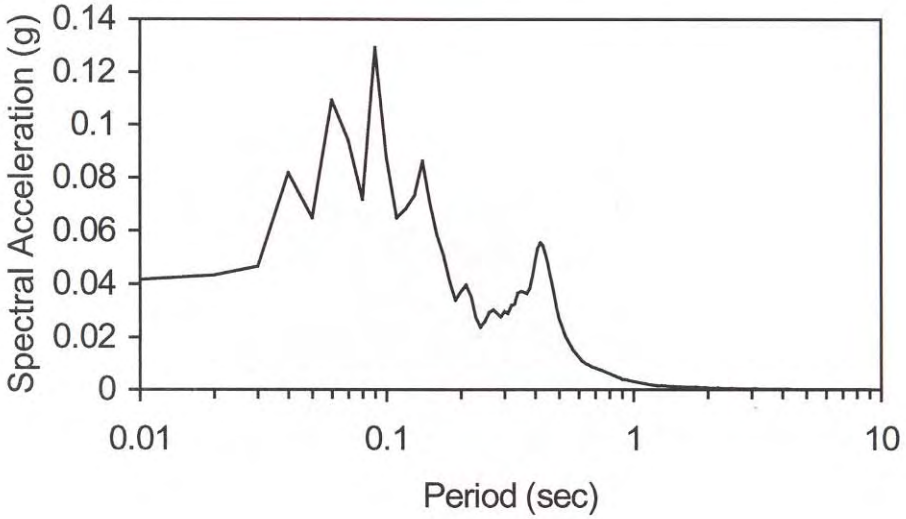
Spectral Acceleration (g)
0
0.02
0.04
0.06
0.08
0.1
0.12
0.14
0.01
0.1
1
10
Period (sec)

Site 22

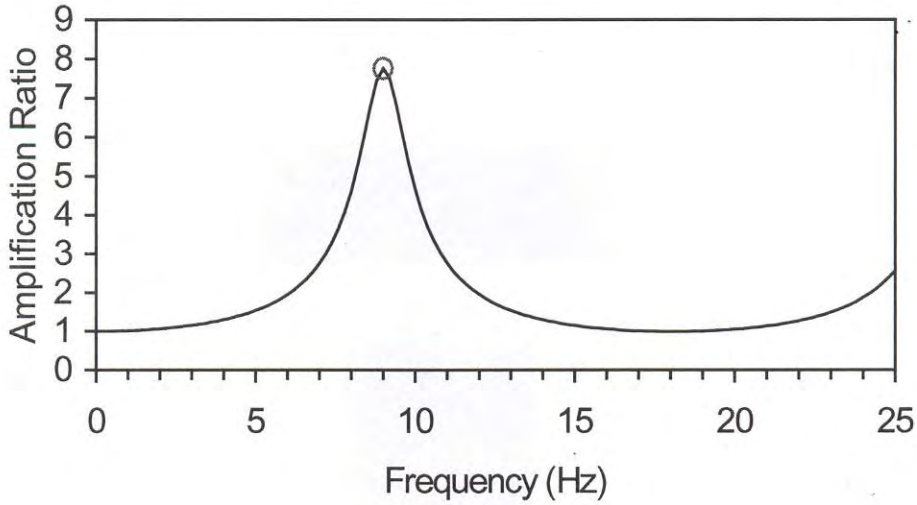
Amplification Ratio
0
1
2
3
4
5
6
7
8
9
0
5
10
15
20
25
Frequency (Hz)

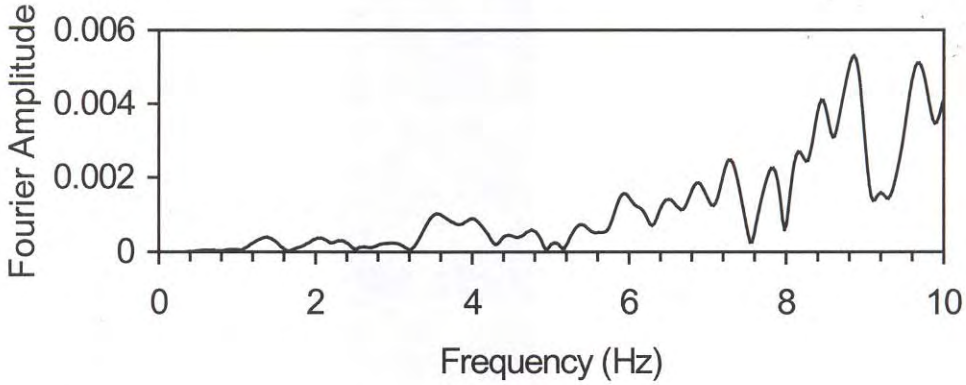
Fourier Amplitude
0
0.002
0.004
0.006
0
2
4
6
8
10
Frequency (Hz)

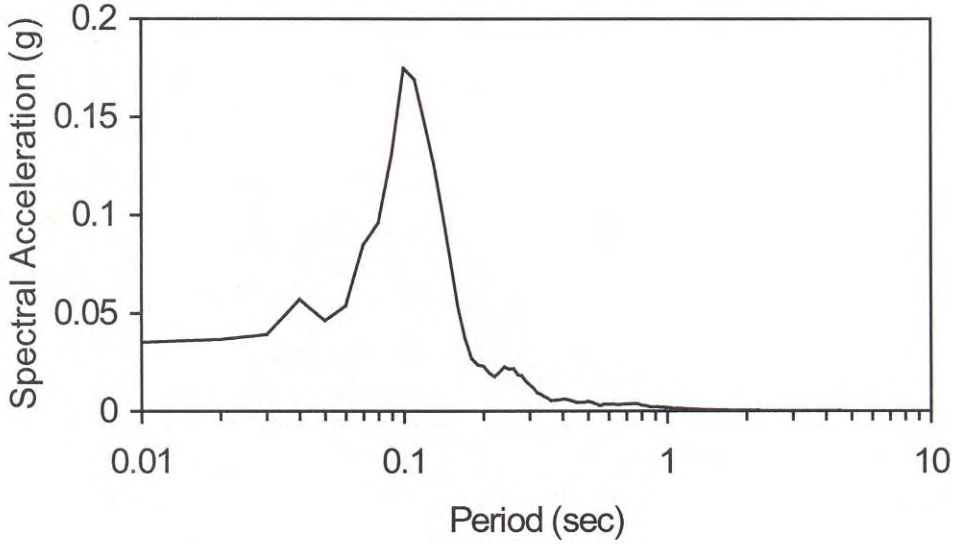
Spectral Acceleration (g)
0
0.05
0.1
0.15
0.2
0.01
0.1
1
10
Period (sec)

Site 25

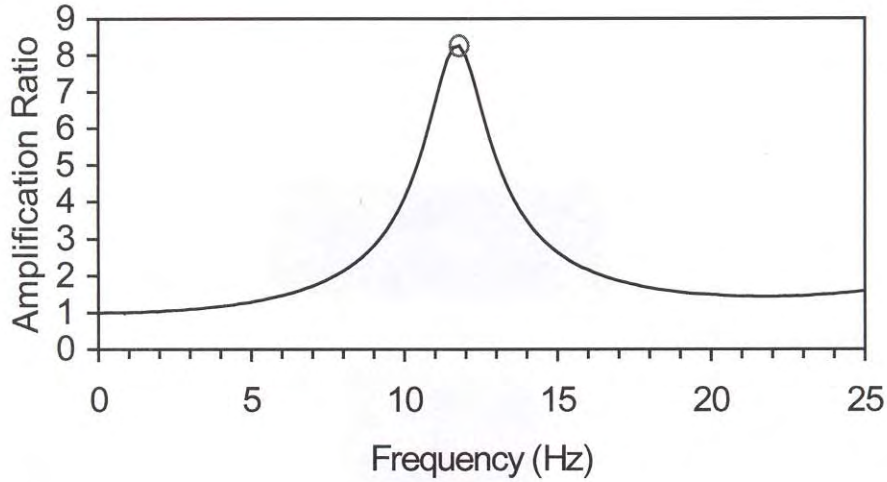
Amplification Ratio
0
1
2
3
4
5
6
7
8
9
0
5
10
15
20
25
Frequency (Hz)

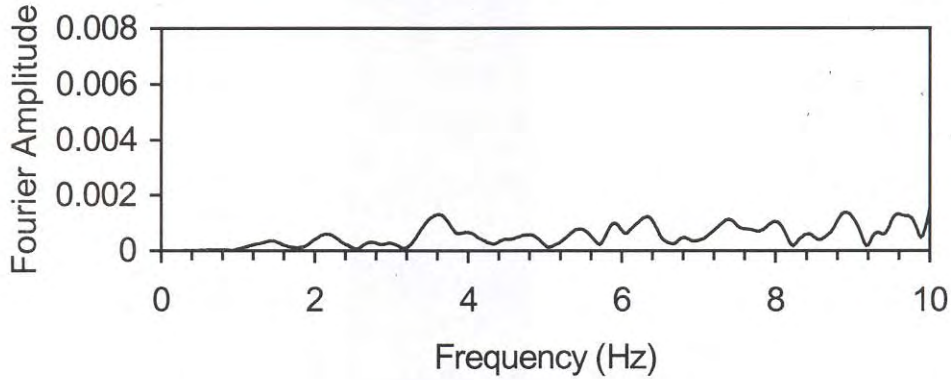
Fourier Amplitude
0
0.002
0.004
0.006
0.008
0
2
4
6
8
10
Frequency (Hz)

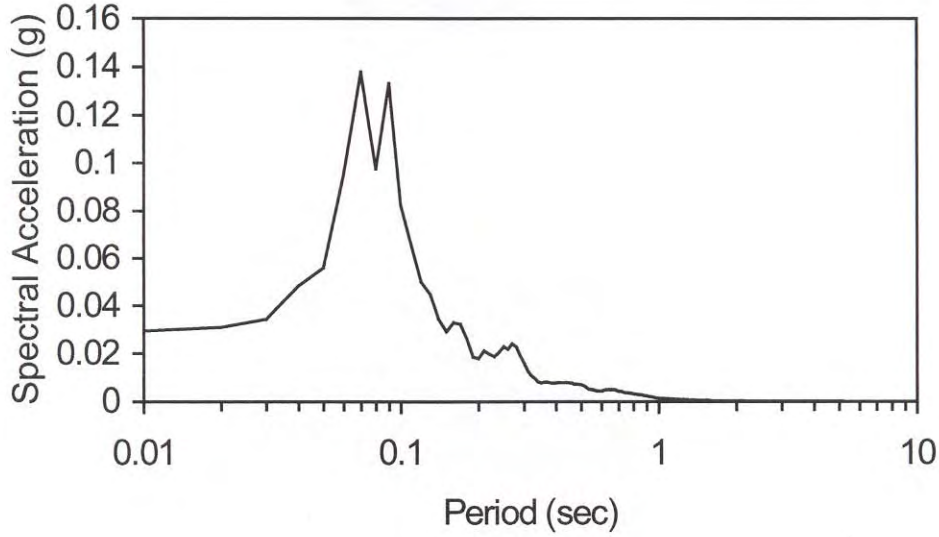
Spectral Acceleration (g)
0
0.02
0.04
0.06
0.08
0.1
0.12
0.14
0.16
0.01
0.1
1
10
Period (sec)

Site 26

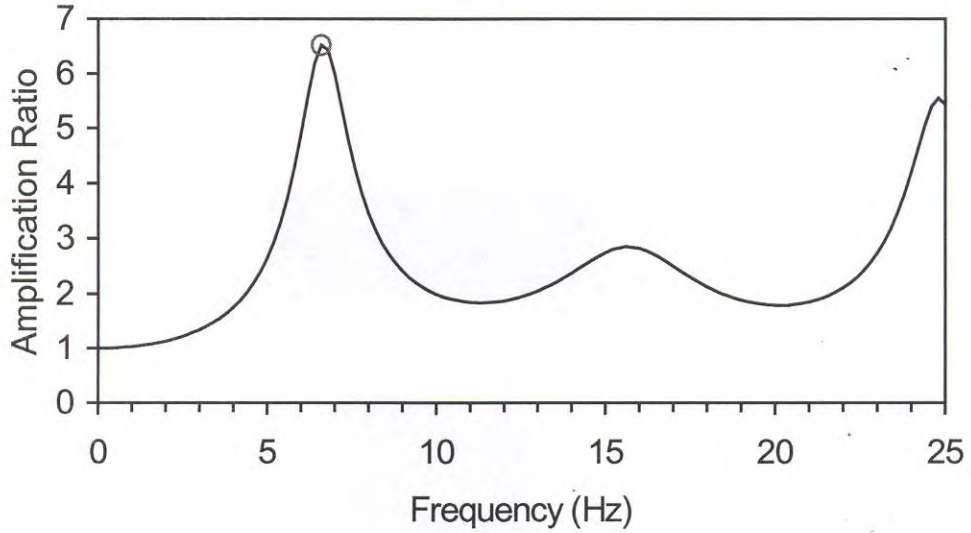
Amplification Ratio
0
1
2
3
4
5
6
7
0
5
10
15
20
25
Frequency (Hz)

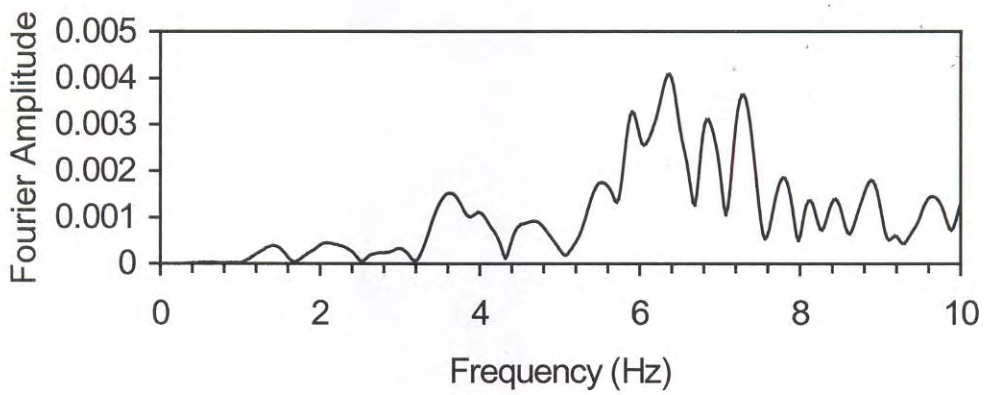
Fourier Amplitude
0
0.001
0.002
0.003
0.004
0.005
0
2
4
6
8
10
Frequency (Hz)

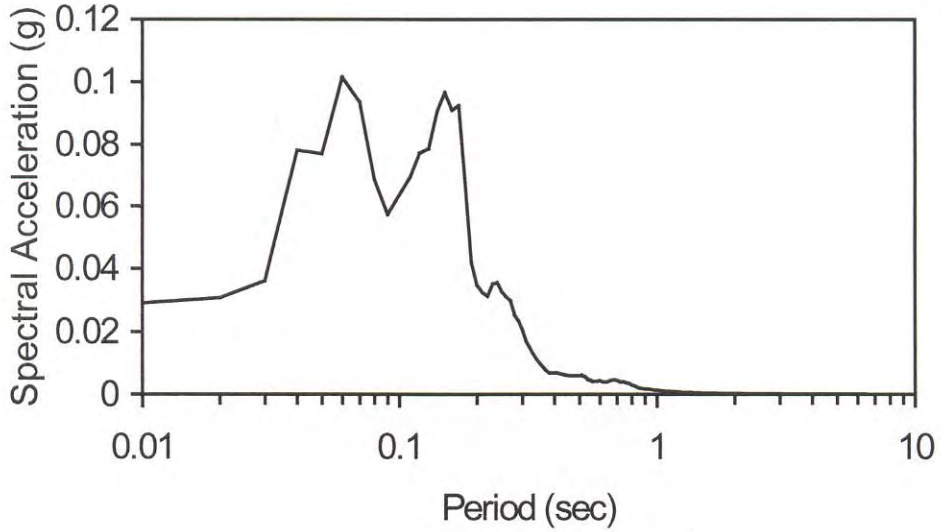
Spectral Acceleration (g)
0
0.02
0.04
0.06
0.08
0.1
0.12
0.01
0.1
1
10
Period (sec)

Site 30

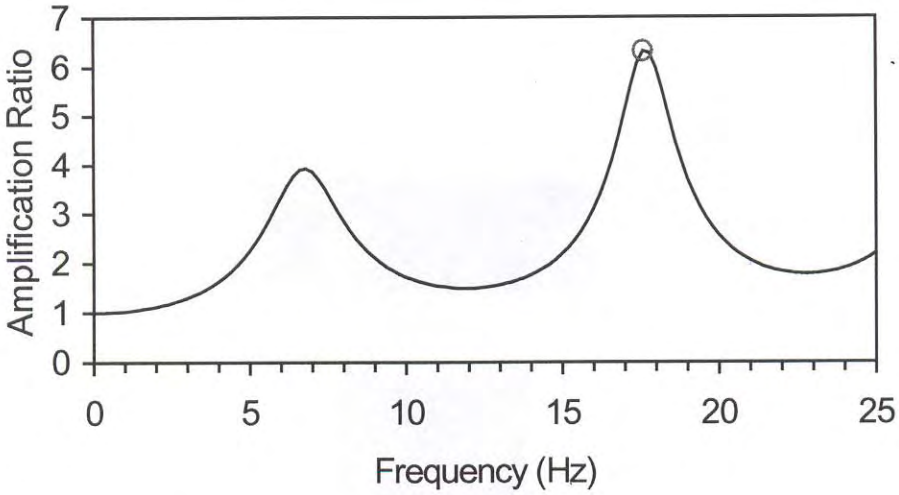
Amplification Ratio
0
1
2
3
4
5
6
7
0
5
10
15
20
25
Frequency (Hz)

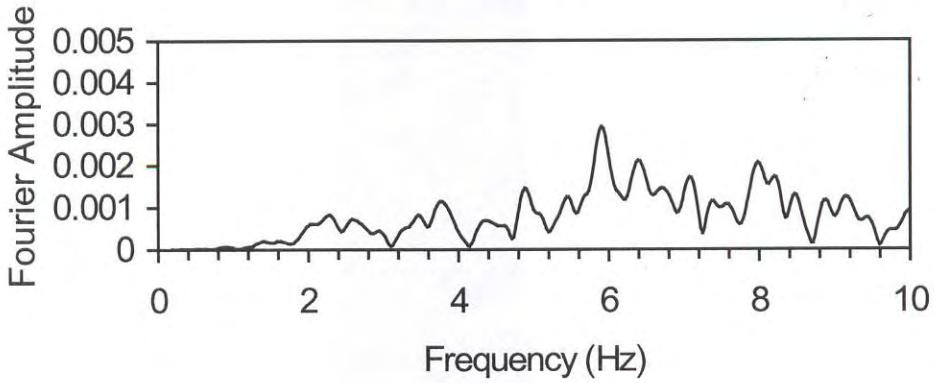
Fourier Amplitude
0
0.001
0.002
0.003
0.004
0.005
0
2
4
6
8
10
Frequency (Hz)

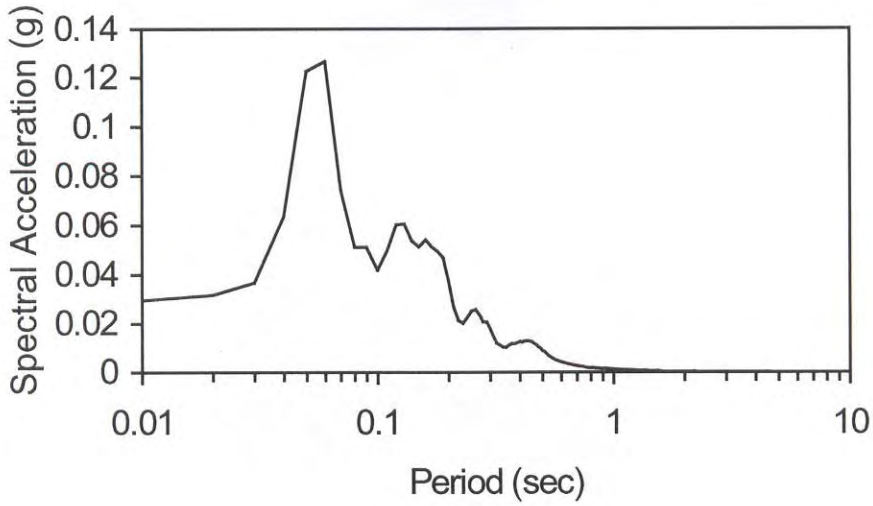
Spectral Acceleration (g)
0
0.02
0.04
0.06
0.08
0.1
0.12
0.14
0.01
0.1
1
10
Period (sec)

Site 31

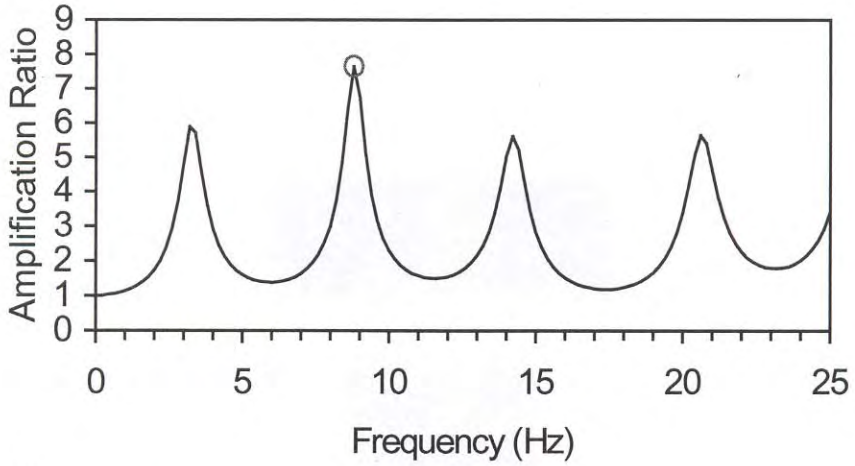
Amplification Ratio
0
1
2
3
4
5
6
7
8
9
0
5
10
15
20
25
Frequency (Hz)

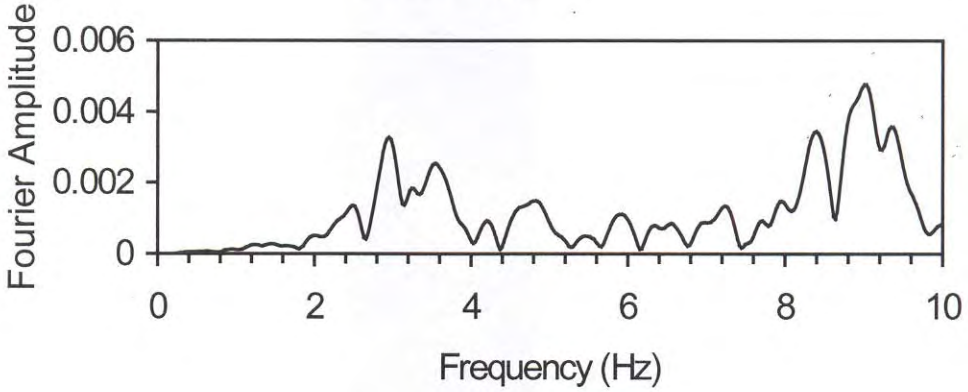
Fourier Amplitude
0
0.002
0.004
0.006
0
2
4
6
8
10
Frequency (Hz)

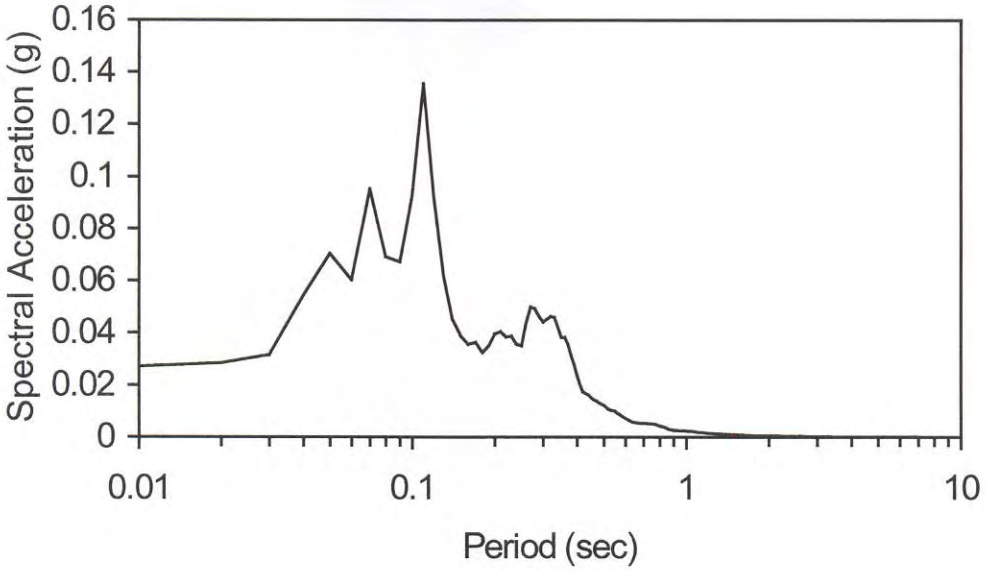
Spectral Acceleration (g)
0
0.02
0.04
0.06
0.08
0.1
0.12
0.14
0.16
0.01
0.1
1
10
Period (sec)

Site 32

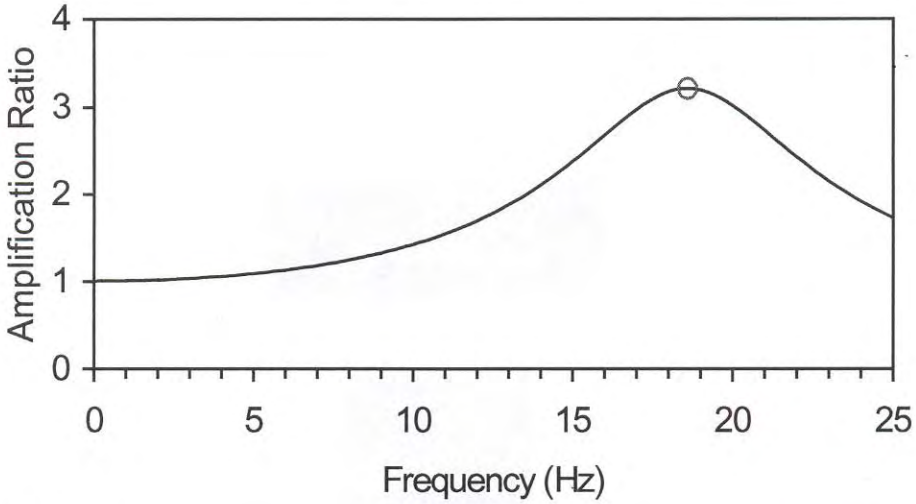
Amplification Ratio
0
1
2
3
4
0
5
10
15
20
25
Frequency (Hz)

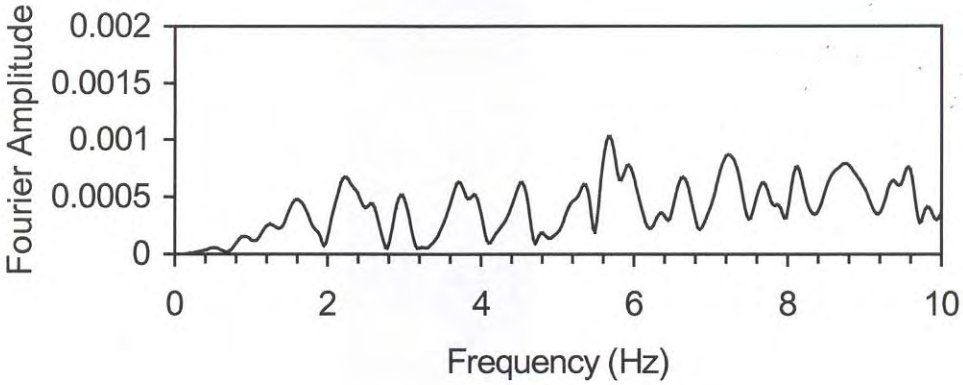
Fourier Amplitude
0
0.0005
0.001
0.0015
0.002
0
2
4
6
8
10
Frequency (Hz)

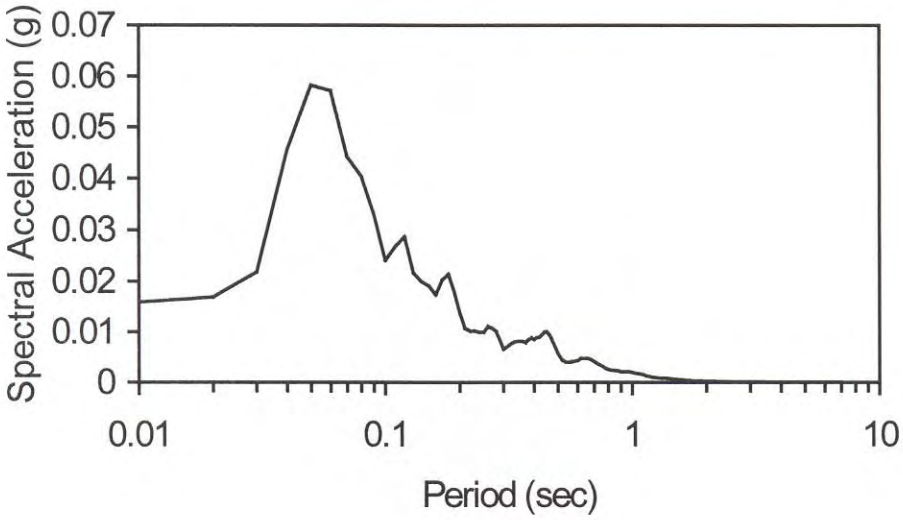
Spectral Acceleration (g)
0
0.01
0.02
0.03
0.04
0.05
0.06
0.07
0.01
0.1
1
10
Period (sec)

Site 33

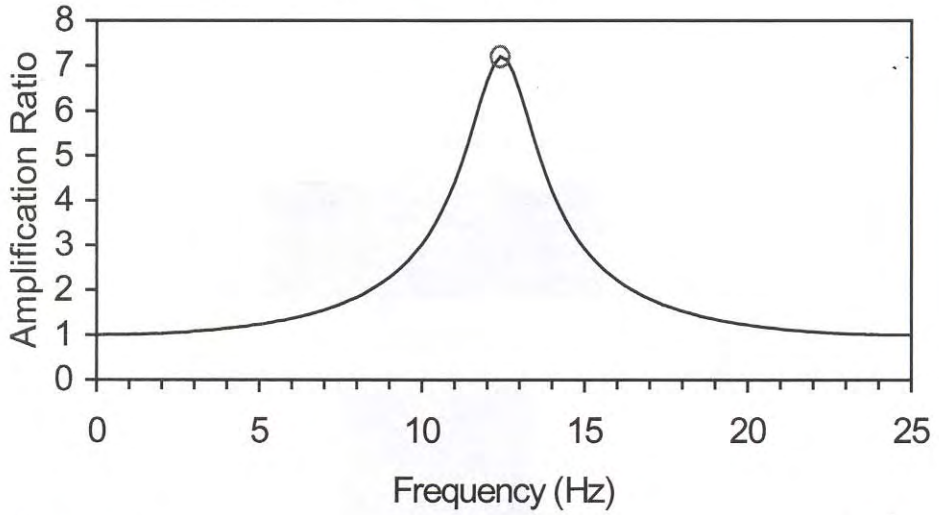
Amplification Ratio
0
1
2
3
4
5
6
7
8
0
5
10
15
20
25
Frequency (Hz)

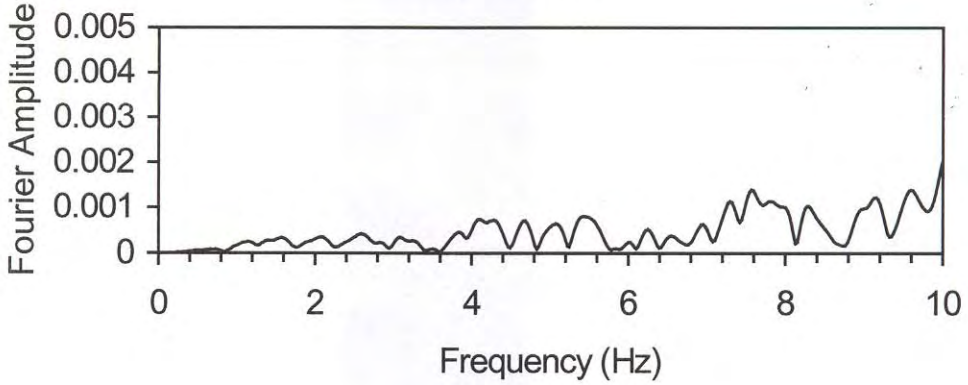
Fourier Amplitude
0
0.001
0.002
0.003
0.004
0.005
0
2
4
6
8
10
Frequency (Hz)

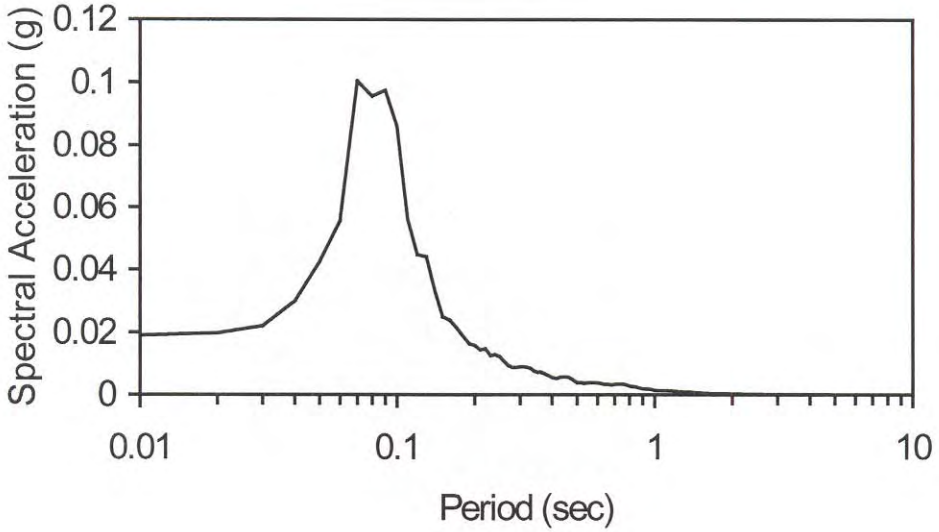
Spectral Acceleration (g)
0
0.02
0.04
0.06
0.08
0.1
0.12
0.01
0.1
1
10
Period (sec)

Site 34

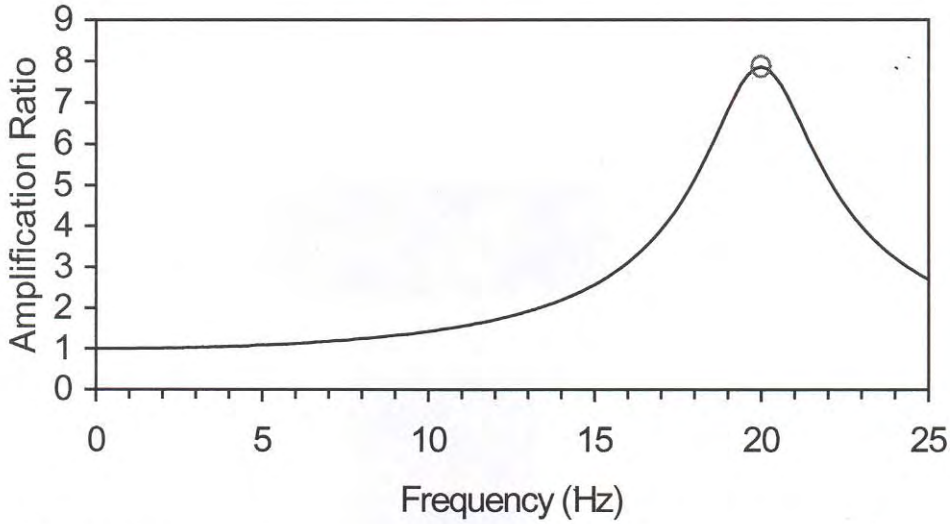
Amplification Ratio
0
1
2
3
4
5
6
7
8
9
0
5
10
15
20
25
Frequency (Hz)

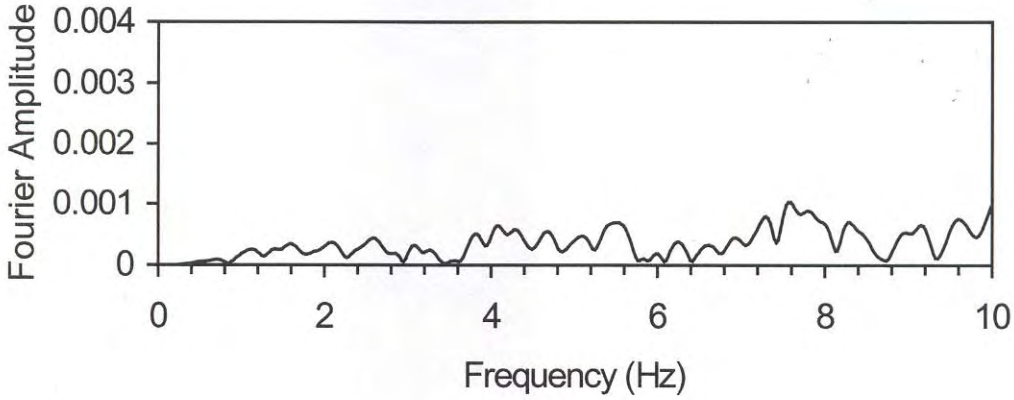
Fourier Amplitude
0
0.001
0.002
0.003
0.004
0
2
4
6
8
10
Frequency (Hz)

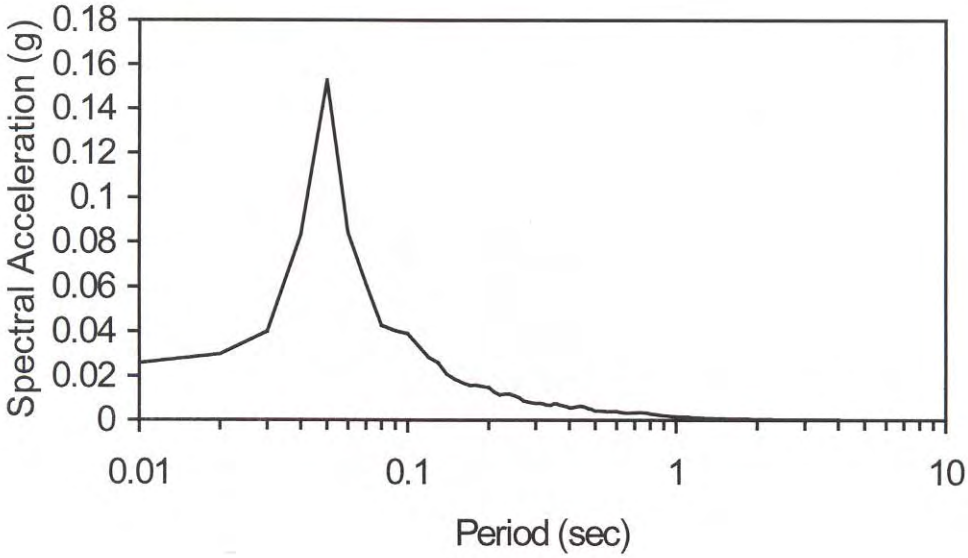
Spectral Acceleration (g)
0
0.02
0.04
0.06
0.08
0.1
0.12
0.14
0.16
0.18
0.01
0.1
1
10
Period (sec)

Site 35

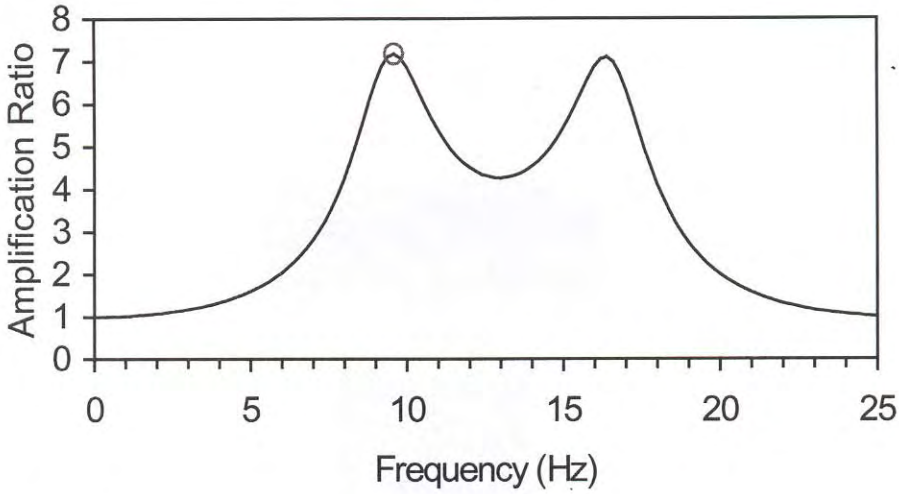
Amplification Ratio
0
1
2
3
4
5
6
7
8
0
5
10
15
20
25
Frequency (Hz)

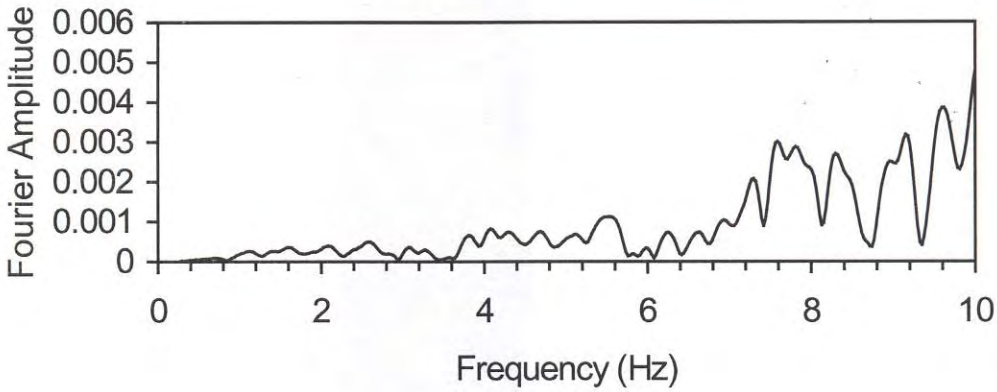
Fourier Amplitude
0
0.001
0.002
0.003
0.004
0.005
0.006
0
2
4
6
8
10
Frequency (Hz)

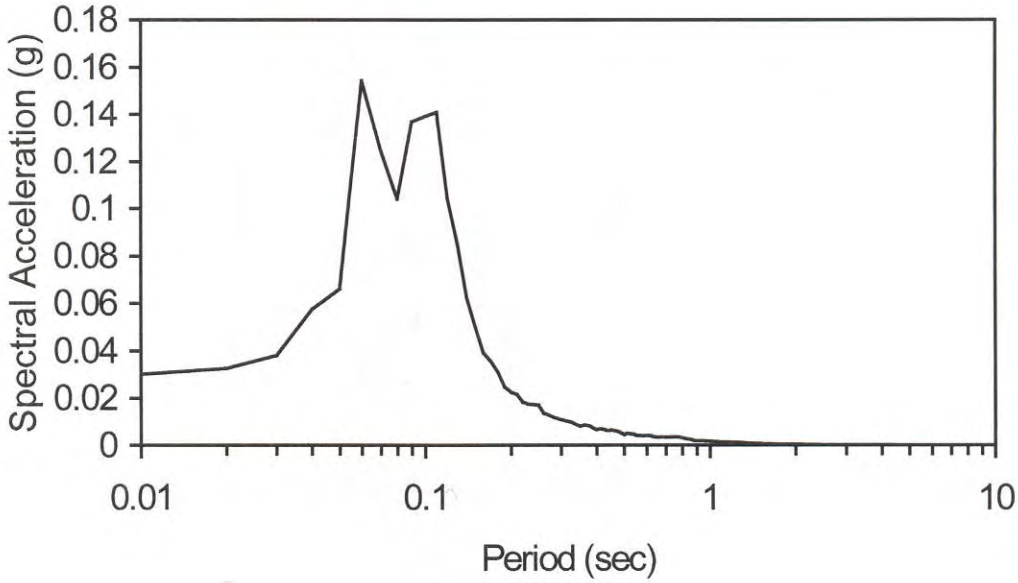
Spectral Acceleration (g)
0
0.02
0.04
0.06
0.08
0.1
0.12
0.14
0.16
0.18
0.01
0.1
1
10
Period (sec)

Site 37

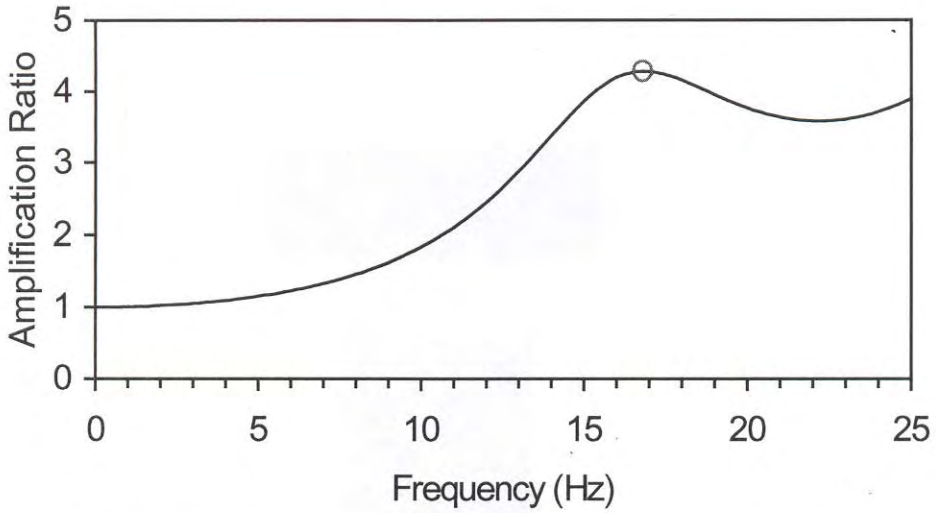
Amplification Ratio
0
1
2
3
4
5
0
5
10
15
20
25
Frequency (Hz)

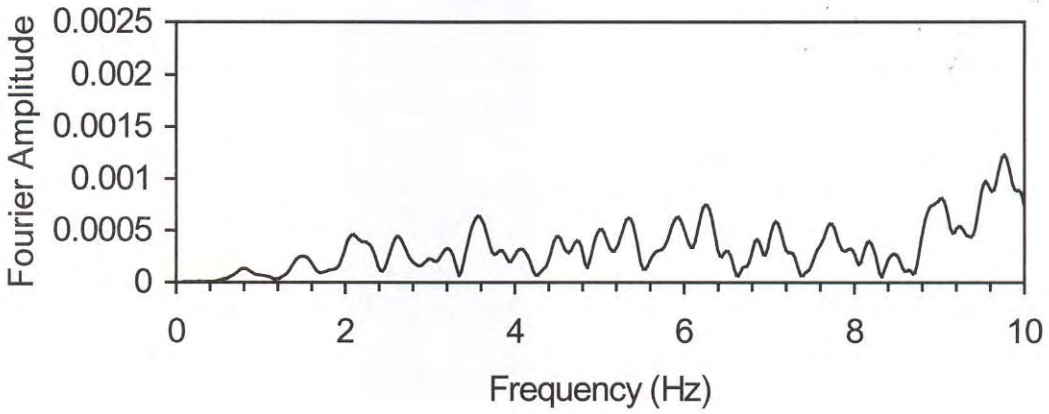
Fourier Amplitude
0
0.0005
0.001
0.0015
0.002
0.0025
0
2
4
6
8
10
Frequency (Hz)

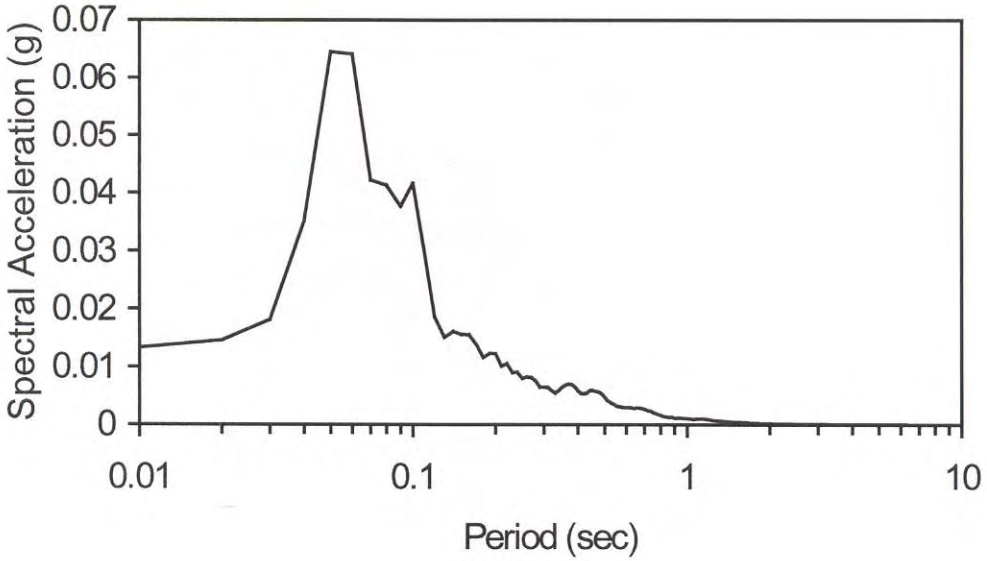
Spectral Acceleration (g)
0
0.01
0.02
0.03
0.04
0.05
0.06
0.07
0.01
0.1
1
10
Period (sec)

Site 38

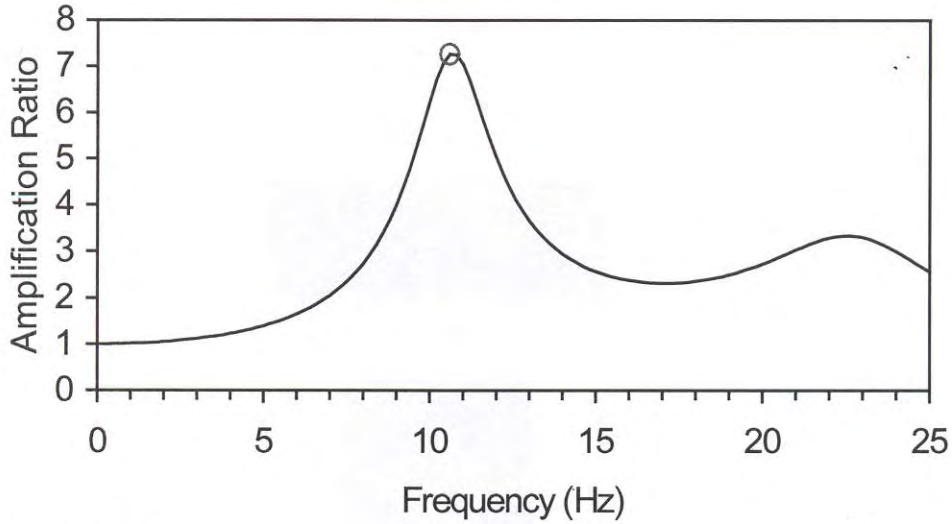
Amplification Ratio
0
1
2
3
4
5
6
7
8
0
5
10
15
20
25
Frequency (Hz)

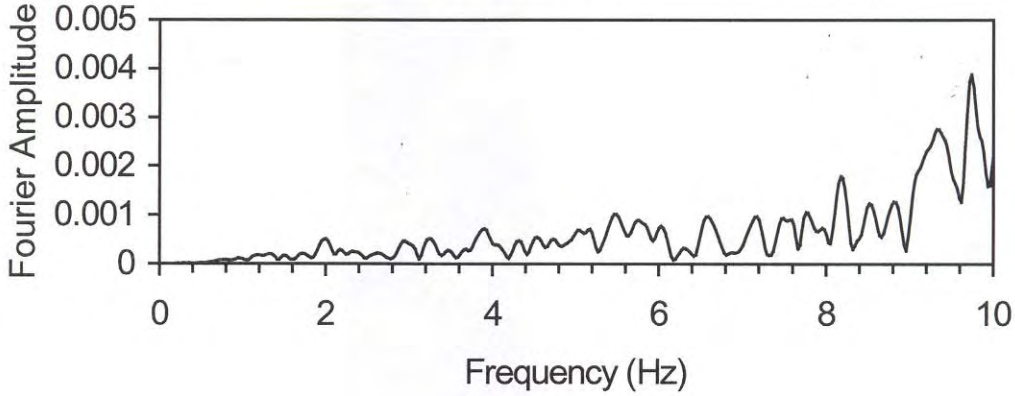
Fourier Amplitude
0
0.001
0.002
0.003
0.004
0.005
0
2
4
6
8
10
Frequency (Hz)

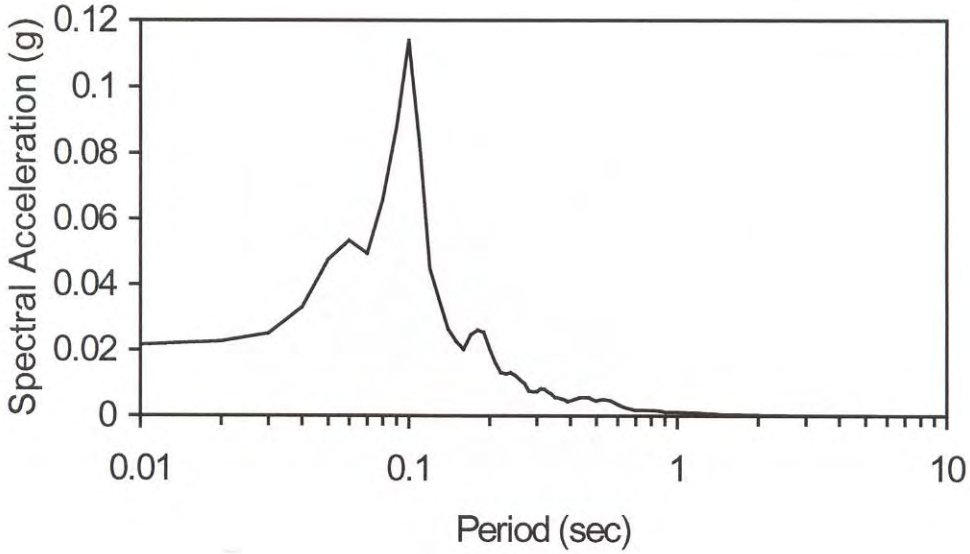
Spectral Acceleration (g)
0
0.02
0.04
0.06
0.08
0.1
0.12
0.01
0.1
1
10
Period (sec)

Site 39

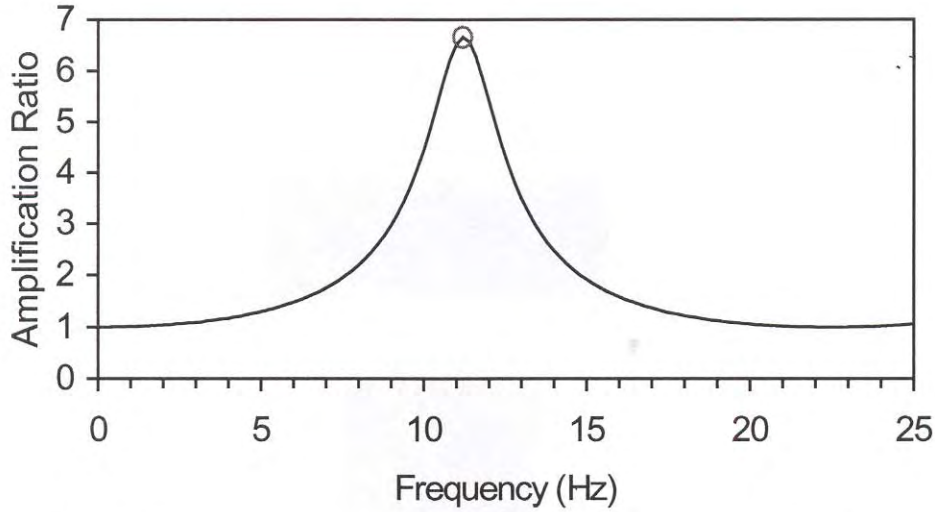
Amplification Ratio
0
1
2
3
4
5
6
7
0
5
10
15
20
25
Frequency (Hz)

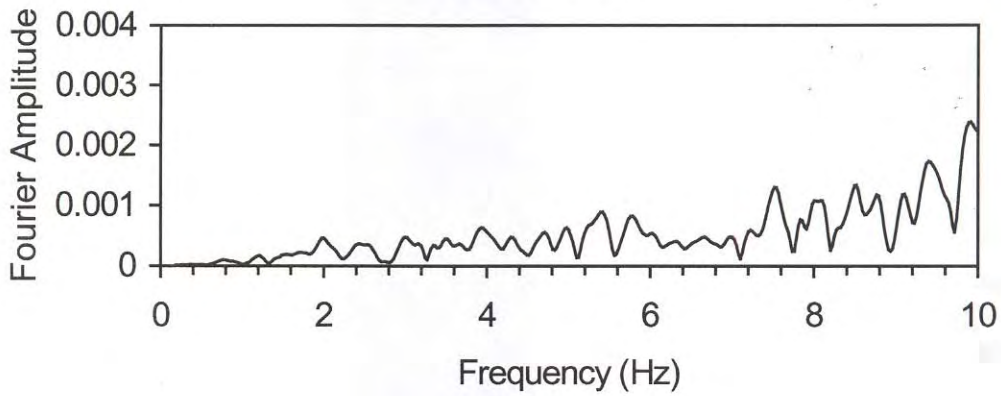
Fourier Amplitude
0
0.001
0.002
0.003
0.004
0
2
4
6
8
10
Frequency (Hz)

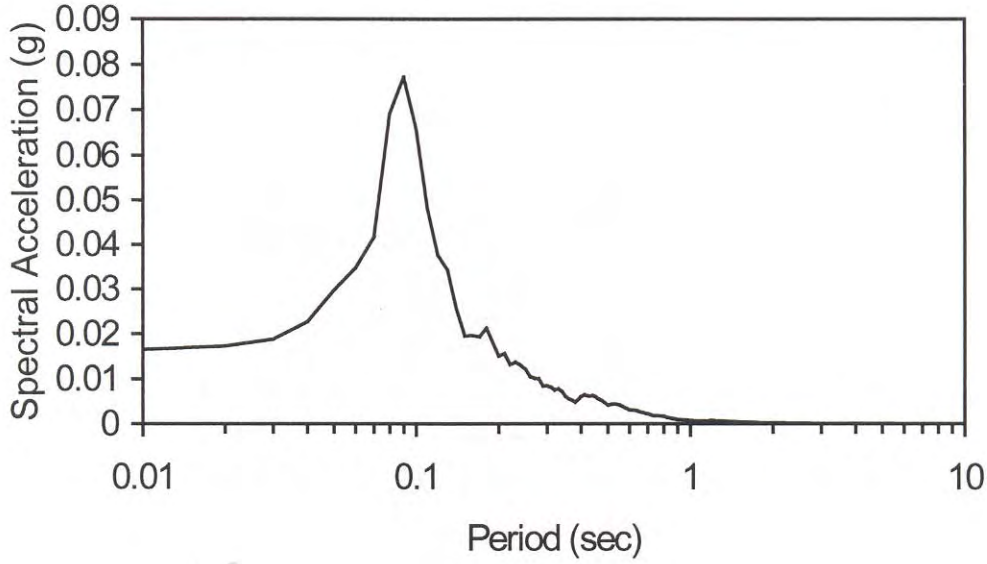
Spectral Acceleration (g)
0
0.01
0.02
0.03
0.04
0.05
0.06
0.07
0.08
0.09
0.01
0.1
1
10
Period (sec)

Site 40

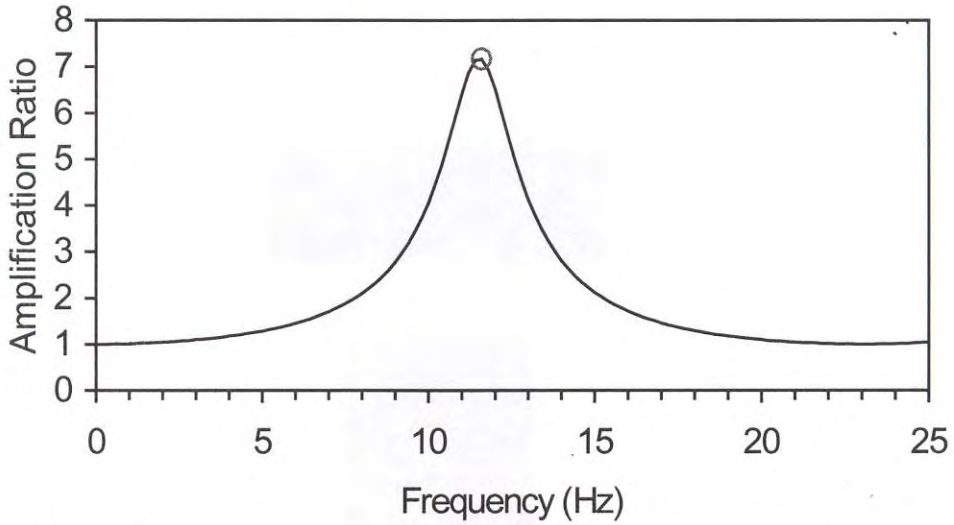
Amplification Ratio
0
1
2
3
4
5
6
7
8
0
5
10
15
20
25
Frequency (Hz)

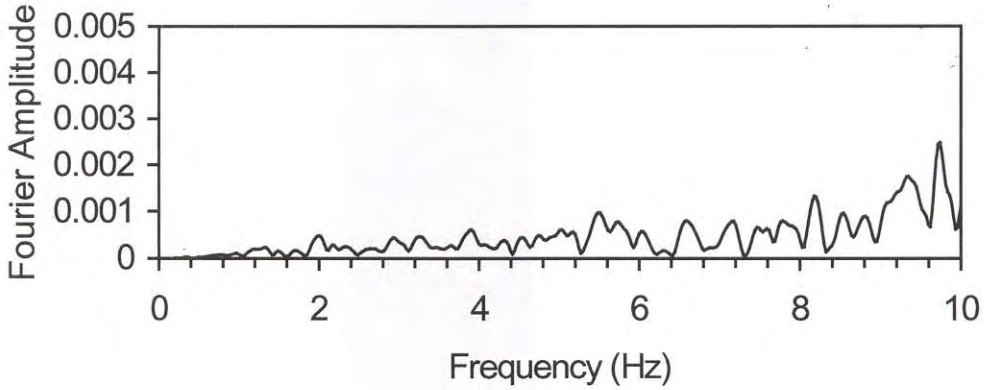
Fourier Amplitude
0
0.001
0.002
0.003
0.004
0.005
0
2
4
6
8
10
Frequency (Hz)

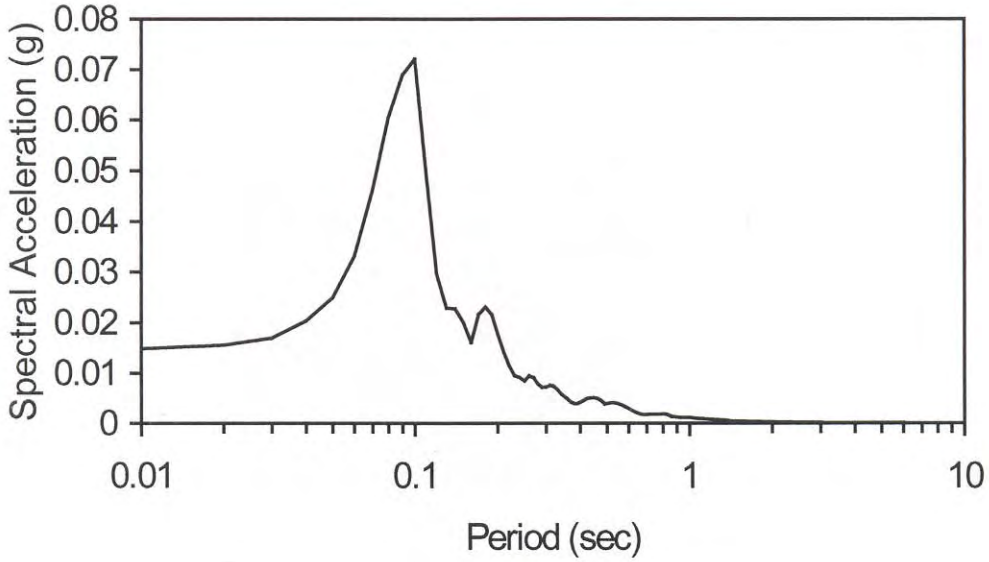
Spectral Acceleration (g)
0
0.01
0.02
0.03
0.04
0.05
0.06
0.07
0.08
0.01
0.1
1
10
Period (sec)

Site 41

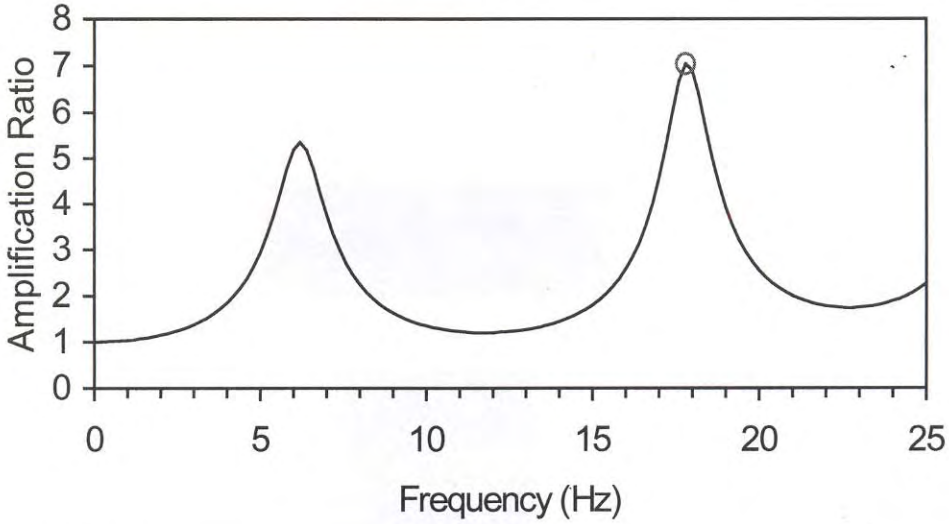
Amplification Ratio
0
1
2
3
4
5
6
7
8
0
5
10
15
20
25
Frequency (Hz)

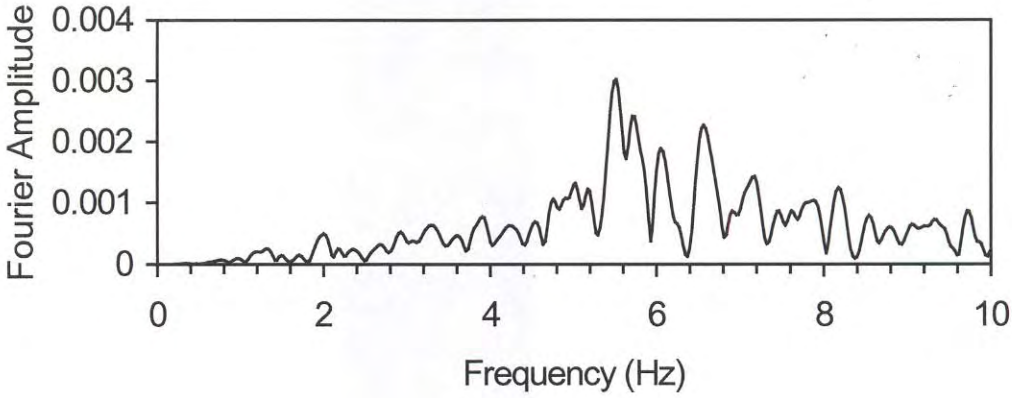
Fourier Amplitude
0
0.001
0.002
0.003
0.004
0
2
4
6
8
10
Frequency (Hz)

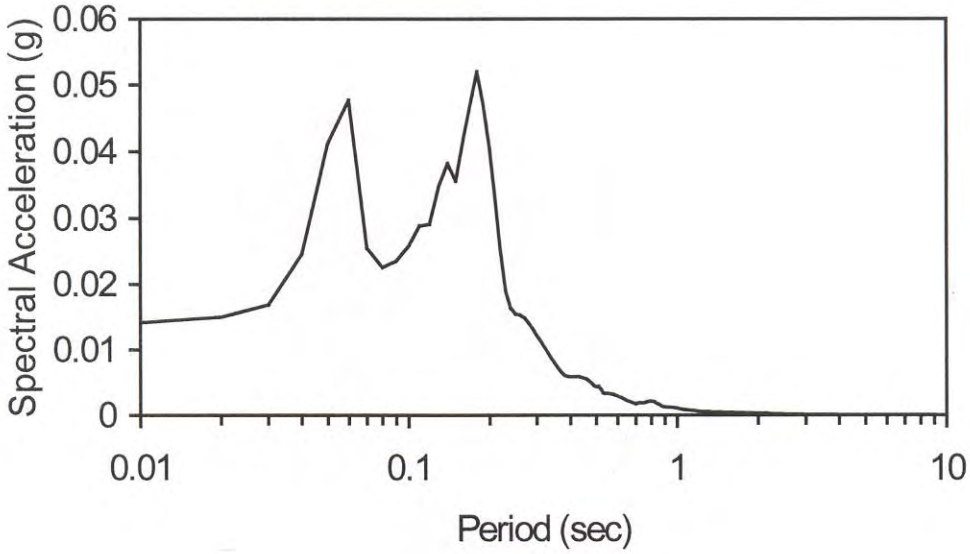
Spectral Acceleration (g)
0
0.01
0.02
0.03
0.04
0.05
0.06
0.01
0.1
1
10
Period (sec)

Site 42

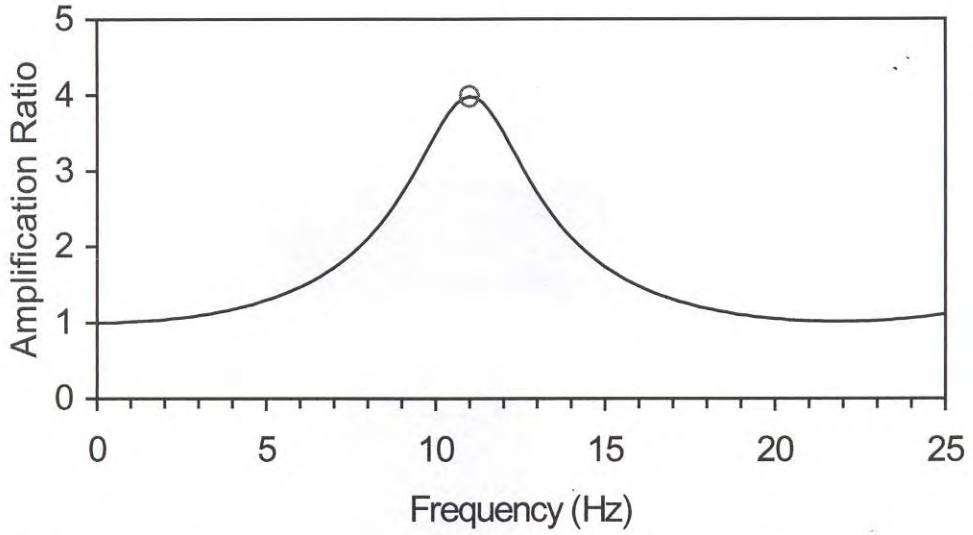
Amplification Ratio
0
1
2
3
4
5
0
5
10
15
20
25
Frequency (Hz)

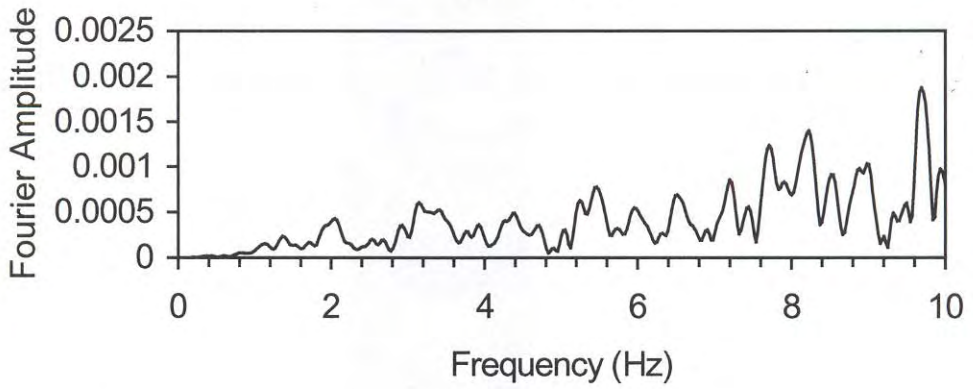
Fourier Amplitude
0
0.0005
0.001
0.0015
0.002
0.0025
0
2
4
6
8
10
Frequency (Hz)

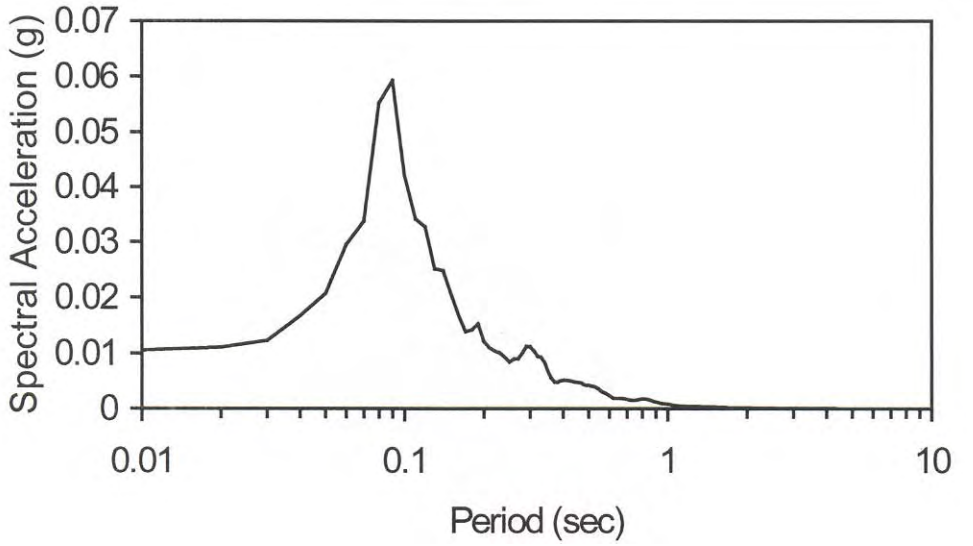
Spectral Acceleration (g)
0
0.01
0.02
0.03
0.04
0.05
0.06
0.07
0.01
0.1
1
10
Period (sec)

APPENDIX C

Site Response – HVSR:

Ambient Noise (dashed line)

Earthquake S-wave (solid line)

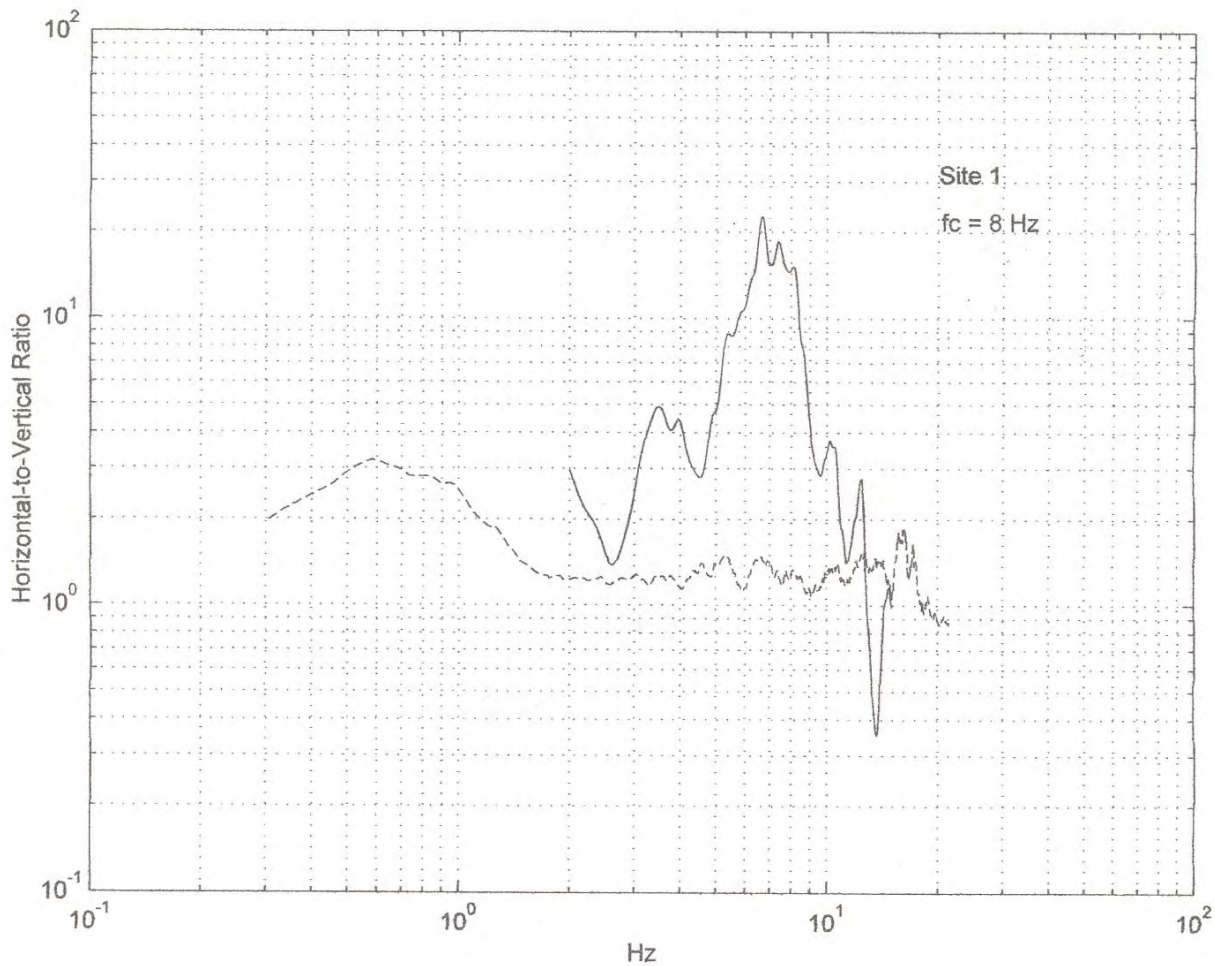
Site 1
fc = 8 Hz
Horizontal-to-Vertical Ratio
Hz
10^{2}
10^{1}
10^{0}
10^{-1}
10^{-1}
10^{0}
10^{1}
10^{2}

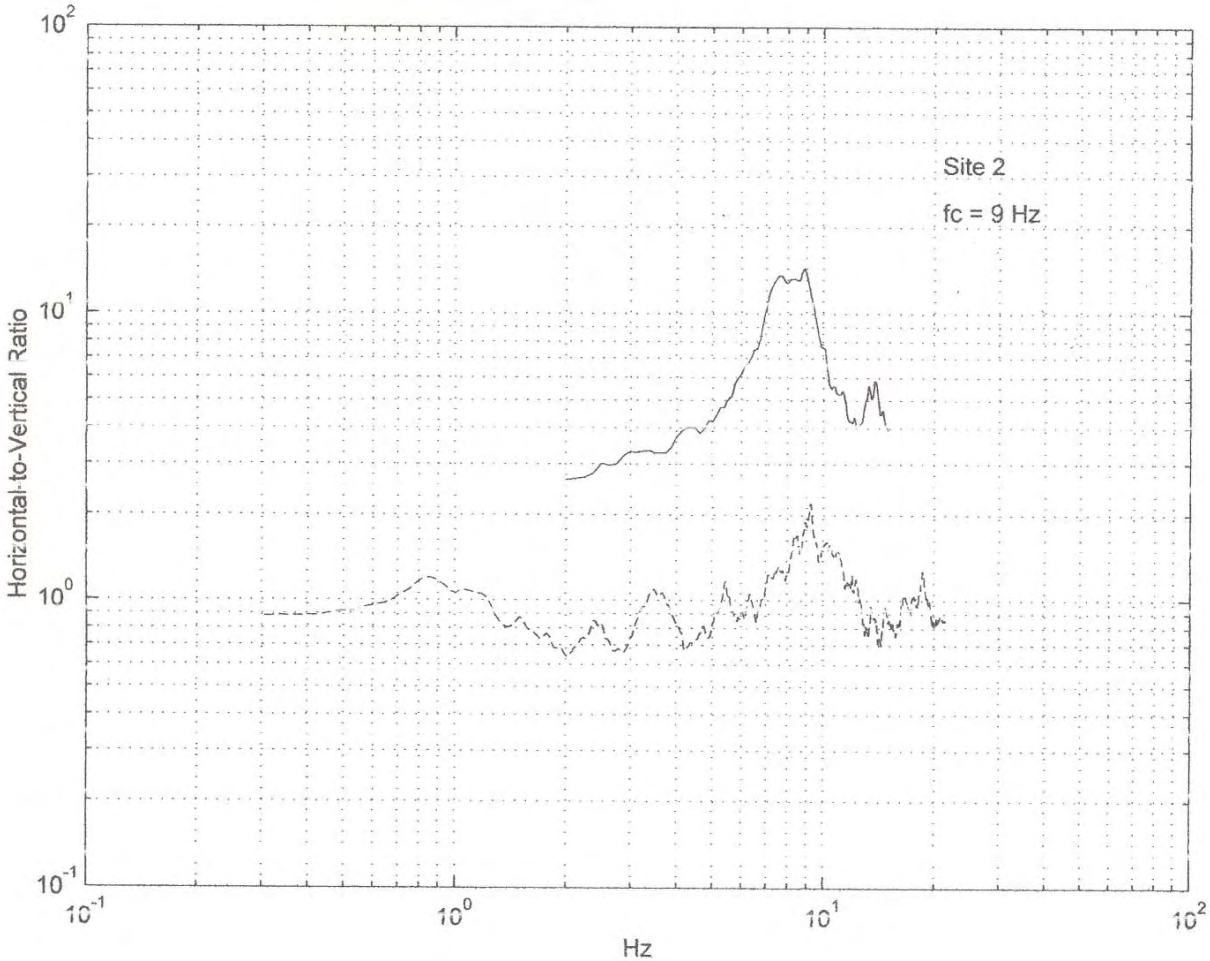
Site 2
fc = 9 Hz
Horizontal-to-Vertical Ratio
Hz
10^{2}
10^{1}
10^{0}
10^{-1}
10^{-1}
10^{0}
10^{1}
10^{2}

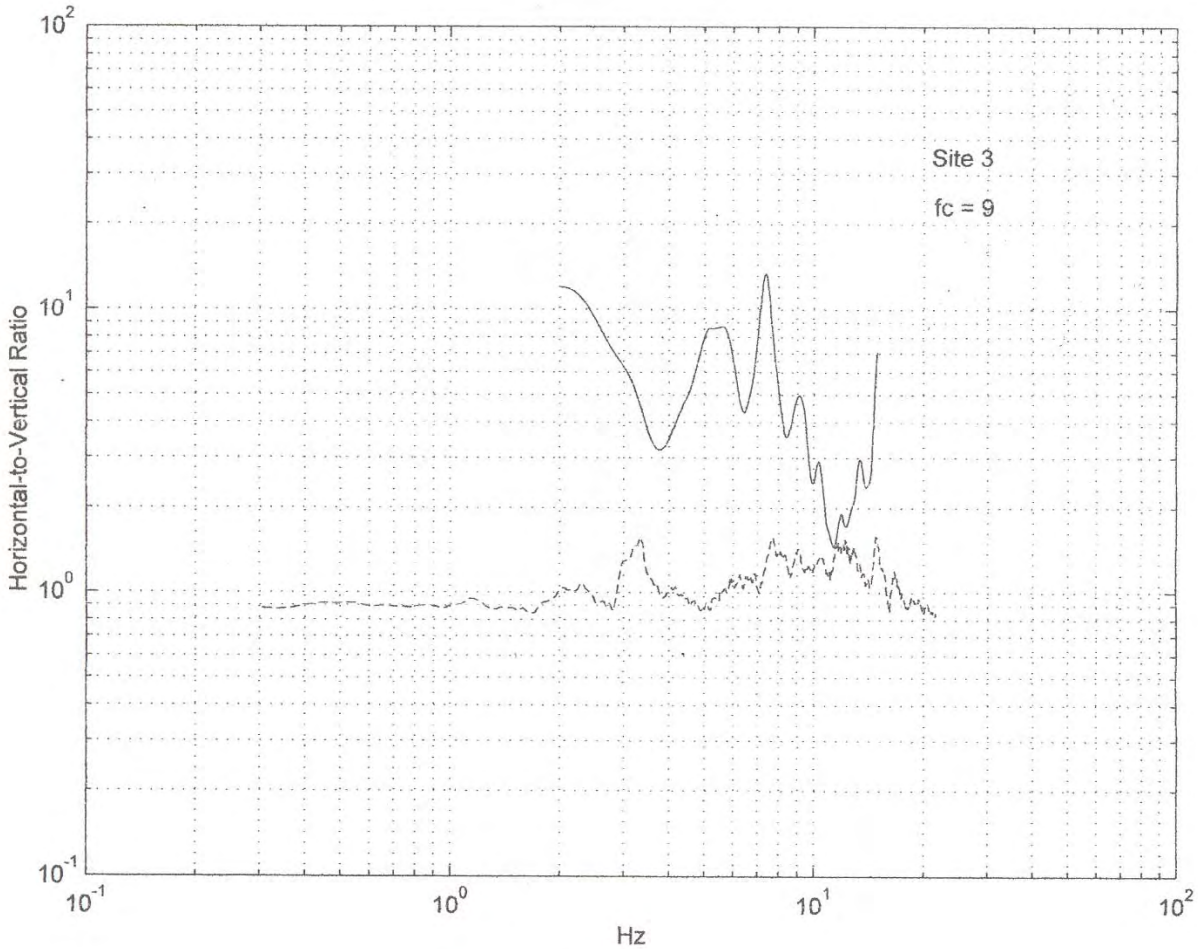
Site 3
fc = 9
Horizontal-to-Vertical Ratio
Hz
10^{2}
10^{1}
10^{0}
10^{-1}
10^{-1}
10^{0}
10^{1}
10^{2}

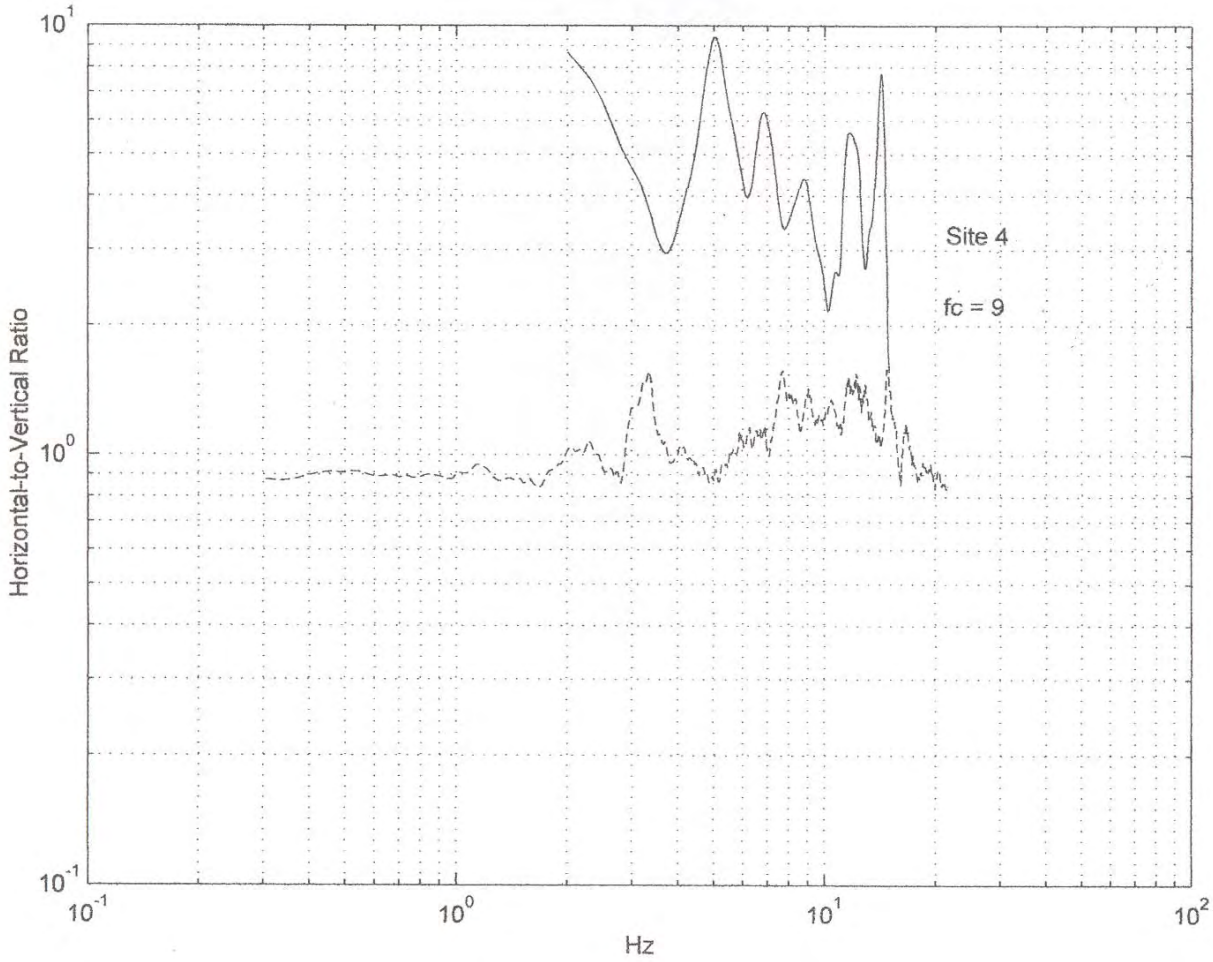
Site 4
fc = 9
Horizontal-to-Vertical Ratio
Hz
10^{1}
10^{0}
10^{-1}
10^{-1}
10^{0}
10^{1}
10^{2}

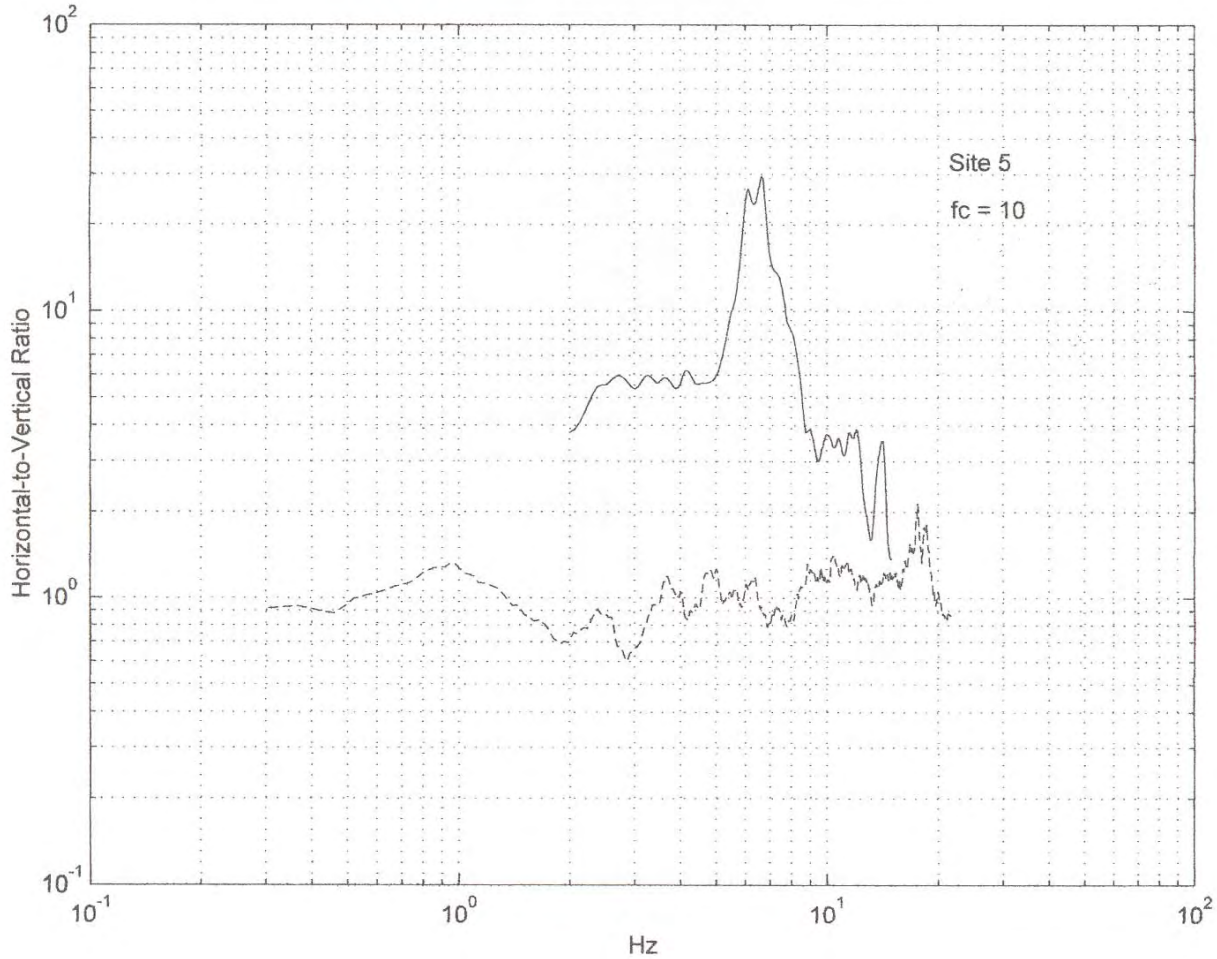
Site 5
fc = 10
Horizontal-to-Vertical Ratio
Hz
10^{2}
10^{1}
10^{0}
10^{-1}
10^{-1}
10^{0}
10^{1}
10^{2}

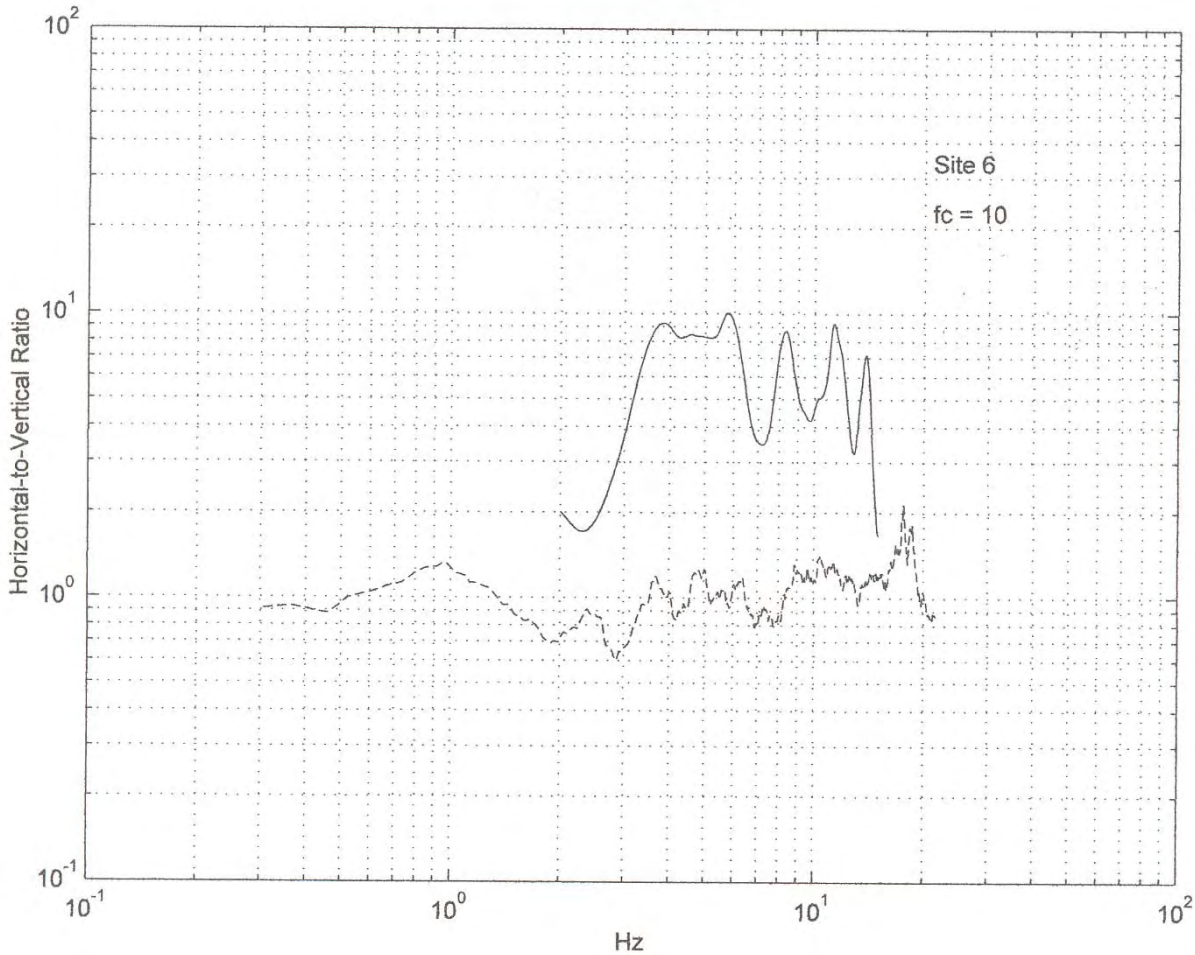
Site 6
fc = 10
Horizontal-to-Vertical Ratio
Hz
10^{2}
10^{1}
10^{0}
10^{-1}
10^{-1}
10^{0}
10^{1}
10^{2}

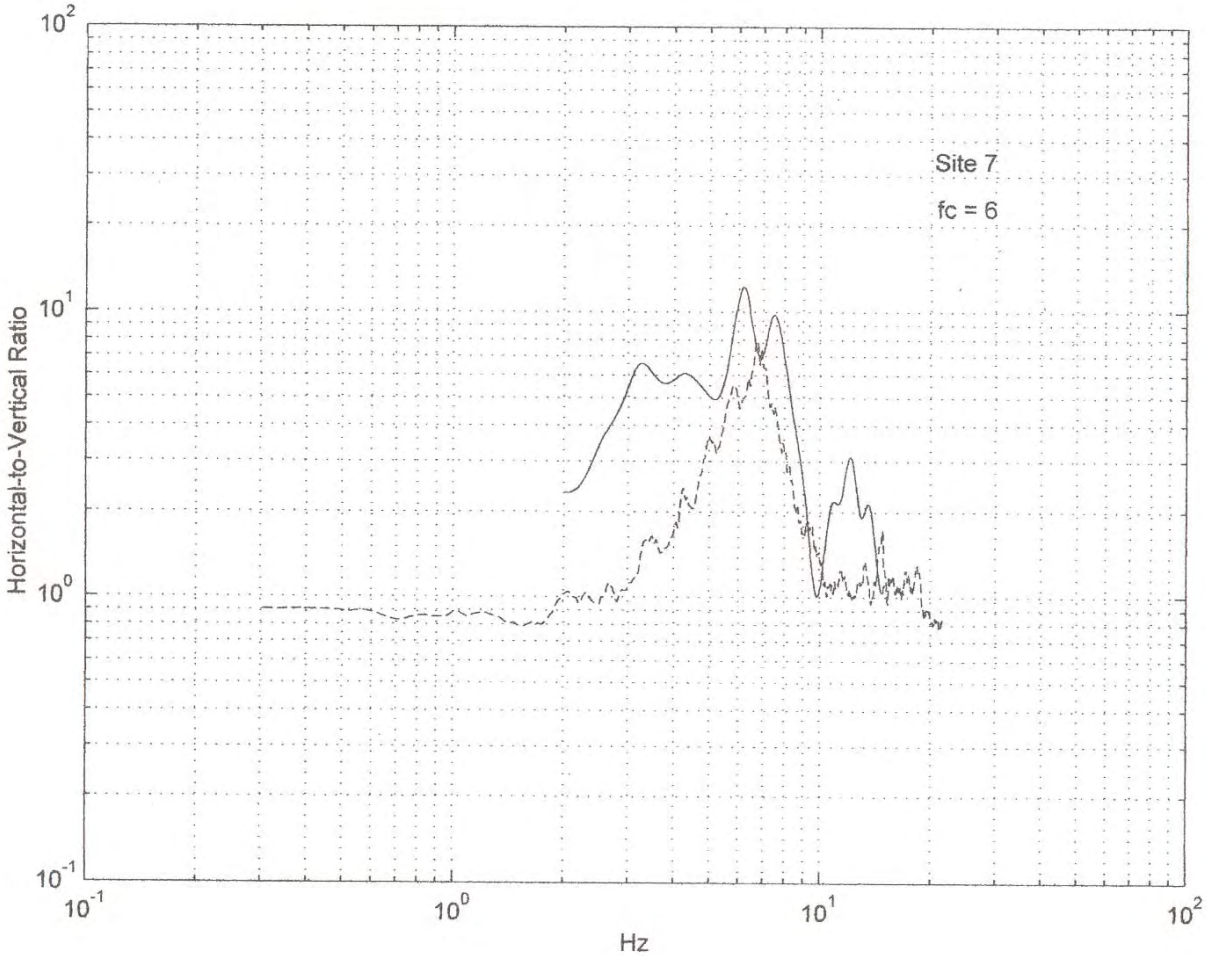
Site 7
fc = 6
Horizontal-to-Vertical Ratio
Hz
10^{2}
10^{1}
10^{0}
10^{-1}
10^{-1}
10^{0}
10^{1}
10^{2}

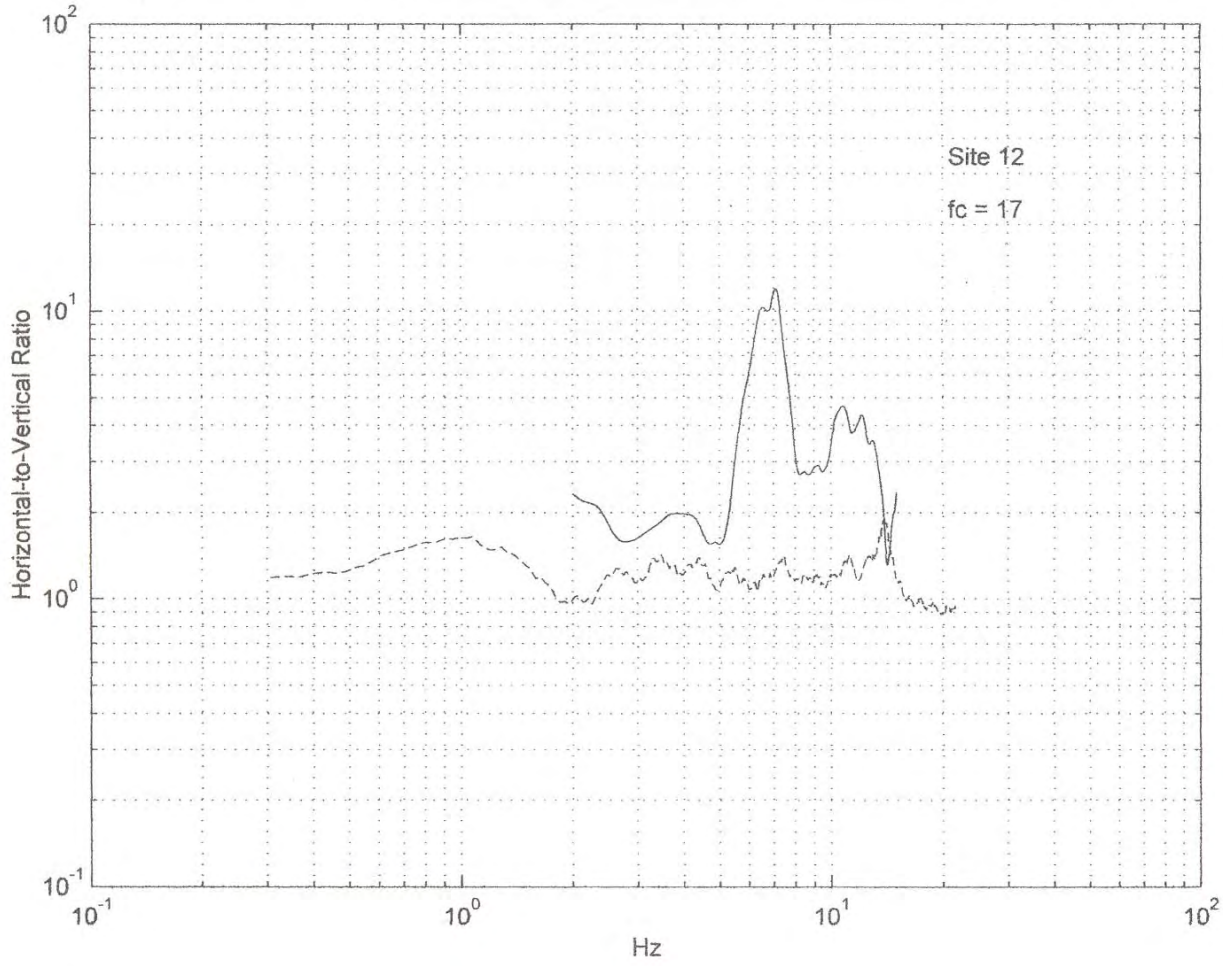
Site 12
fc = 17
Horizontal-to-Vertical Ratio
Hz
10^{2}
10^{1}
10^{0}
10^{-1}
10^{-1}
10^{0}
10^{1}
10^{2}

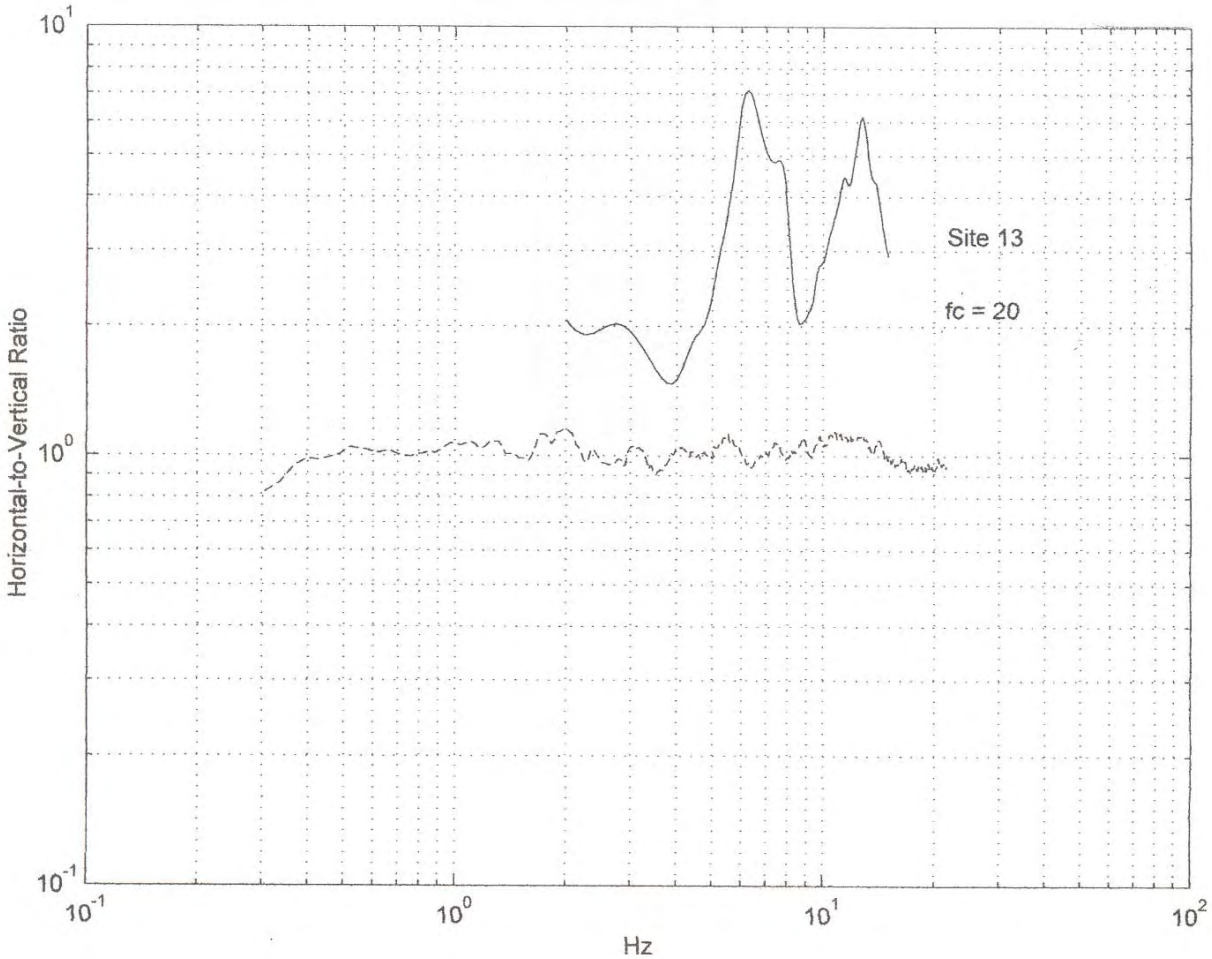
Site 13
fc = 20
Horizontal-to-Vertical Ratio
Hz
10^{1}
10^{0}
10^{-1}
10^{-1}
10^{0}
10^{1}
10^{2}

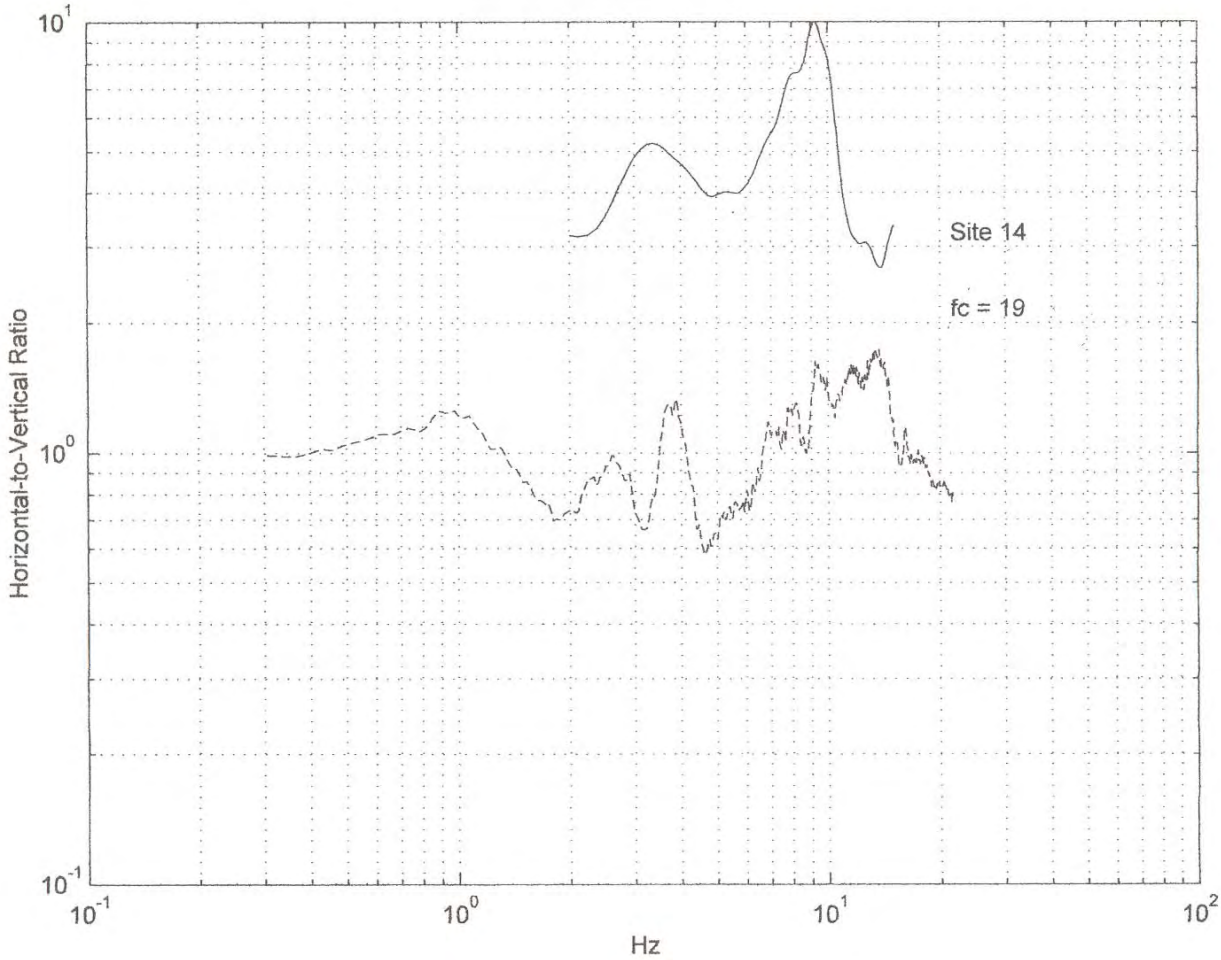
Site 14
fc = 19
Horizontal-to-Vertical Ratio
Hz
10^{1}
10^{0}
10^{-1}
10^{-1}
10^{0}
10^{1}
10^{2}

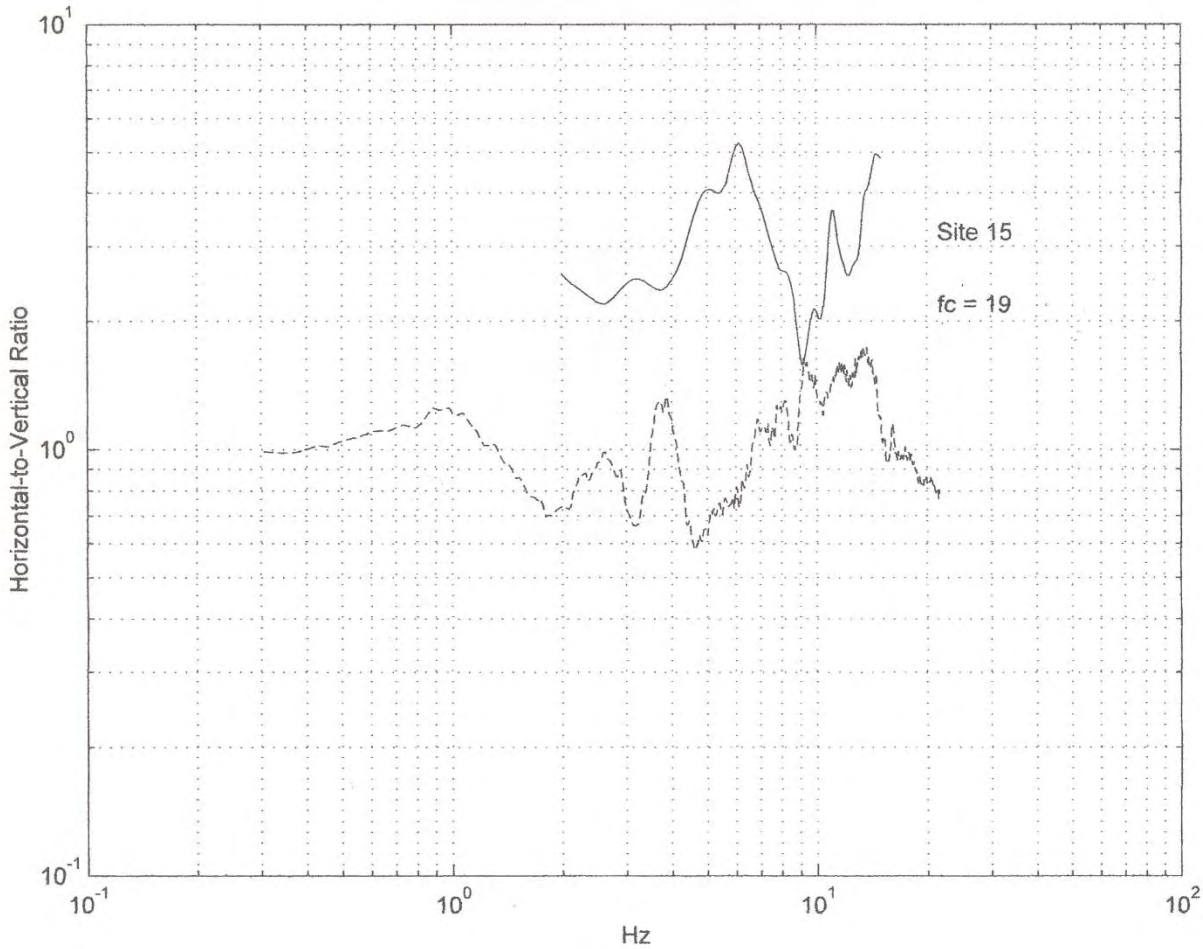
Site 15
fc = 19
Horizontal-to-Vertical Ratio
Hz
10^{1}
10^{0}
10^{-1}
10^{-1}
10^{0}
10^{1}
10^{2}

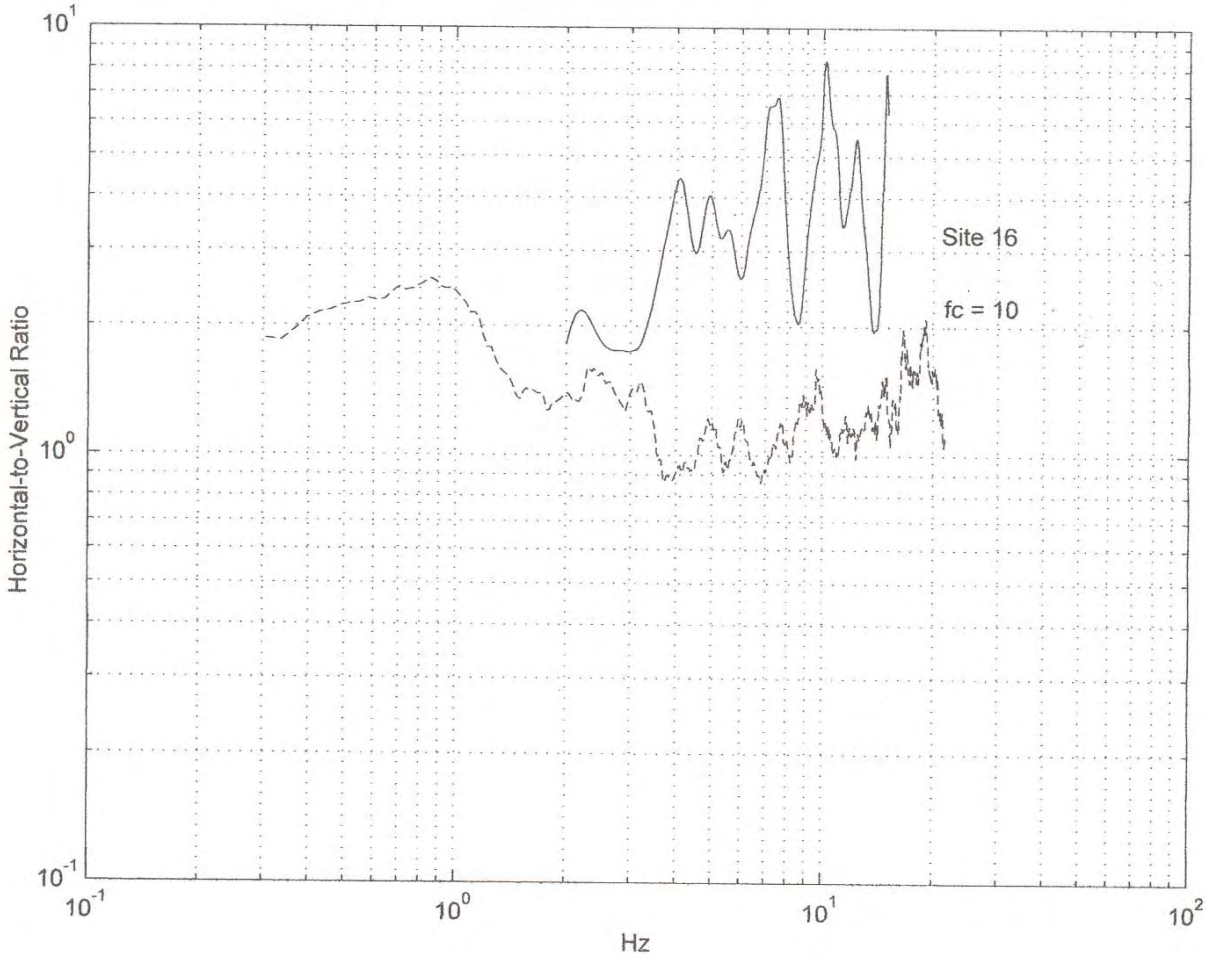
Site 16
fc = 10
Horizontal-to-Vertical Ratio
Hz
10^{1}
10^{0}
10^{-1}
10^{-1}
10^{0}
10^{1}
10^{2}

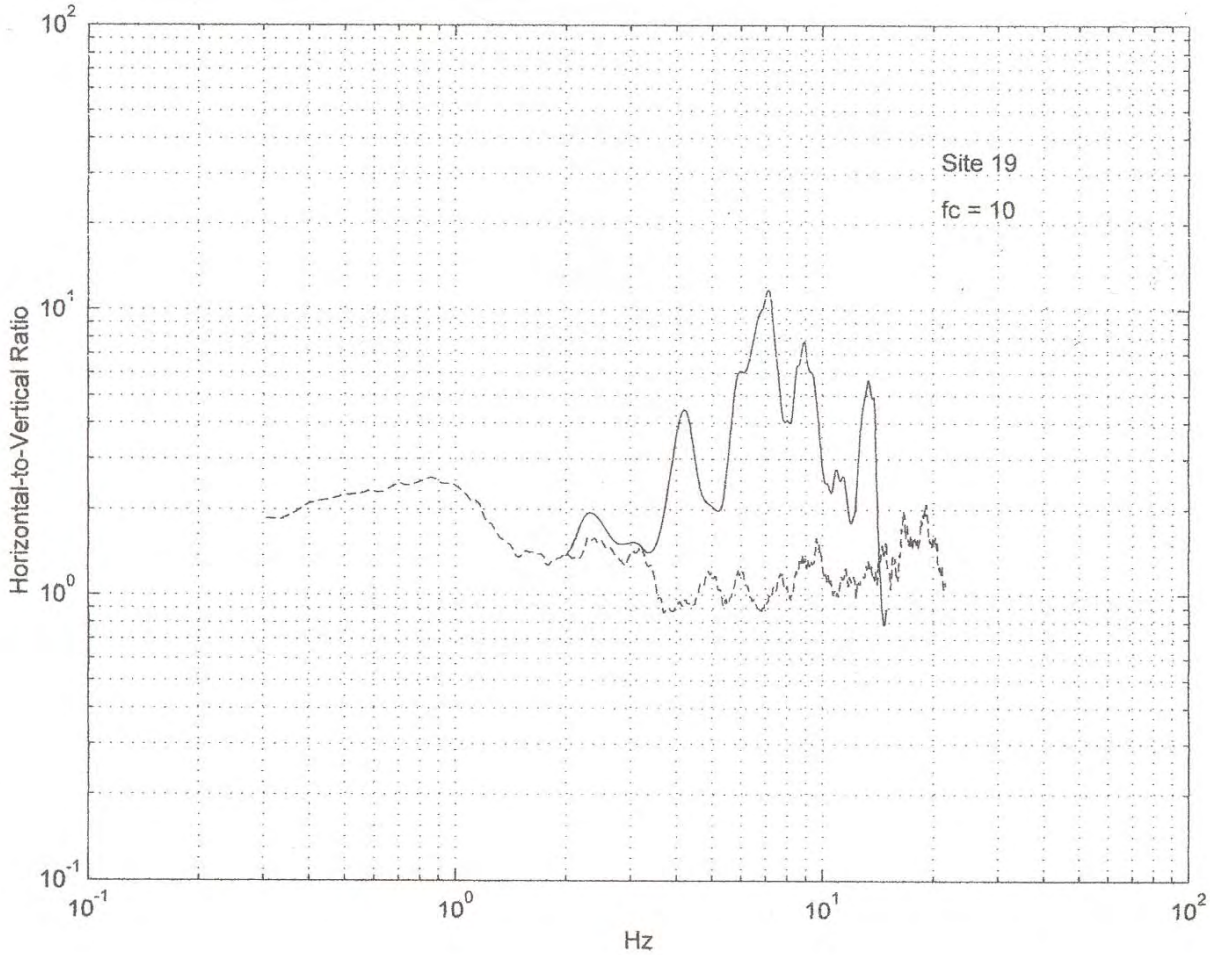
Site 19
fc = 10
Horizontal-to-Vertical Ratio
Hz
10^{2}
10^{1}
10^{0}
10^{-1}
10^{-1}
10^{0}
10^{1}
10^{2}

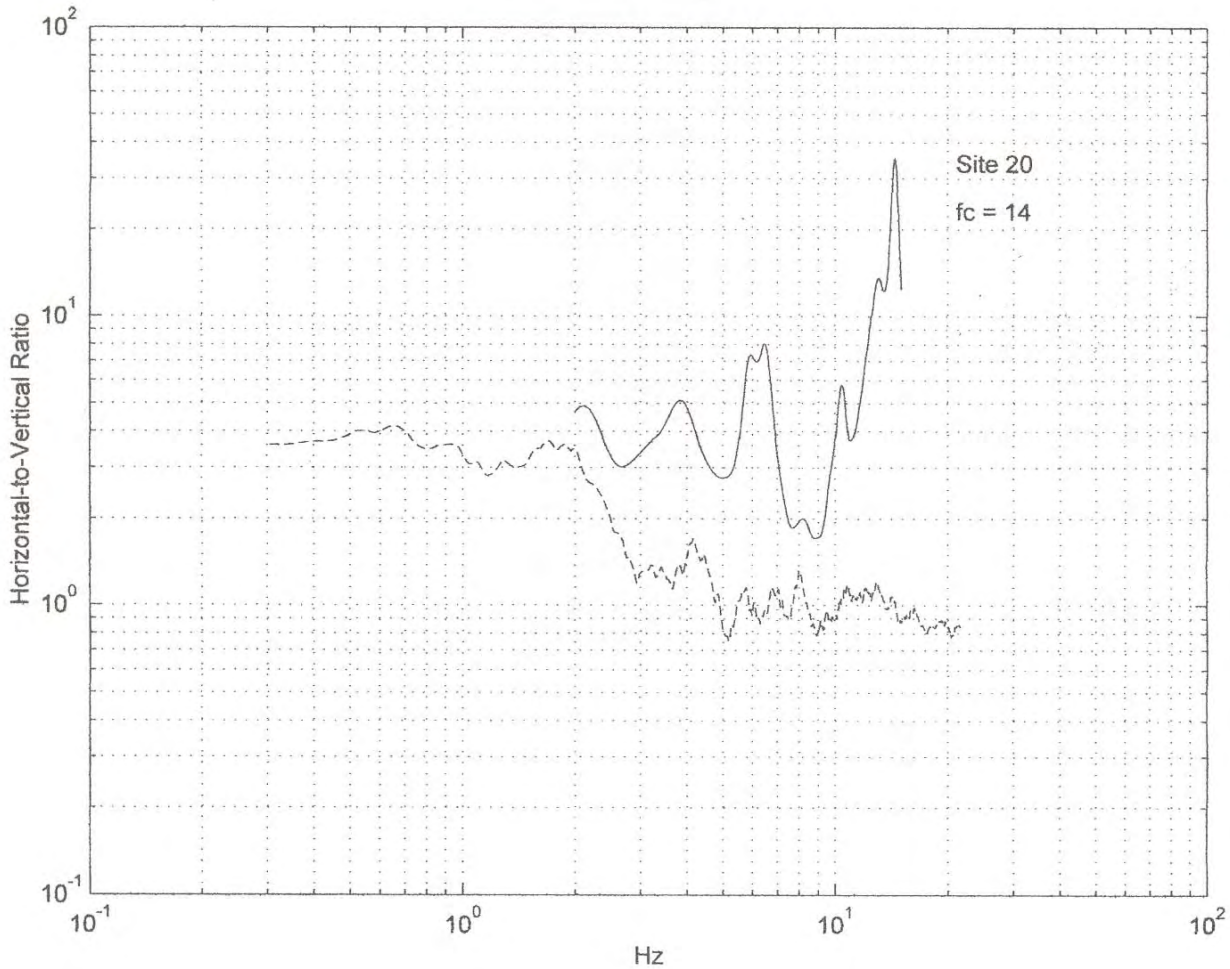
Site 20
fc = 14
Horizontal-to-Vertical Ratio
Hz
10^{2}
10^{1}
10^{0}
10^{-1}
10^{-1}
10^{0}
10^{1}
10^{2}

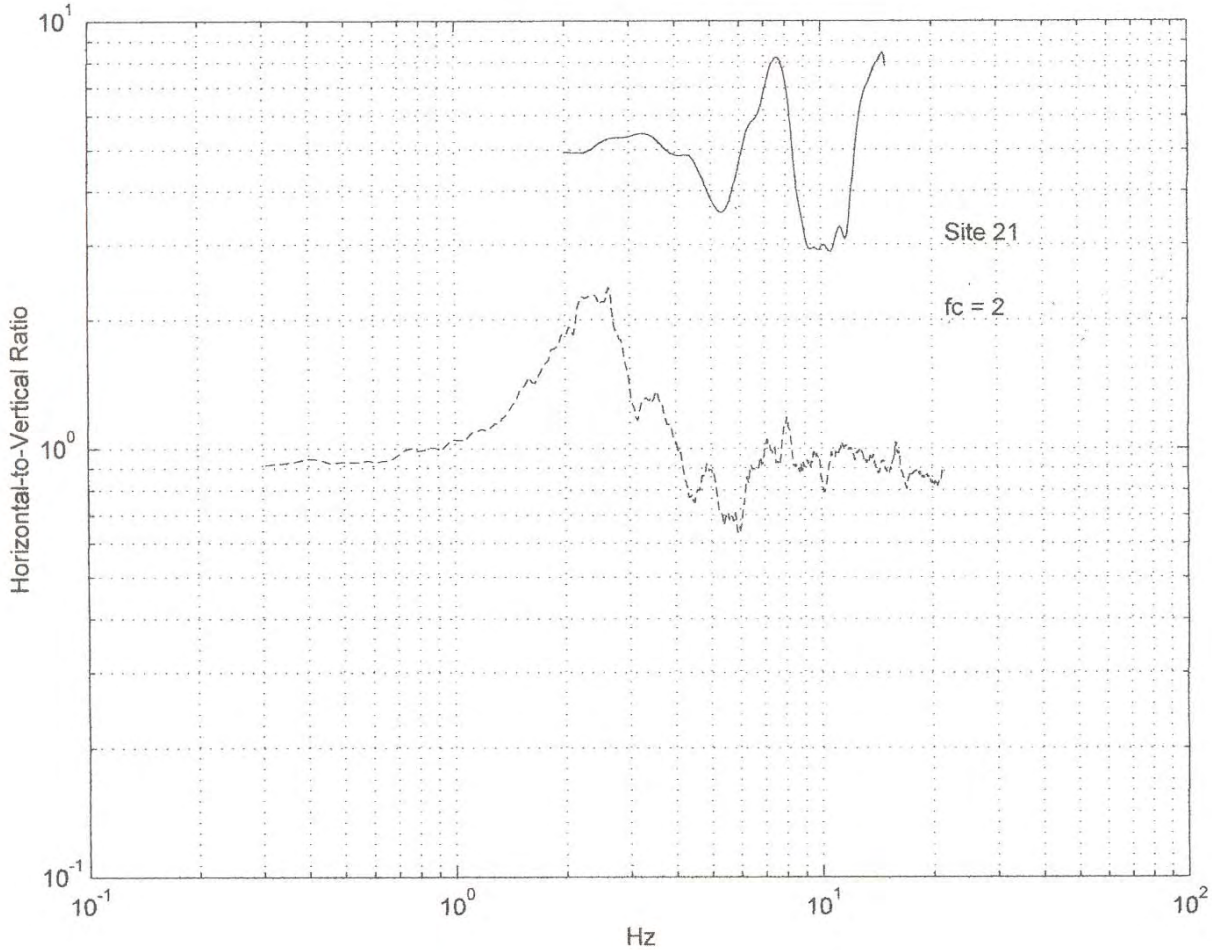
Site 21
fc = 2
Horizontal-to-Vertical Ratio
Hz
10^{1}
10^{0}
10^{-1}
10^{-1}
10^{0}
10^{1}
10^{2}

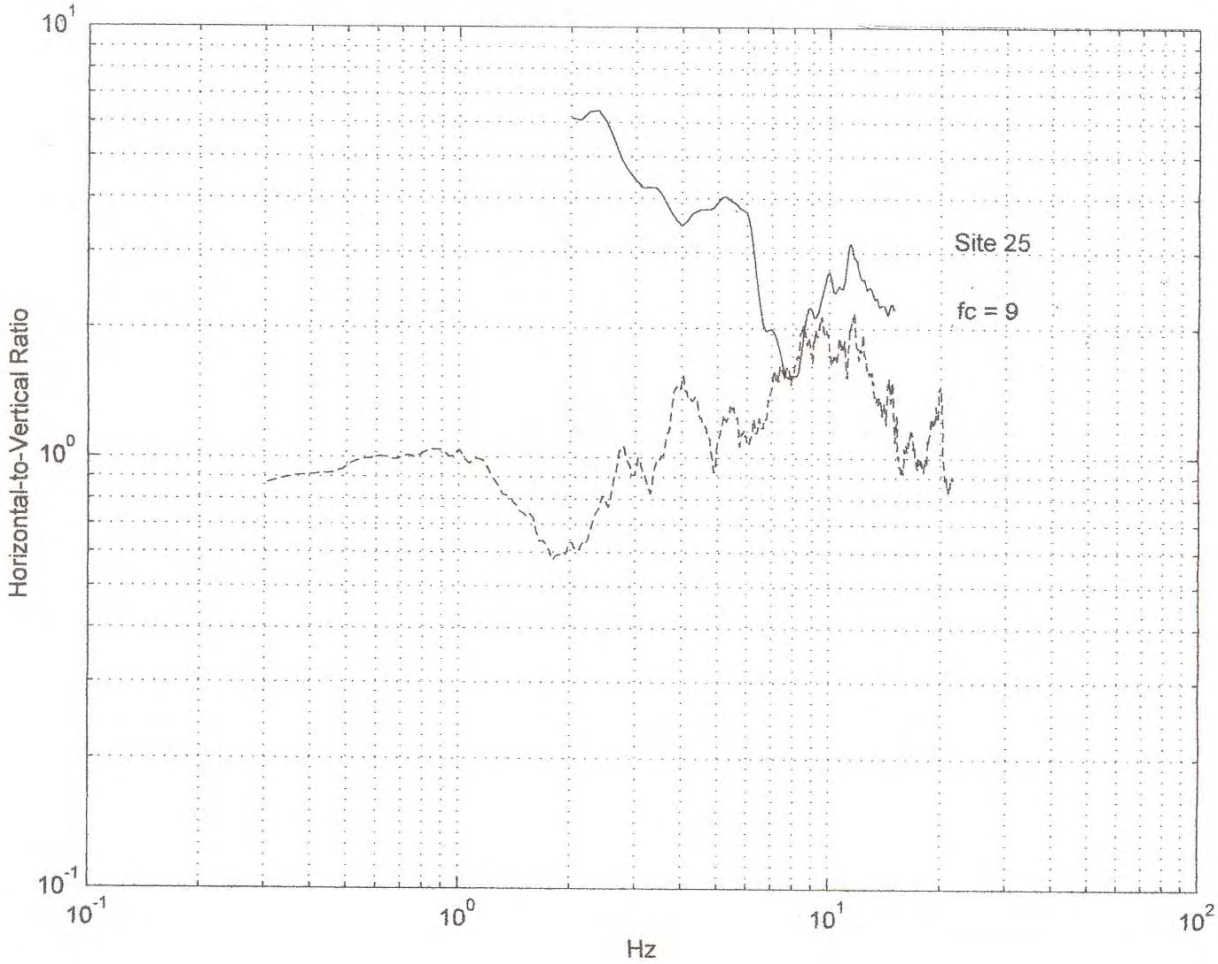
Site 25
fc = 9
Horizontal-to-Vertical Ratio
Hz
10^{1}
10^{0}
10^{-1}
10^{-1}
10^{0}
10^{1}
10^{2}

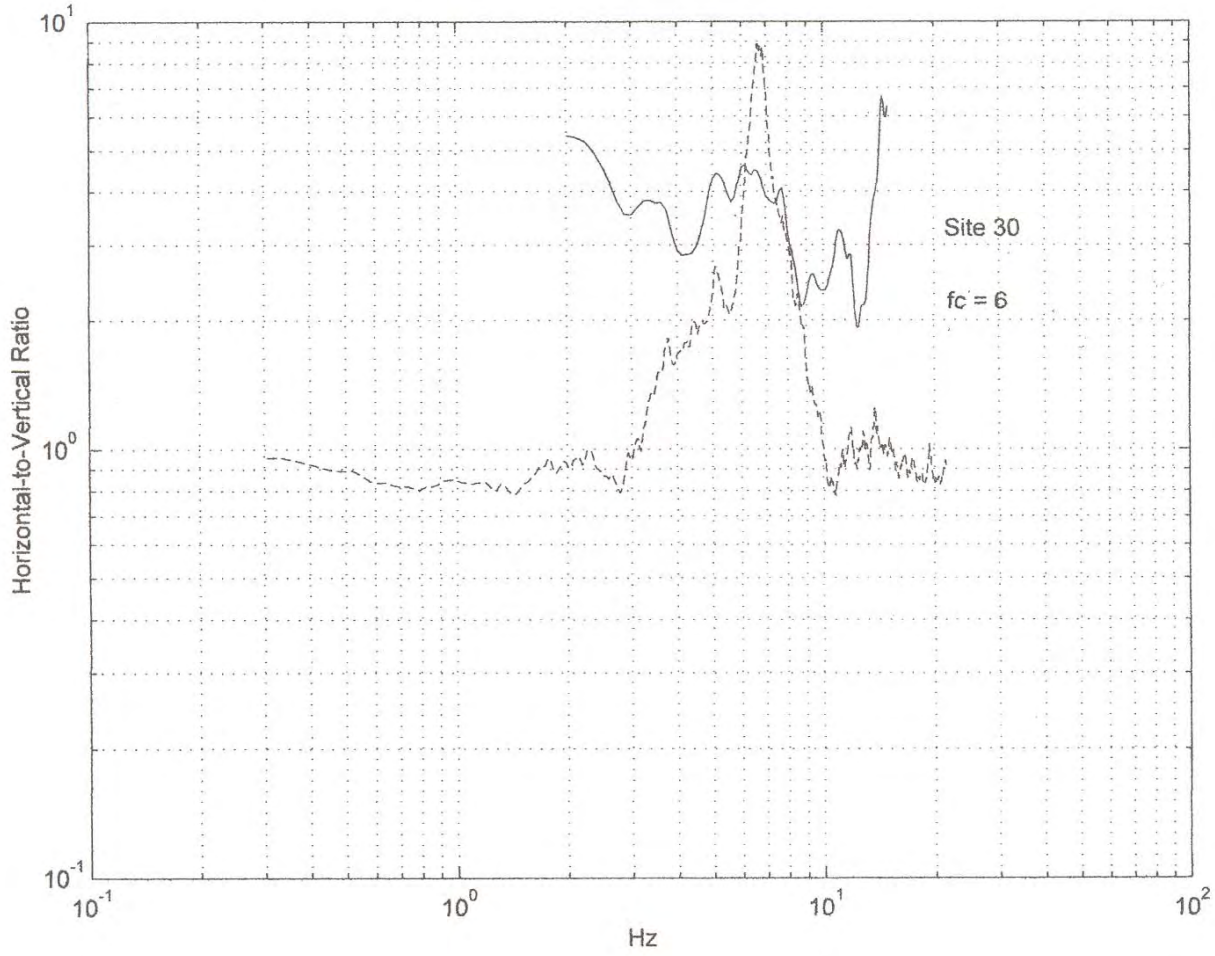
Site 30
fc = 6
Horizontal-to-Vertical Ratio
Hz
10^{1}
10^{0}
10^{-1}
10^{-1}
10^{0}
10^{1}
10^{2}

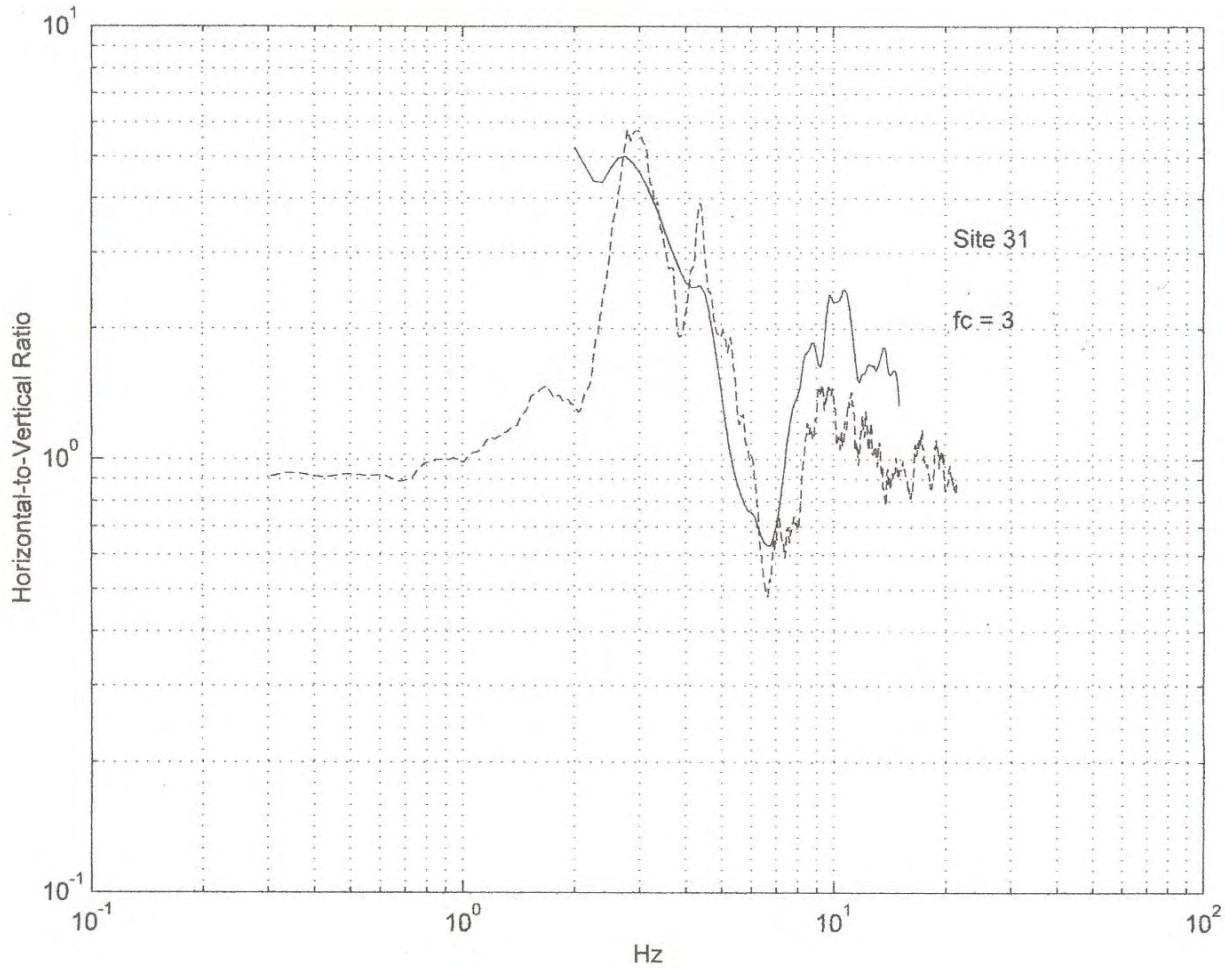
Site 31
fc = 3
Horizontal-to-Vertical Ratio
Hz
10^{1}
10^{0}
10^{-1}
10^{-1}
10^{0}
10^{1}
10^{2}

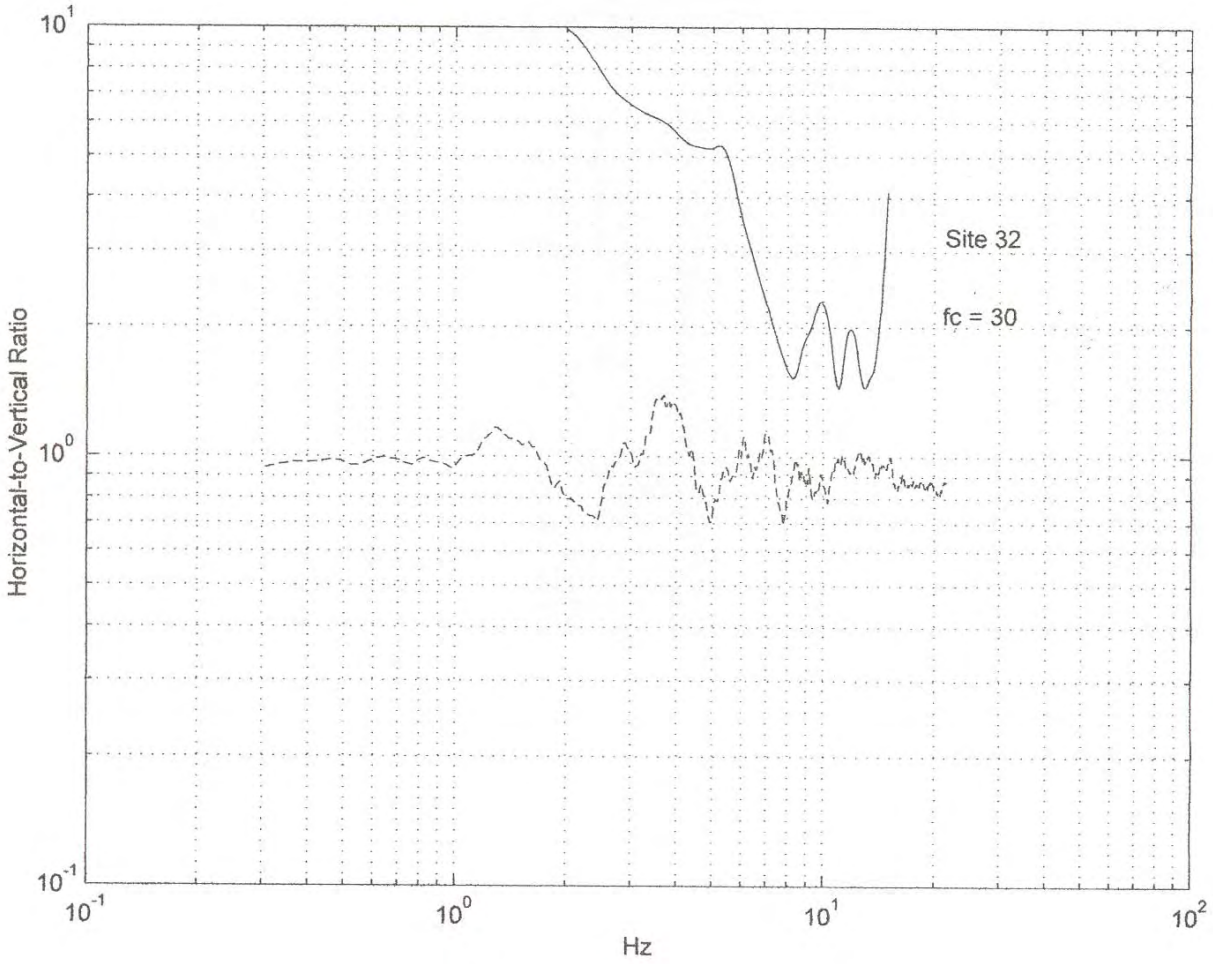
Site 32
fc = 30
Horizontal-to-Vertical Ratio
Hz
10^{1}
10^{0}
10^{-1}
10^{-1}
10^{0}
10^{1}
10^{2}

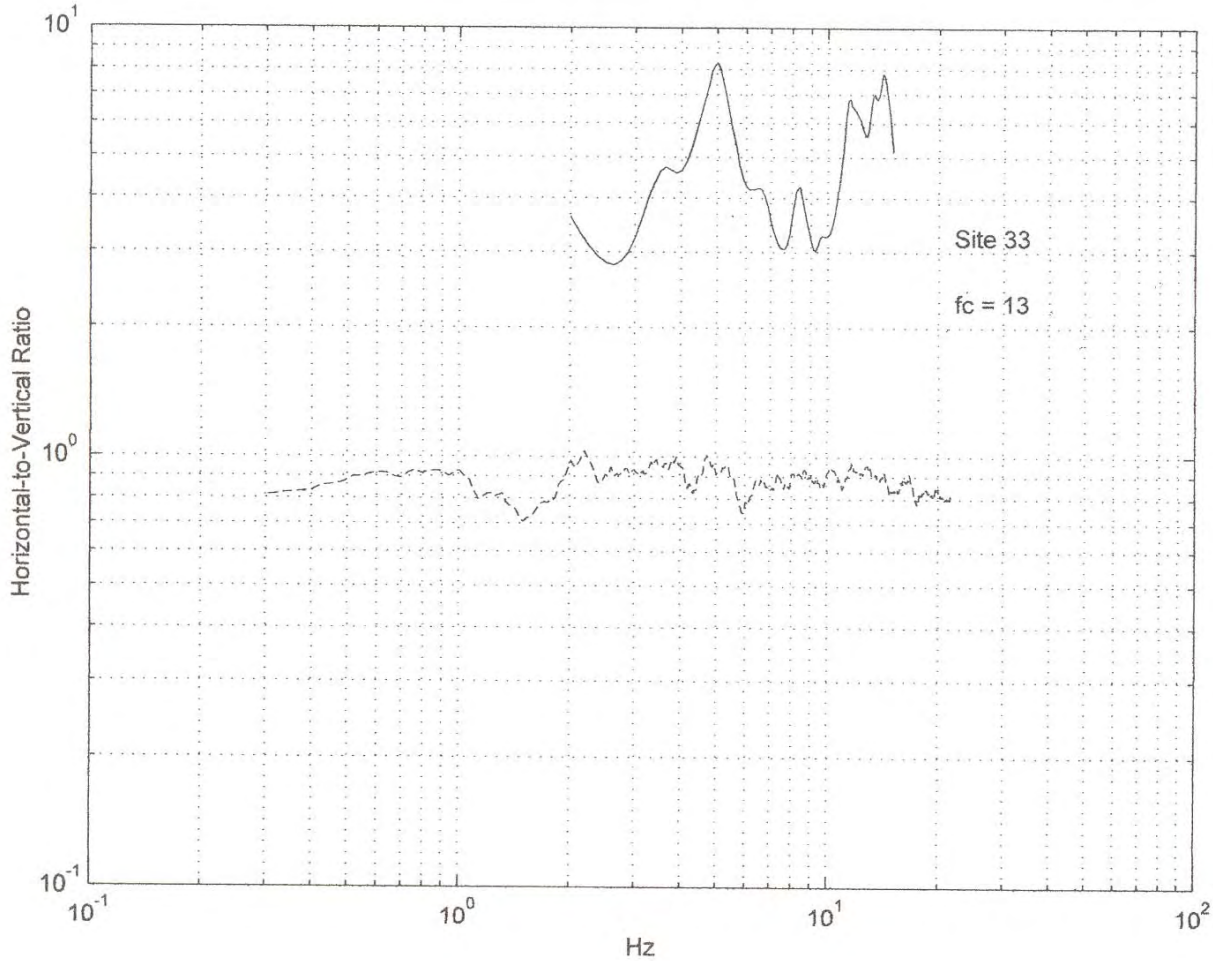
Site 33
fc = 13
Horizontal-to-Vertical Ratio
Hz
10^{1}
10^{0}
10^{-1}
10^{-1}
10^{0}
10^{1}
10^{2}

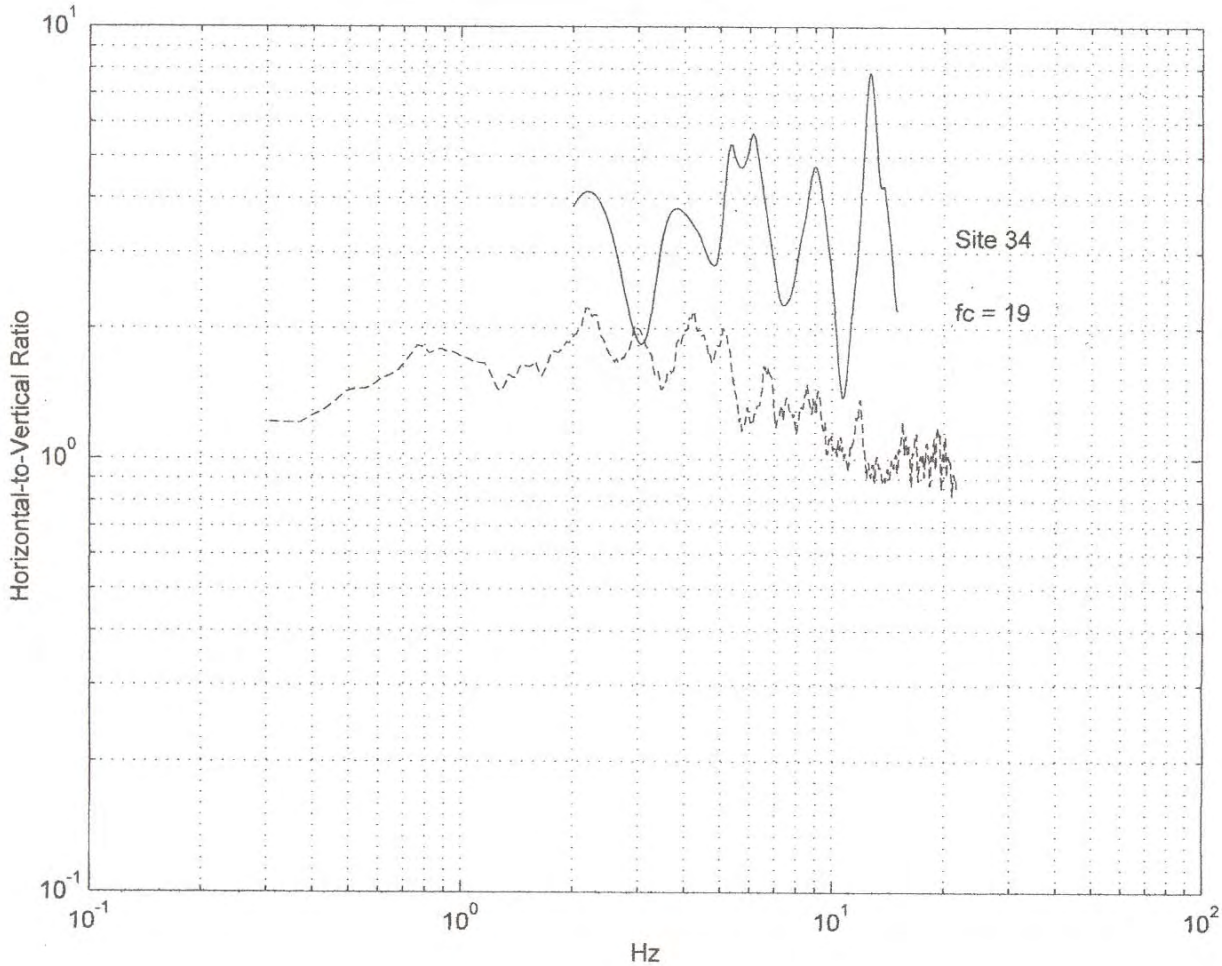
Site 34
fc = 19
Horizontal-to-Vertical Ratio
Hz
10^{1}
10^{0}
10^{-1}
10^{-1}
10^{0}
10^{1}
10^{2}

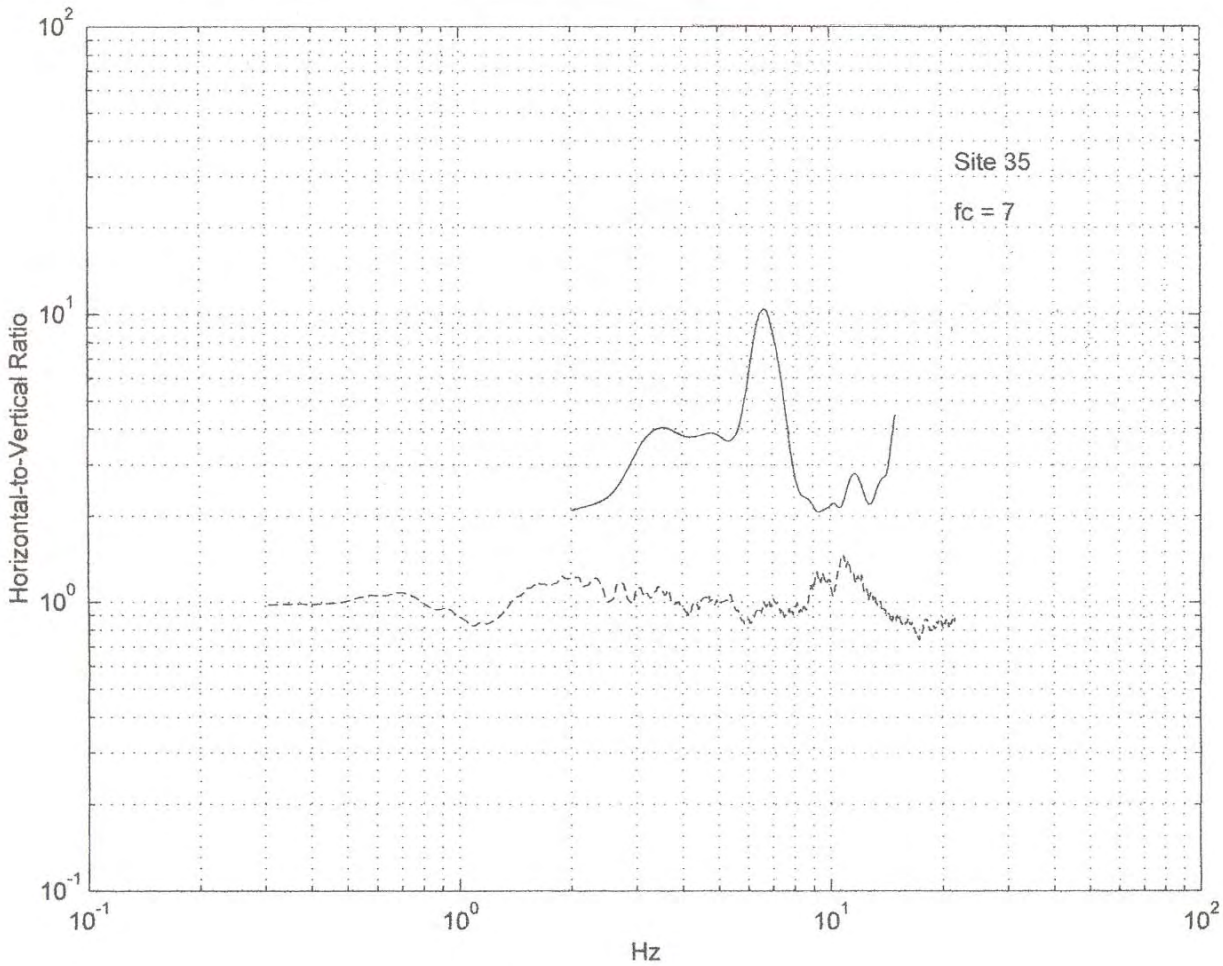
Site 35
fc = 7
Horizontal-to-Vertical Ratio
Hz
10^{2}
10^{1}
10^{0}
10^{-1}
10^{-1}
10^{0}
10^{1}
10^{2}

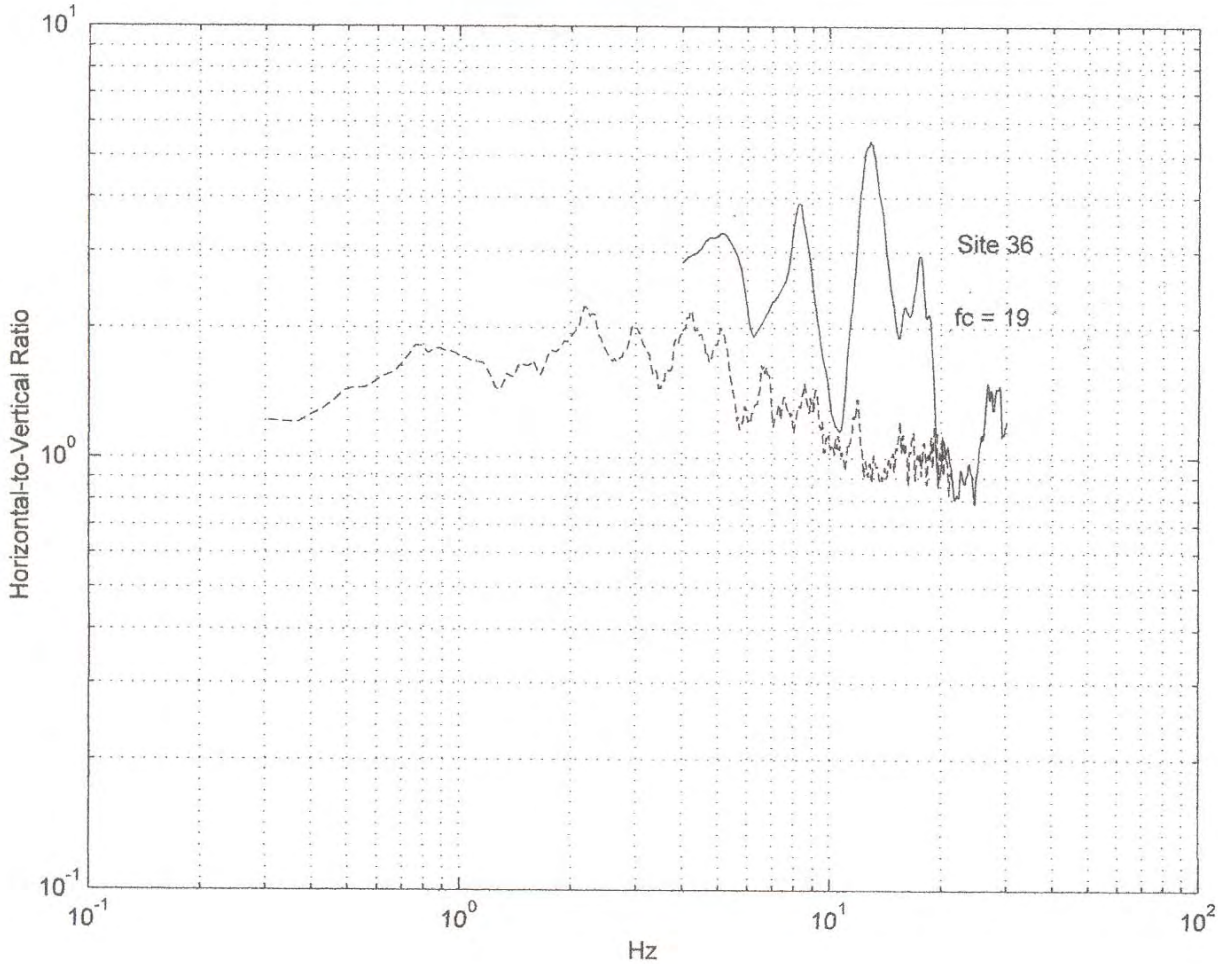
Site 36
fc = 19
Horizontal-to-Vertical Ratio
Hz
10^{1}
10^{0}
10^{-1}
10^{-1}
10^{0}
10^{1}
10^{2}

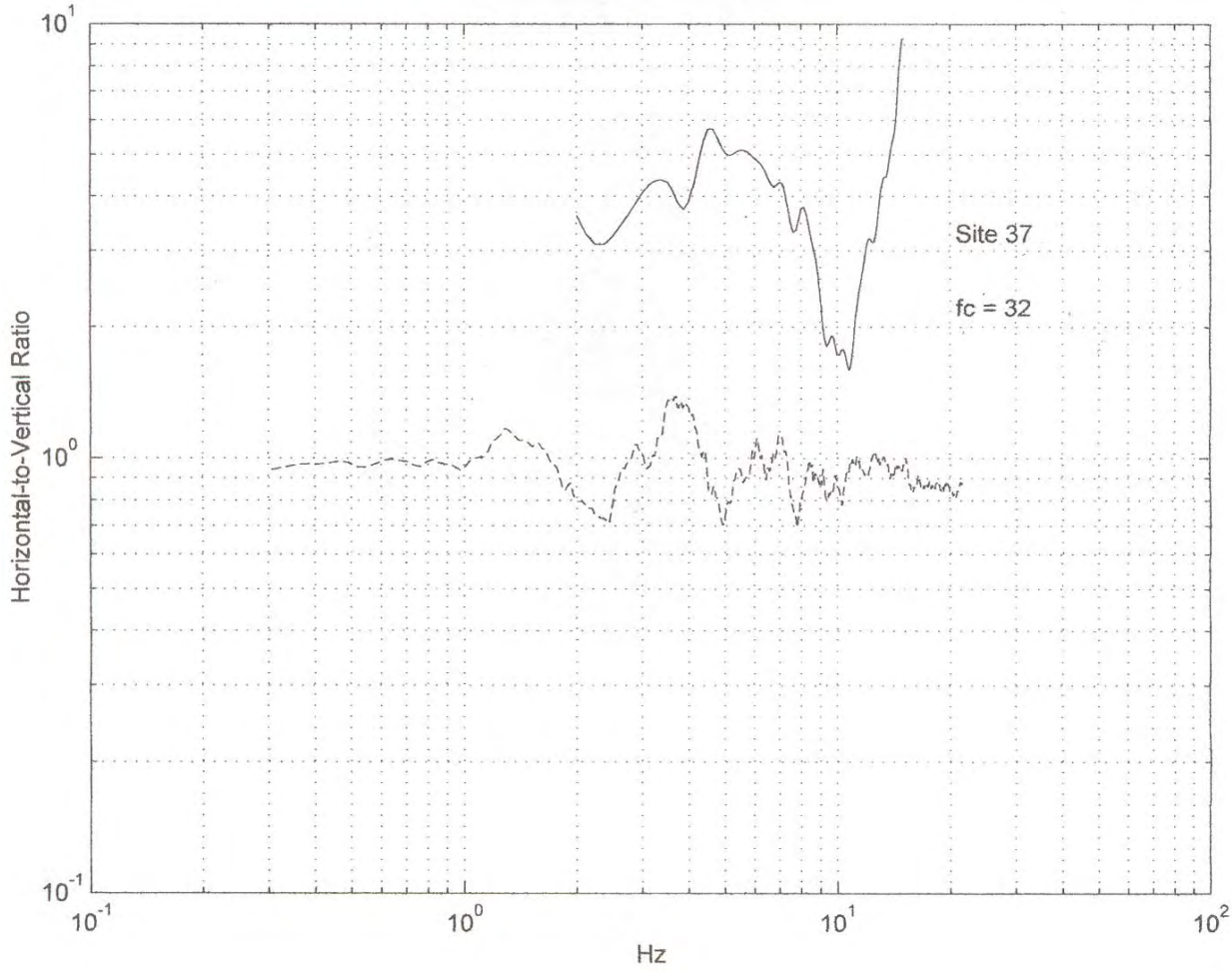
Site 37
fc = 32
Horizontal-to-Vertical Ratio
Hz
10^{1}
10^{0}
10^{-1}
10^{-1}
10^{0}
10^{1}
10^{2}

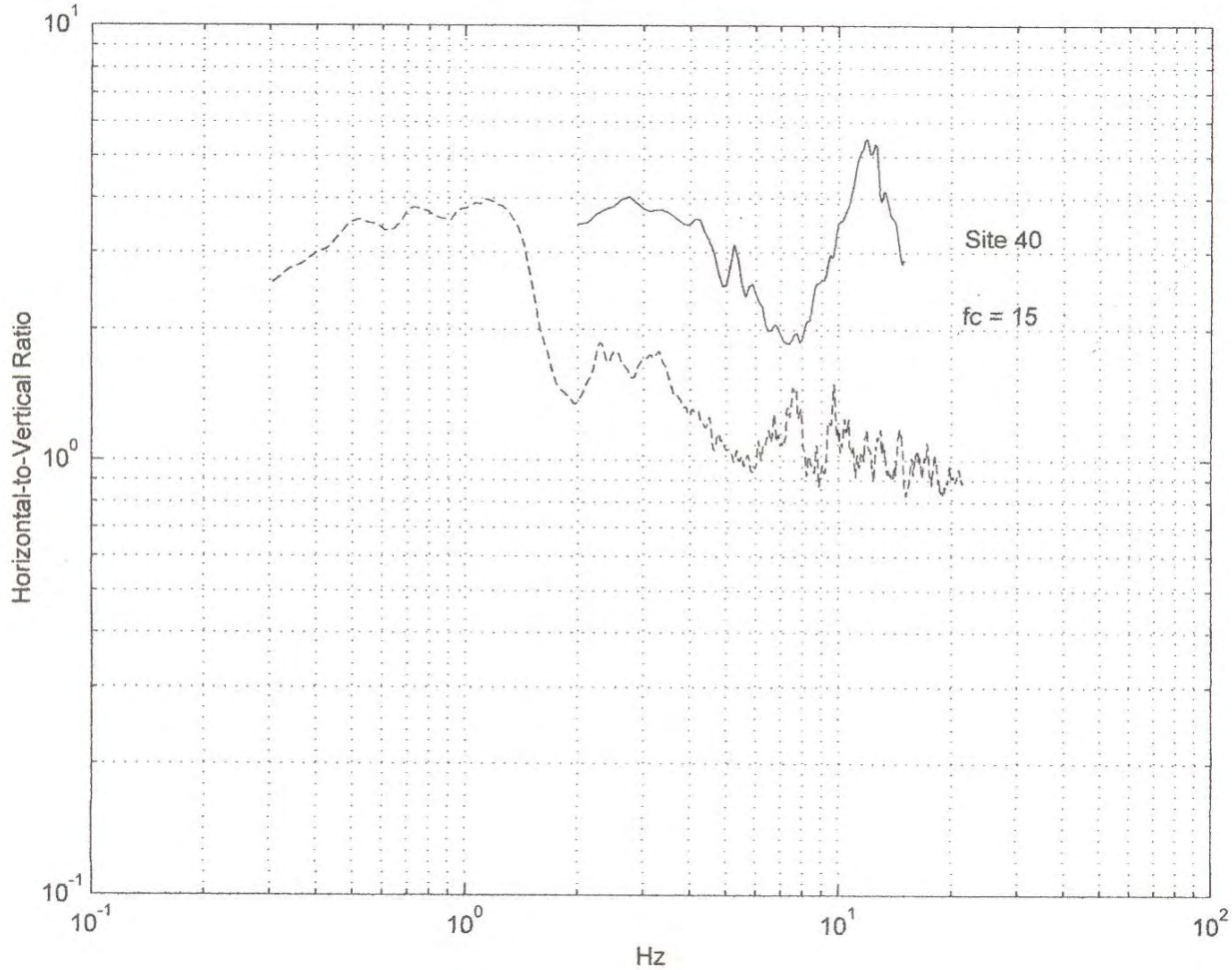
Site 40
fc = 15
Horizontal-to-Vertical Ratio
Hz
10^{1}
10^{0}
10^{-1}
10^{-1}
10^{0}
10^{1}
10^{2}

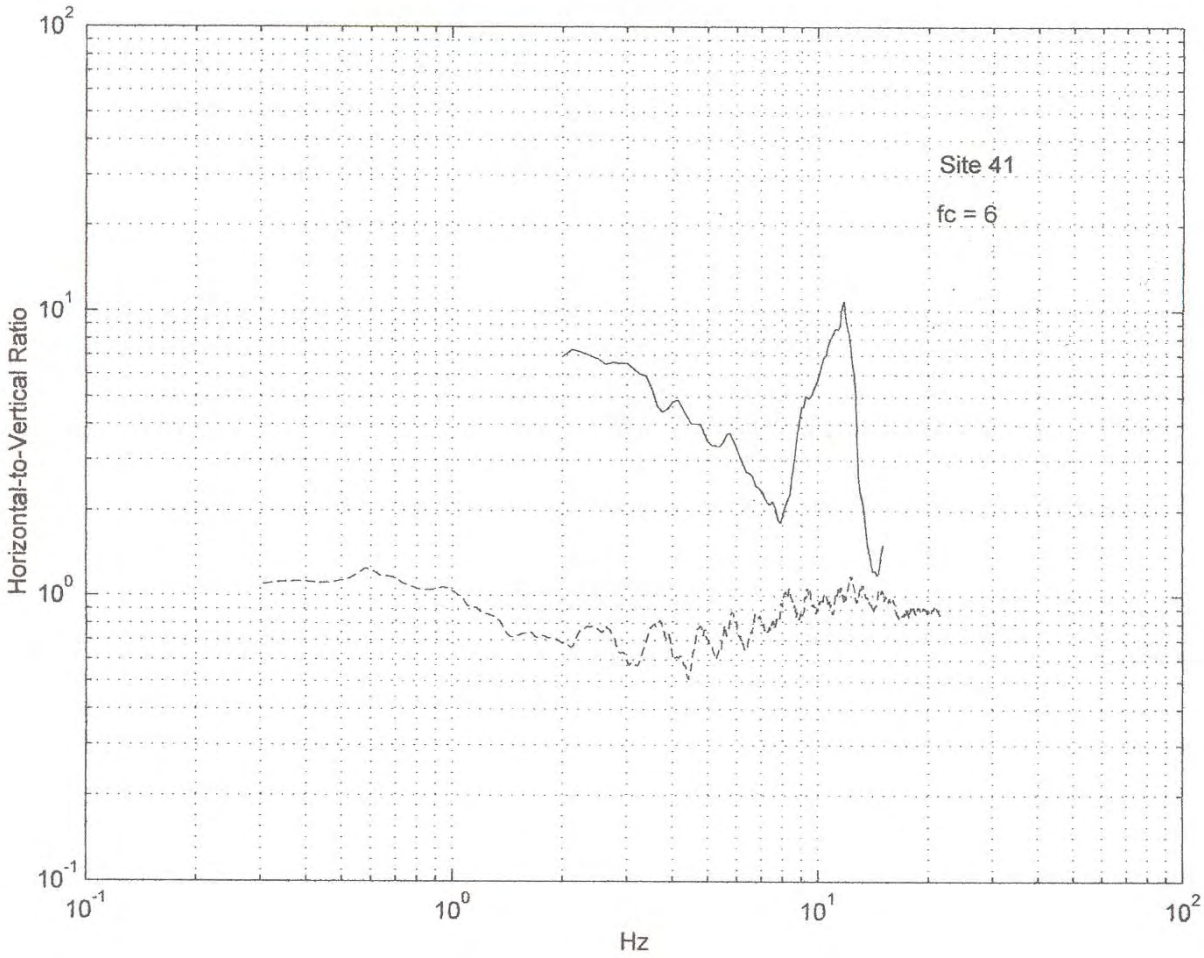
Site 41
fc = 6
Horizontal-to-Vertical Ratio
Hz
10^{2}
10^{1}
10^{0}
10^{-1}
10^{-1}
10^{0}
10^{1}
10^{2}

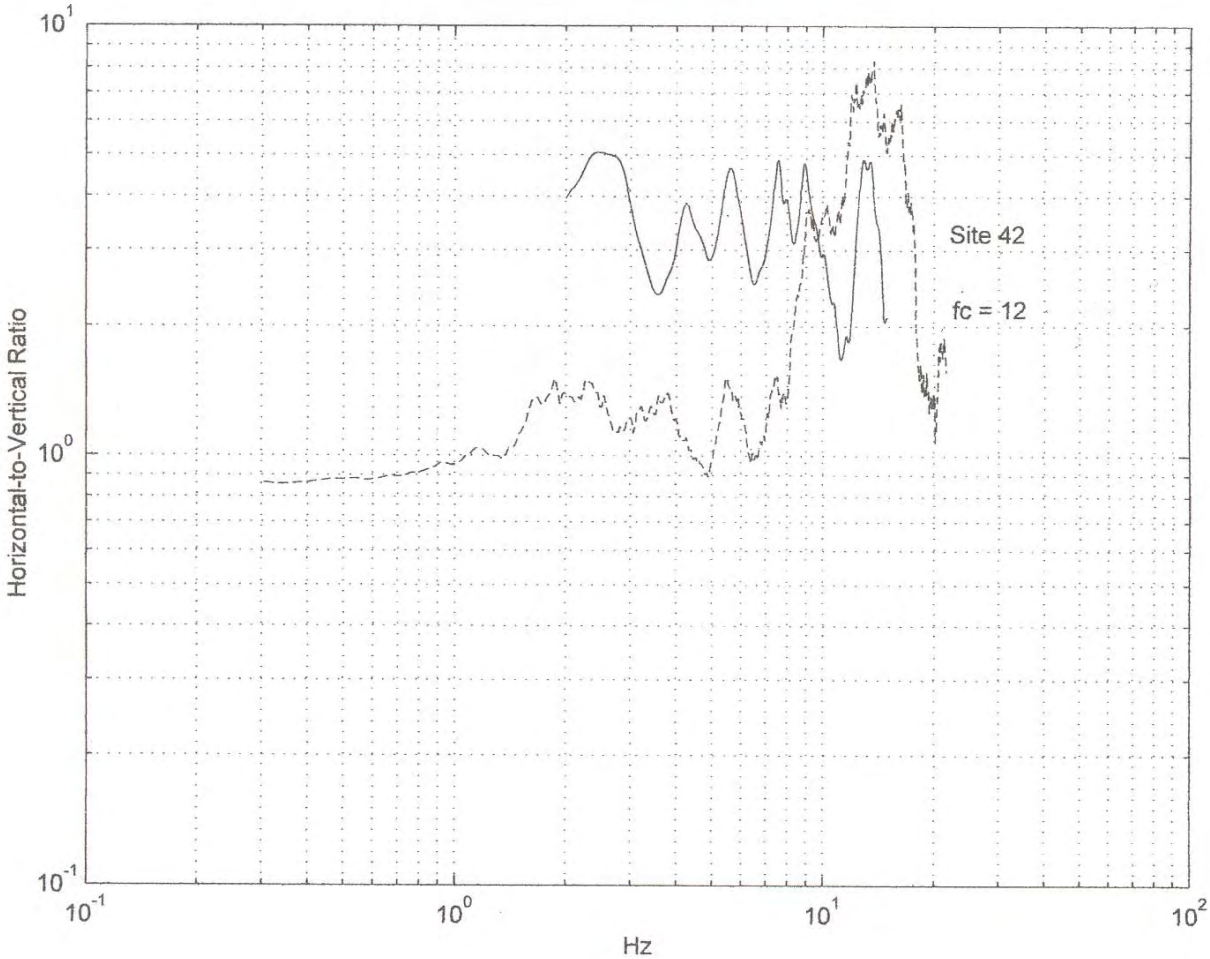
Site 42
fc = 12
Horizontal-to-Vertical Ratio
Hz
10^{1}
10^{0}
10^{-1}
10^{-1}
10^{0}
10^{1}
10^{2}